Modeling and Design of an Independent Solar House

Mark Pasini

A Thesis

In

The Department

Of

Building, Civil and Environmental Engineering

Presented in Partial Fulfillment of the Requirements
for the Degree of Master of Applied Science (Building Engineering) at
Concordia University
Montreal, Quebec, Canada

March 2006

Your file Votre référence
ISBN: 978-0-494-16245-3
Our file Notre référence
ISBN: 978-0-494-16245-3

ABSTRACT

Modeling and Design of an Independent Solar House

Design tools that are flexible enough to simulate homes that contain custom designs that harness energy from renewable energy sources, particularly solar energy are rare and usually in the form of black-box software. This thesis presents the simulation of the thermal behavior of a completely self-sufficient $75m^2$ home by developing a custom simulation program that incorporates mathematical models of most of the significant energy subsystems of the home. Mathematical models use thermal networks to model heat flow and heat storage. Simulations are performed using transient one-dimensional heat flow models. Simulation and design of a photovoltaic-thermal system is focused on due to the lack of design tools that are able to simulate this emerging technology. Simulations and experiments reveal that an overall yearly solar energy utilization efficiency of approximately between 30% - 40% can be achieved by capturing the heat from the solar panels. Simulations also show that with the proper use of thermal storage and motorized shading, the heating load on a typical cold winter night that follows a cold, sunny winter day is only 3 kWh. On a hot, sunny summer day simulations reveal that only 4.5 kWh of cooling is required with the proper use of thermal storage and motorized shading controlled based on room temperature and solar gains. A case study of the 2005 Solar Decathlon Home is presented including preliminary results which are used to verify the software models presented in the thesis.

ACKNOWLEDGEMENTS

I would like to express my gratitude to my supervisor, Dr. A.K. Athienitis, for his expert guidance, encouragement, and support during my graduate studies.

I would like to acknowledge all the Canadian Solar Decathlon Team members without whom the solar house could not have been designed and built for all of their countless hours of hard work and dedication.

Special thanks and appreciation also go to my family for their moral support and encouragement.

I would also like to thank Howard Yaphe for his assistance with this project and CanLyte for partial financial support.

I would also like to thank Dr. Kwang-wook Park for his expert guidance.

Finally, I would like to thank the Natural Sciences and Engineering Research Council of Canada for supporting me with an Industrial Scholarship.

TABLE OF CONTENTS

LIST OF FIGURES

LIST OF TABLES

NOMENCLATURE

α	Solar altitude
α_i	Absorptance of inner glazing
α_o	Absorptance of outer glazing
α_s	Absorptance of single glazing
β	Tilt angle
γ	Surface solar azimuth
δ	Declination angle
θ	Angle of incidence
θ'	Angle of refraction
k_b	Thermal conductivity of brick
ρ_g	Reflectance of ground
ρ_b	Density of brick
ρ_o	Reflectance of outer glazing
τ	Transmittance of glazing
τ_b	Transmittance of atmosphere
τ_{b_open}	Fraction of shade covering window when shade open
τ_{b_redu}	Fraction of shade covering window when shade closed
τ_e	Effective transmittance of double glazing
φ	Solar azimuth
ψ	Surface azimuth
Aw	Area of window

Ad	Area of door
c_b	Specific heat of brick
C2	Capacitance of brick
DT	Difference between maximum and minimum outdoor temperature
f_f	Fraction of framing out of total wall area
Gai	Solar radiation absorbed by inner glazing
Gao	Solar radiation absorbed by outer glazing
Gb	Beam component of solar radiation through windows
Gd	Diffuse component of solar radiation through windows
Gt	Total solar radiation transmitted through windows
hc	Convective heat transfer coefficient
h_{gap}	Heat transfer coefficient inside double glazed window cavity
ho	Exterior heat transfer film coefficient
hi	Interior heat transfer film coefficient
hr_{low_e}	Radiative heat transfer coefficient with low e coating
it	Hour index (0 .. 23)
iw	Index of window orientation (1: South, 2: East, 3: West, 4: North)
Ib	Direct beam solar radiation
Idg	Diffuse ground solar radiation
Ids	Diffuse sky solar radiation
Ion	Extraterrestrial solar radiation
kl	Extinction coefficient
L	Latitude

n_d	Number indicating day of year (1 .. 365)
Q_{blind_rooom}	Heat transferred from shade to room
Qgg	Solar radiation absorbed by glazings and released to room air
r	Component reflectivity
R	Thermal resistance
R1	Thermal resistance from shade to outside
R_{1o}	Thermal resistance between room air and outside
R2	Thermal resistance from shade to room air
$R_{\#a\_\#c}$	Thermal resistance between air and bricks
$R_{\#a\_r}$	Thermal resistance between air surrounding bricks and room air
Rext	Thermal resistance of external insulation
Rf	Thermal resistance of framing
Rw	Thermal resistance of window
schedule	Shading schedule
shadefac	Fraction of shade covering window
S	Solar radiation incident on walls and floor
T_6	Room air temperature
T#a	Temperature of control volume of air surrounding brick
T#c	Temperature of control volume of brick
To	Outdoor temperature
Tomean	Mean outdoor temperature
Ts#	Temperature of control volume of floor surface
$U_{\#b\_\#b}$	Conductance between adjacent bricks

Uinf	Air infiltration (air exchanges per hour)
V	Velocity profile of air through bricks
w_t	Period of temperature profile
z	Zenith angle

CHAPTER 1

INTRODUCTION

1.1 Introduction

Engineers and architects that are interested in designing an energy efficient home are faced with the challenge of creating a structure which maximizes the use of solar energy, uses energy efficient construction methods, appliances and systems, yet represents an aesthetically appealing and economically viable alternative to the consumer. Building energy efficient homes and multi-residential buildings has been a priority since the energy crisis of the 1970's. Although the focus faded somewhat in the 1980's and 1990's due to the drop in the price of oil, the world finally realized through a combination of rising oil prices, reduced supply of fossil fuels, and a greater concern for the long term survival of the earth in general, that energy efficiency must become a primary design criteria for not only vehicles, but also appliances, heating, ventilation and air conditioning (HVAC) systems, and home and building construction methods. This is also evident in the significant increase in the use of renewable energies such as photovoltaics, solar thermal, wind, and micro-turbines, to the point where the production of some of them, noticeably photovoltaics, is not sufficient to supply the demand [Barnett (2003)].

Although it may seem that research and development in the area of harnessing the sun's energy and transforming it into other useful forms has been around since the 1970's, it was in fact in 1860 that this research began. Auguste Mouchout, a mathematics instructor at the Lyce de Tours, out of concern of Europe's dependence on coal, invented a system of converting solar energy into mechanical power. Stemming from this research, in 1885

the first flat-plate solar collector was invented [Smith (1995)]. The concept of thermal storage is nothing new as well. Since the age of the pyramids, man has been finding ways of storing the energy of the earth and sun for later use. One aspect of thermal storage systems that lacks a significant amount of research however is that of control. To truly optimize the performance of a passive thermal storage system, one must have an algorithm which effectively controls solar radiation. Due to the high costs associated with photovoltaics, methods of integrating the panels into the roof and façade of the building are being researched. PV-thermal refers photovoltaic systems installed in a way in which the heat that is generated can be harnessed and used for common loads such as space and water heating, thereby increasing the overall efficiency of the system with minimal increase in cost. However, designing homes with custom features are difficult to simulate due to a lack of software which is easily configurable to handle non-conventional sources of energy. This thesis describes the design of custom software using that simulates the thermal behavior of a home by modeling aspects including the envelope, shading, PV-thermal and thermal storage system. A case study is also presented which was built based on the results of the research performed for this thesis. Preliminary results from the case study are then used to validate the software program.

1.2 Research Motivation

Due to the almost unlimited possibilities that exist when attempting to design a net-zero energy home, this thesis aims to present the manner in which such a home may be designed based on solar energy utilization – from simulation to construction. Little information is available that covers innovative building integrated photovoltaics (BIPV) designs, let alone designs that integrate into the HVAC system in order to increase the

efficiency of the photovoltaic system. Research shows that PV-thermal systems are cost effect and of better environmental impact compared with standard PV modules [Tripanagnostopoulos (2004)]. Research in the area of thermal storage also exists which looks at how to size it, where it should be located, and how the energy should be transferred to the space [Charron (2005)]. However, little or no work has been focused on developing control algorithms or techniques which control shading, lights, and HVAC at the same time. Software exists that simulates the electrical performance of PV systems, but there is no record of software that simulates the thermal energy characteristics. Work must be done in order to optimize the performance of these systems when working in unison to achieve the same common goal – that is, to create a comfortable environment using the least amount of energy possible. This thesis demonstrates that energy simulations should be performed in parallel with architectural decisions when determining building envelope criteria such as the building's aspect ratio, windows and insulation in order to minimize the size of heating and cooling equipment. Although software exists today to accomplish this, such as TRNSYS and ESP-r, such program are difficult to learn and cannot handle custom energy saving features since most software programs that exist today are not up to date with the latest research. For example, none of this software allows for programmable control algorithms for motorized blinds. In the case of a solar house one needs to optimize the portion of solar energy admitted through the windows by automatically controlling the blind position based on outside temperature, indoor conditions, and solar radiation.

1.3 Scope and Objectives

This thesis is focused on the development of a computer model for energy analysis of a solar home implementing advanced solar technologies, particularly a building-integrated photovoltaic-thermal system, passive solar design systems, and controlled motorized blinds. Extensive simulations were performed using a program developed in MathCAD 2001i that simulates the control of the significant systems that affect the thermal behavior of a house in order to choose appropriate building technologies and mechanical systems and to develop algorithms which attempt to maintain a comfortable living environment year-round while minimizing energy consumption.

The result of the thesis were used to design and build a net-zero energy home for the Canadian entry in the 2005 Solar Decathlon Competition, which went on to win the Most Energy Efficient Design award from the National Association of Home Builders. The home also received an award from BP solar for the innovative method of integrating the PV panels into the roof that allows the panels to act as a roofing material as well as a source of electrical and thermal energy for the home. Preliminary test results are also discussed which were recorded during the pre-competition testing of a mock-up of the Solar House from the Solar House itself.

1.4 Overview of the Thesis

Chapter 2 begins with a review of current housing technology necessary for both accurately simulating a net-zero home as well as building it in the most energy efficient manner. The review focuses on energy-efficient electricity-powered HVAC technology, such as heat pumps, followed by photovoltaic technology, including amorphous, polycrystalline, and thin film as well as inverter and battery charging technologies.

Building envelope technologies are then examined including insulation and windows. Lighting technology including dimming methods and control algorithms is reviewed due to its importance for the Solar Decathlon Competition since the ability to accurately control the lighting is crucial to saving energy in a home. Chapter 3 presents the simulation model for the house and the simulations that were performed using energy simulation programs developed over the course of this research project. Chapter 4 describes the 2005 Solar Decathlon House which served as a test case for the simulation software and technologies developed and researched as a result of this thesis. Chapter 5 performs verification of some of the models presented in Chapter 3 by examining the preliminary test results obtained from the mock-up of the Solar House and the actual Solar Decathlon House which were tested at Concordia University's Loyola Campus in Montreal, Canada. Chapter 6 presents conclusions from this study. Recommendations for future work are also presented.

CHAPTER 2

REVIEW OF BUILDING SOLAR AND ENERGY TECHNOLOGIES

2.1 Introduction

The aim of this review is to examine the state of current housing technology, mechanical systems, and active solar energy products in order to develop a suitable solar house design tool and to design a net-zero energy solar house. Mechanical systems are researched in order to be able to model an appropriate method of adding and removing thermal energy from the home. A review of active solar technology and roof integration techniques is reviewed in order to understand and be able to accurately model the photovoltaic-thermal system. Windows and insulation are then examined since they represent the key elements of the building envelope which must be optimized in order to maximize energy efficiency and return on investment. Lighting technology is examined since it is an integral part of energy efficiency in residential buildings and is therefore an important aspect of the system design process of an energy efficient structure. The results from the review were used to choose appropriate systems for use in a case study that was simulated to evaluate their predicted energy performance when integrated.

2.2 Heating, Ventilation and Air Conditioning

There are many different ways of heating a house. There is heating directly using electricity (baseboard heaters or electric forced air furnaces), natural gas, wood, oil, and heat pumps. Heat pumps are considered a good match for solar buildings due to their high efficiency. For heat pumps, the COP can be as high as 5 in some cases, with a COP of 3 being quite common. A COP of 3 means they are 3 times as efficient as heating with electricity. Air-source heat pumps however lose their effectiveness (their COP drops to 1) when the inlet air temperature drops below around -15°C. There are methods however to avoid this: use a ground source heat pump (GSHP) or some other source of warmer air (warm air from under PV which is explained in more detail in Chapter 3). A GSHP ensures an inlet temperature of around 6°C, depending on the geographical location, how deeps the pipe is below the ground, and how many feet of pipe are used. An alternative to the GSHP is to use a water-source heat pump that can use heat from the PV system or the solar thermal collector to store heat in thermally insulated water tanks so that on cold, overcast days the heat pump has a source of heat. This was the concept chosen for the Solar Decathlon House since transportation did not allow for a typical GSHP. The advantage of this would be that no digging is required; the disadvantage would be that air from the PV is only warmed up when it is sunny [Pasini and Athienitis (2006)].

2.2.1 HVAC Control

The simplest means of control is the thermostat. Thermostats can either be analog or digital, meaning the setpoint can be manually adjusted with a dial or lever or can be programmed depending on occupant preferences. These preferences could include time of day setpoints, setpoints based on occupancy of the space, or in most advanced

situations, setpoints based on load management algorithms that take energy cost and availability into consideration. Another method of control that is emerging is the modulation of the power of compressors. Controlling the power of the system can be accomplished by either having a compressor with multiple speeds or by having multiple compressors and deciding when each compressor turns on. The benefits of controlling the output power of the system include better part-load performance, reduced compressor cycling, and the potential for improved humidity management (Roth (2004)]. By having a variable speed drive modulating the motor's speed, the compressor's output can be matched to the load sensed by the unit's control system. In the case of the Solar Decathlon House, the heat pump had two separate compressors, one 9000 BTU and one 12000 BTU, to allow for more precise heating and cooling based on varying needs.

2.3 Photovoltaics

In order to make an educated choice regarding the best product for integration into the Solar Decathlon Home, like any other net-zero home, a review of photovoltaic technology was performed. Details of the PV system of the Solar Decathlon Home can be found in Chapter 4.

2.3.1 Introduction

The conversion of the energy carried by optical electromagnetic radiation into electrical energy is a physical phenomenon known as the photovoltaic effect. Solar cells carry out such conversions, and it is with solar cells that solar panels are produced. The first efficient solar cell was developed in 1954 by Chapin, Fuller and Pearson [Araujo (1998)]. A solar cell functions in a similar manner to a battery; when a load is connected across

the terminals a current is produced that flows from the positive terminal, through the load, then back through the negative terminal. The solar cells are connected in series and in parallel in order to produce the desired voltage and current of the module. A graph of the typical current and voltage characteristics of a solar cell are shown in Figure 2.1. It can be seen that the cell acts as a current source over a range of voltages. It can also be seen that the operating temperature of the cell affects the performance of the cell; a rise in temperature results in a lower maximum voltage and therefore lower power output. Solar radiation on the other hand is proportional to the current; the larger the solar radiation value, the large the current and therefore power.

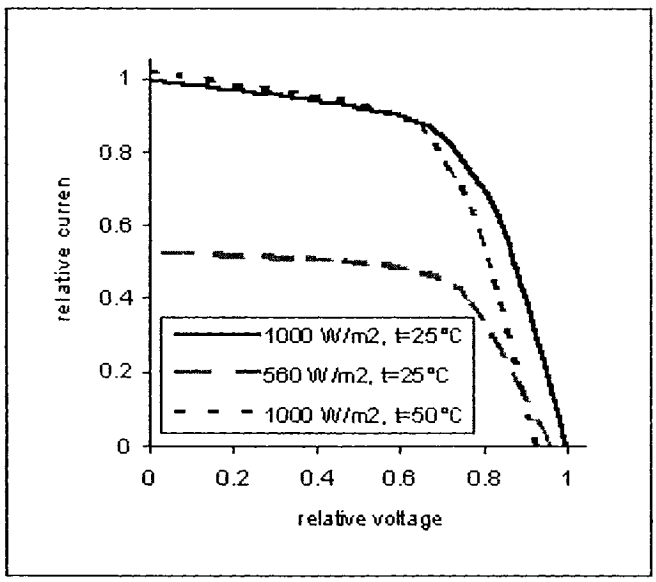

Figure 2.1: Typical Photovoltaic I-V curve (http://www.scolar.org.uk/)

To understand the operation of a PV cell, the nature of the material and the nature of sunlight must be considered. Solar cells consist of two types of material, often p-type silicon and n-type silicon. Light of certain wavelengths is able to ionize the atoms in the silicon and the internal field produced by the junction separates some of the positive charges ("holes") from the negative charges (electrons) within the photovoltaic device.

The holes are swept into the positive or p-layer and the electrons are swept into the negative or n-layer. Although these opposite charges are attracted to each other, most of them can only recombine by passing through an external circuit outside the material because of the internal potential energy barrier. Therefore if a circuit is made power can be produced from the cells under illumination, since the free electrons have to pass through the load to recombine with the positive holes [Araujo (1998)].

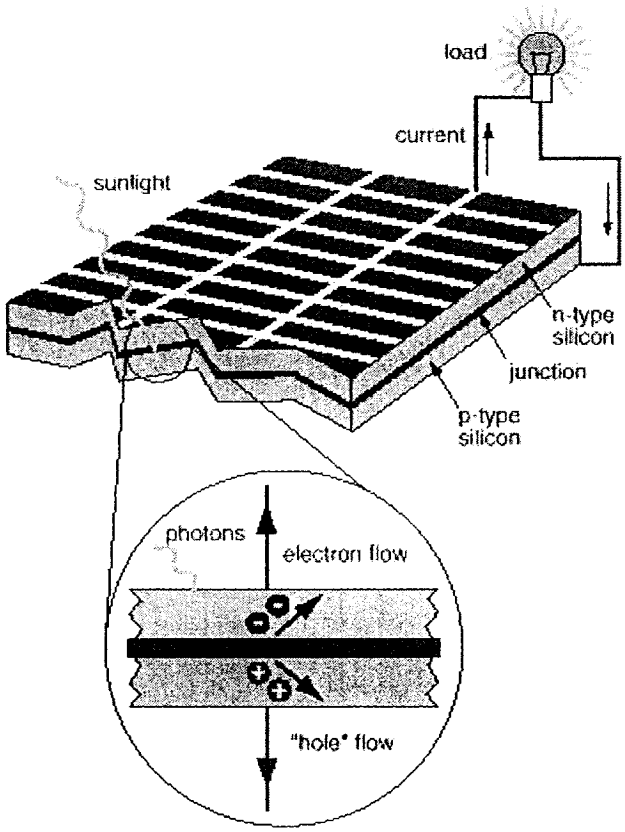

Figure 2.2: Schematic of how photovoltaic cells work (HowStuffWorks.com)

2.3.2 PV Technologies

2.3.2.1 Crystalline

Historically, crystalline silicon (c-Si) has been used as the light-absorbing semiconductor in most solar cells, even though it is a relatively poor absorber of light and requires a considerable thickness (several hundred microns) of material. Nevertheless, it has proved convenient because it yields stable solar cells with good efficiencies (11-16%, half to two-thirds of the theoretical maximum) and uses process technology developed from the huge knowledge base of the microelectronics industry. Two types of crystalline silicon are used in the industry. The first is monocrystalline, produced by slicing wafers (up to 150mm diameter and 350 microns thick) from a high-purity single crystal boule. The second is multicrystalline silicon, made by sawing a cast block of silicon first into bars and then wafers. For both mono- and multicrystalline Si, a semiconductor homojunction is formed by diffusing phosphorus (an n-type dopant) into the top surface of the boron doped (p-type) Si wafer. Screen-printed contacts are applied to the front and rear of the cell, with the front contact pattern specially designed to allow maximum light exposure of the Si material with minimum electrical (resistive) losses in the cell. The most efficient production cells use monocrystalline c-Si with laser grooved, buried grid contacts for maximum light absorption and current collection. Some companies are producing technologies that by-pass some of the inefficiencies of the crystal growth/casting and wafer sawing route. One route is to grow a ribbon of silicon, either as a plain two-dimensional strip or as an octagonal column, by pulling it from a silicon melt. Another is to melt silicon powder on a cheap conducting substrate. These processes may bring with them other issues of lower growth/pulling rates and poorer uniformity and surface

roughness. Each c-Si cell generates about 0.5V, so 36 cells are usually soldered together in series to produce a module with an output to charge a 12V battery. The cells are hermetically sealed under toughened, high transmission glass to produce highly reliable, weather resistant modules that usually carry a warranty of up to 25 years [NEEC (2005)].

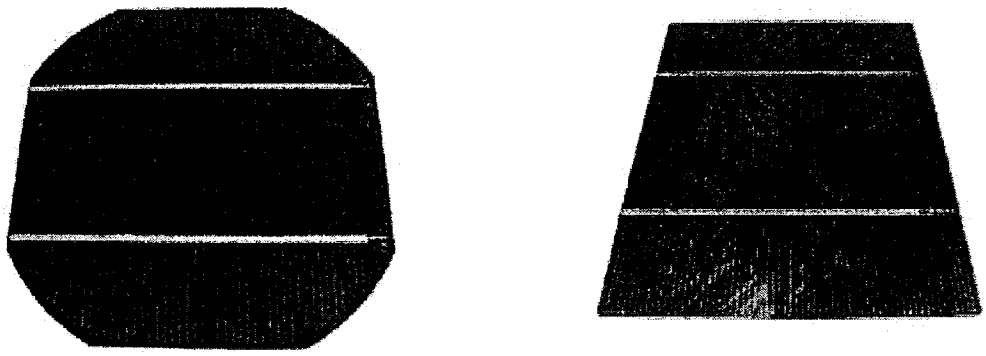

Figure 2.3: Mono-Crystalline (left) and Poly-Crystalline (right) cells (National Energy Efficiency Committee)

2.3.2.2 Thin-Film

Thin film technologies are all complex. They have taken at least twenty years, supported in some cases by major corporations, to get from the stage of promising research (about 8% efficiency at $1cm^2$ scale) to the first manufacturing plants producing early product.

Amorphous silicon is the most well developed of the thin film technologies. In its simplest form, the cell structure has a single sequence of p-i-n layers. Such cells suffer from significant degradation in their power output (in the range 15-35%) when exposed to the sun. The mechanism of degradation is called the Staebler-Wronski Effect, after its discoverers. Better stability requires the use of a thinner layer in order to increase the electric field strength across the material. However, this reduces light absorption and hence cell efficiency. This has led the industry to develop tandem and even triple layer

devices that contain p-i-n cells stacked one on top of the other. In the cell at the base of the structure, the a-Si is sometimes alloyed with germanium to reduce its band gap and further improve light absorption. All this added complexity has a downside though; the processes are more complex and process yields are likely to be lower. In order to build up a practically useful voltage from thin film cells, their manufacture usually includes a laser scribing sequence that enables the front and back of adjacent cells to be directly interconnected in series, with no need for further solder connection between cells.

As before, thin film cells are laminated to produce a weather resistant and environmentally robust module. Although they are less efficient (production modules range from 5 to 8%), thin films are potentially cheaper than c-Si because of their lower materials costs and larger substrate size. However, some thin film materials have shown degradation of performance over time and stabilized efficiencies can be 15-35% lower than initial values. Many thin film technologies have demonstrated best cell efficiencies at research scale above 13%, and best prototype module efficiencies above 10%. The technology that is most successful in achieving low manufacturing costs in the long run is likely to be the one that can deliver the highest stable efficiencies (probably at least 10%) with the highest process yields [Solarbuzz (2006)]

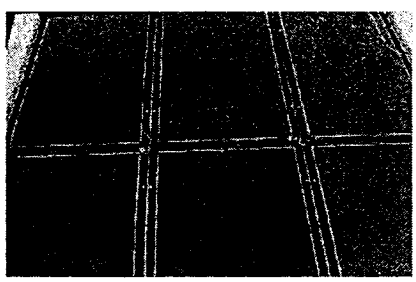

Figure 2.4: Amorphous PV Modules (National Energy Efficiency Committee)

Copper indium diselenide (CIS) is a more recent thin-film PV material. Siemens Solar developed a process for depositing layers of the three elements on a substrate in a vacuum, and Shell Solar later acquired the technology when it bought Siemens Solar. CIS modules currently on the market reach stable efficiencies of more than 11%. National Renewable Energy Laboratory (NREL) scientists have achieved cell efficiencies of 19.2% with the semiconductor. Research now focuses on increasing efficiency, reducing costs, and raising the production yield of CIS panels. Scientists predict that thin-film technology will eventually halve the present production cost per unit kilowatt peak (kWp), which is the peak power that a solar panel can produce at optimum intensity and sun angle (90°). This implies a cost reduction for a complete system of 35% or more [AIP (2006)].

Thin film technologies in general have been shown to perform significantly better (up to 40%) in low-light, non-ideal orientation, and high temperature situations (such as Building Integrated Photovoltaics) [van Cleef (2001)].

2.3.2.3 Building Integrated Photovoltaics (BIPV)

Building Integrated Photovoltaics (BIPV) is the integration of photovoltaics (PV) into the building envelope. The PV modules serve the dual function of building skin—replacing conventional building envelope materials—and power generator. By avoiding the cost of conventional materials, the incremental cost of photovoltaics is reduced and its life-cycle cost is improved. That is, BIPV systems often have lower overall costs than PV systems requiring separate, dedicated, mounting systems [Strong (2006)].

Figure 2.5 shows examples of BIPV. Shown from left to right are a PV skylight entryway, APS factory in Fairfield, CA, and Intercultural Center, Georgetown University, Washington D.C.

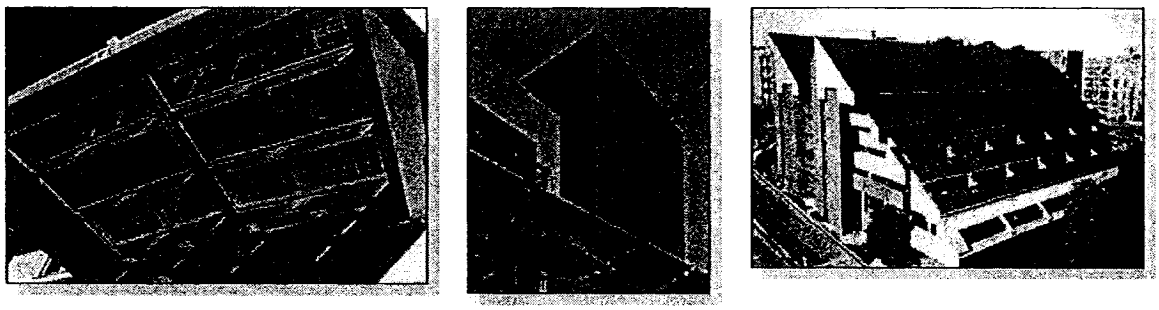

Figure 2.5: Examples of BIPV (Courtesy of DOE/NREL)

2.3.2.4 Grid Tied and Off-Grid Systems

Grid tied systems require no storage equipment (i.e. batteries). The crucial issue relative to the PV Systems discussed below is the technical aspects of tying into the electricity grid. In these applications, grid-tied inverters must be used that meet the requirements of the utilities. They must not emit "noise" which can interfere with the reception of equipment (e.g. televisions), switch off in the case of a grid failure and retain acceptable levels of harmonic distortion (i.e. quality of voltage and current output waveforms). This type of system tends to be an optimum configuration from an economic viewpoint because all the electricity is utilized by the owner during the day and any surplus is exported to the grid. Meanwhile, the cost of storage to meet night-time needs is avoided, because the owner simply draws on the grid in the usual way. Also, with access to the grid, the system does not need to be sized to meet peak loads.

Most off-grid systems use batteries to store power for use during periods of low or no sunlight. These systems can also be referred to as Hybrid when the addition of a generator is added for times when the batteries have run out of power and there is no sun. The extra cost of these systems can usually be justified in remote locations when the cost of bringing the grid is similar to the cost of the system.

2.3.3 Balance of System

2.3.3.1 Charge Controller

PV systems that contain a battery bank for storage of energy, which are usually off-grid systems, require a charge controller to regulate the voltage at which the batteries are charged. A charge controller regulates the voltage and current coming from the solar panels going to the battery. Most panels generate 15.5V to 20V, so if there is no regulation the batteries will be damaged from overcharging. Most batteries need around 14V to 14.5V to get fully charged. Generally, there is no need for a charge controller with the small trickle charge panels, such as the 1W to 5W panels. A rough rule is that if the panel generates 1/60th or less per day of the rated battery capacity, you don't need one. The reason why panels do not generate 12V is that the panels will provide power only under perfect conditions and full sun. This is not something you can count on in most places. The panels need to provide some extra voltage so that when the sun is low in the sky, or you have heavy haze, cloud cover, or high temperatures, you still get some output from the panel. The charge controller regulates this 16V to 20V output of the panel down to what the battery needs at the time [Windsun (2006)]. This voltage will vary from about

10.5V to 14.5V, depending on the state of charge of the battery, the type of battery, and temperature (refer to Chapter 2.3.4)

2.3.3.2 Maximum Power Point Tracking (MPPT)

In order to maximize the output of the solar modules, several technologies exist. Solar cells have a point at which maximum power output occurs; this point will vary depending on the amount of solar radiation and temperature. A Maximum Power Point Tracker (MPPT) will therefore calculate the optimal current in order to generate the maximum power output from the module at all times and under all conditions. MPPT's are most effective under conditions of cloudy or hazy days - when the extra power is needed the most. In cold weather conditions, solar module output increases when sun hours are low and you need the most power.

2.3.3.3 Inverter

An inverter converts DC (direct current) power in to AC (alternating current), which is the typical power supply found in homes and businesses. Inverters have come a long way since their inception, with efficiencies in the range of 95%. Early inverter had efficiencies in the range of 60%, but with the introduction of solid state inverters in the 1980's efficiencies jumped to 90% [Trace (2006)].

2.3.4 Batteries

Batteries, or storage cells, are electrochemical devices. The principle components include one positive and one negative electrode comprised of numerous plates or tubes each made of dissimilar active material and an electrolyte all encased within a sealed or open container. A chemical reaction takes place when a load is connected to the two

electrodes, discharging the battery. The positive electrode absorbs negatively charged electrons from the load, while the negative electrode releases electrons to the positive plate. The electrolyte serves as the means by which the electricity, in the form of ions, moves. The reverse process occurs when the battery is charged.

When not connected to any load or charge current the battery's open voltage represents the potential energy between the electrodes that may be measured to determine the batteries state of charge. When fully charged this voltage will differ depending upon the type of battery - for example, each cell of a lead acid battery will have a VOC of about 2.1VDC, while nickel-cadmium will show 1.25VDC at 25° C. Rechargeable batteries are the most effective storage mechanism available. Notwithstanding this, the electrochemical conversion process of the battery utilizes about 20-25% of energy produced, so storage is only about 75% efficient. The storage capacity of batteries is rated in ampere hours, which is the current that it delivers over a set number of hours at a normal voltage at a temperature of 25°C. Batteries must therefore be protected from the elements. Stationary lead (low or non-antimony) acid and nickel-cadmium are the types of batteries applicable to remote power systems. Within the lead acid category there are further classifications of vented and sealed batteries, also known as valve-regulated, and differing construction. With vented batteries, care must be taken to ensure adequate ventilation is provided. Sealed batteries recombine the oxygen that is normally produced on the positive plate with the hydrogen produced by the negative plate into water, thereby replacing the moisture in the battery. The oxygen is trapped in the cell by pressurized caps that lead to recombination. Sealed batteries are more expensive but are better suited for remote applications since little or no maintenance is required.

Antimony is the alloy added to lead to increase its hardness. The high antimony content also reduces long discharge capability characteristic of remote power installation and increases the gases produced by the cells thus they should be avoided in remote power applications. Nickel-Cadmium (ni-cad) batteries are generally 3 - 4 times the cost of lead acid cells thus their use is typically restricted to specialized situations of extreme hot or cold temperatures [Matrix Energy (2006)].

2.4 Solar Thermal Collectors

At the heart of a solar thermal system is the solar collector. It absorbs solar radiation, converts it into heat, and transfers useful heat to the solar system. There are a number of different design concepts for collectors: besides simple absorbers used for swimming pool heating, more sophisticated systems have also been developed for higher temperatures, such as integral storage collector systems, flat-plate collectors, evacuated flat-plate collectors and evacuated-tube collectors. In the case of the Solar Decathlon Home, the solar thermal collector was used as a source of heat for the heat pump which enables it to be used for a greater amount of time throughout the year in Canada. This review of collector technology was done to evaluate which technology would be most appropriate for Canada's climate.

2.4.1 Flat-plate collectors

The majority of solar collectors that are sold in many countries are of the flat-plate variety. The main components of these are a transparent front cover, collector housing and an absorber. The absorber, inside the flat plate collector housing, converts sunlight to

heat and transfers it to water in the absorber tubes. As the collector can reach stagnation temperatures up to 200°C (i.e. when no water flows through), all the materials used must be able to resist such heat. Therefore, the absorber is usually made of metal materials such as copper, steel or aluminum. The collector housing can be made of plastic, metal or wood, and the glass front cover must be sealed so that heat does not escape, and dirt, insects or humidity do not get into the collector itself. Many collectors also have controlled ventilation, so as to avoid condensation inside the glass front cover. The collector housing is highly insulated at the back and sides, keeping heat losses low. However, there are still some collector heat losses, mainly due to the temperature difference between the absorber and ambient air, and these are subdivided into convection and radiation losses. The former are caused by air movements, while the latter are caused by exchange of heat by radiation between the absorber and the environment. A sheet of glass covers the collector as it faces the sun, and this helps to prevent most of the convection losses. Furthermore, it reduces heat radiation from the absorber into the environment in a similar way as a greenhouse does. However, the glass also reflects a small part of the sunlight, which does not then reach the absorber at all. Figure 2.6 shows the processes occurring at a flat-plate collector.

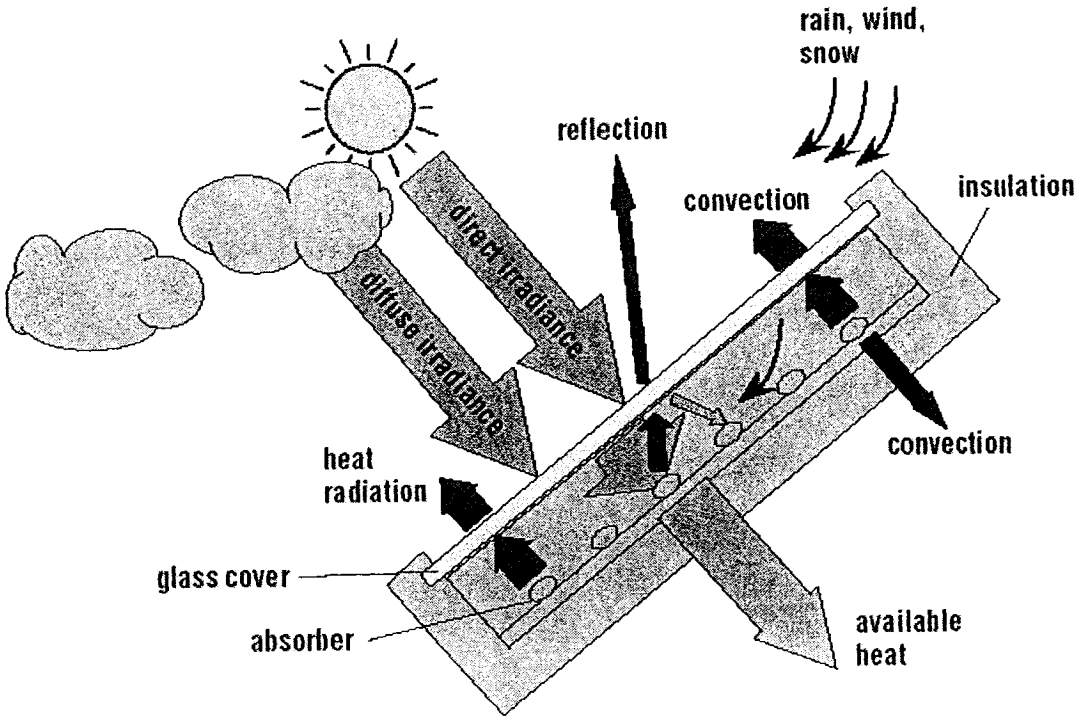

Figure 2.6: Processes at a flat-plate collector (Volker 2004)

2.4.2 Glazed flat-plate collector

In this type of collector a flat absorber efficiently transforms sunlight into heat. To minimize heat escaping, the plate is located between a glazing (glass pane or transparent material) and an insulating panel. The glazing is chosen so that a maximum amount of sunlight will pass though it and reach the absorber.

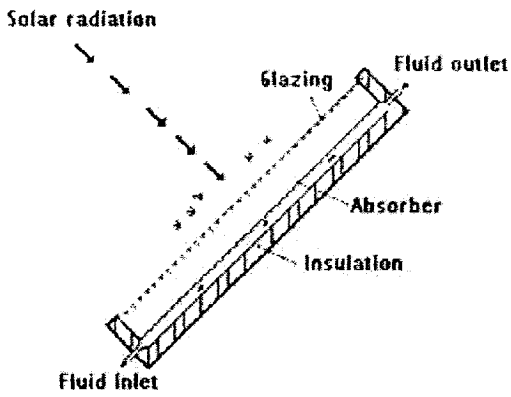

Figure 2.7: Glazed flat-plate collector

2.4.3 Unglazed flat-plate solar collectors

In North America unglazed flat-plate collectors currently account for the most area installed per year of any solar collector. Because they are not insulated, these collectors are best suited for low temperature applications where the demand temperature is below 30°C. Unglazed flat-plate collectors are usually made of black plastic that has been stabilized to withstand ultraviolet light. Since these collectors have no glazing, a larger portion of the sun's energy is absorbed. However, because they are not insulated a large portion of the heat absorbed is lost, particularly when it is windy and not warm outside. They transfer heat so well to air (and from air) that they can actually 'capture' heat during the night when it is hot and windy outside!

2.4.4 Selective absorbers

Black materials absorb sunlight very well, and heat up as a result. Since metallic materials do not naturally have a black surface, they need to be coated for selective absorption. Black, temperature-resistant lacquer can serve this purpose, but there are

much better materials for absorber coating. If a black surface heats up, it emits part of the heat energy again as heat radiation, as can be shown with electrical hotplates: when the hotplate is on, heat radiation can be felt on the skin without touching the hotplate itself. A black lacquered absorber shows the same effect, transferring only part of the absorbed heat to the water that flows through the absorber tubes, while radiating some heat back into the environment. So-called selective coatings absorb the sunlight almost as well as black lacquered surfaces, and re-emit a much smaller amount of heat radiation. While the coating processes needed for these materials are more complicated than those for lacquering, this is compensated for by much higher efficiencies. As a result, many absorbers today have selective coatings, with materials used including black chrome, black nickel or TiNOX.

2.4.5 Evacuated-tube collectors

Convection heat loss due to air movements inside the collector can be significantly reduced by maintaining a vacuum between the front cover and the absorber of a flat plate collector. As the ambient air pressure would then force the front cover against the absorber, small supports must be used between the back of the collector and the cover, to keep the cover itself in shape. It is difficult to maintain the vacuum over a long period of time, since ambient air will always find a way between the glass and the housing to get into the collector, and an evacuated flat-plate collector therefore has to be evacuated again from time to time. These disadvantages can be avoided with evacuated-tube collectors. The high (almost complete) vacuum inside the closed glass tube of the evacuated-tube collector is more stable over a long period of time than in an evacuated

flat-plate collector. Due to their shape, glass tubes can better resist the ambient air pressure, and therefore no supports are needed between the back and front sides. An evacuated-tube collector comprises a closed glass tube, inside which is a metal absorber sheet with a heat pipe in the middle, containing a temperature-sensitive medium such as methanol. The sun heats up and vaporizes this heat pipe fluid, and the vapor then rises to the condenser and heat exchanger at the end of the pipe. There, the steam condenses, and transfers heat to the heat carrier of the solar cycle, water with antifreeze agent. The condensed fluid flows back to the bottom of the heat pipe where the sun begins heating it up again. To work properly, the pipes must have a minimum angle of inclination, in order for the steam to rise and the fluid to flow back. A cross-section of the evacuated-tube collector and the principle of its operation are shown in Figure 2.8. With some evacuated-tube collectors, the heat pipe passes through the end of the glass tube, so that the heat transfer medium of the solar cycle can flow directly through it. A heat exchanger is not needed with this type of collector, and the collector does not have to be mounted at the minimum angle of inclination [Quaschning (2004)].

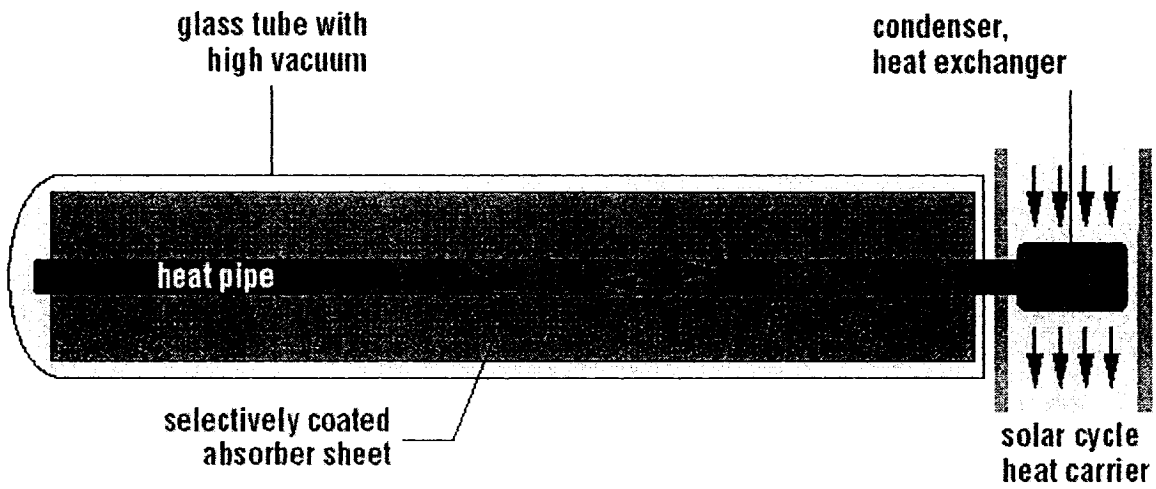

Figure 2.8: Principle of an evacuated tube collector with heat pipe; view from top (Volker 2004)

A significantly higher energy gain can be obtained with evacuated-tube collectors, especially during the cooler months of the year. Thus, a solar system using evacuated tube collectors requires a smaller collector area than one using standard flat-plate collectors.

The specific collector price for evacuated-tube collectors is higher than that for flat-plate systems. A further consideration is that tube collectors cannot be directly integrated into a roof, so they must always be installed on top of it, reducing their architectural possibilities.

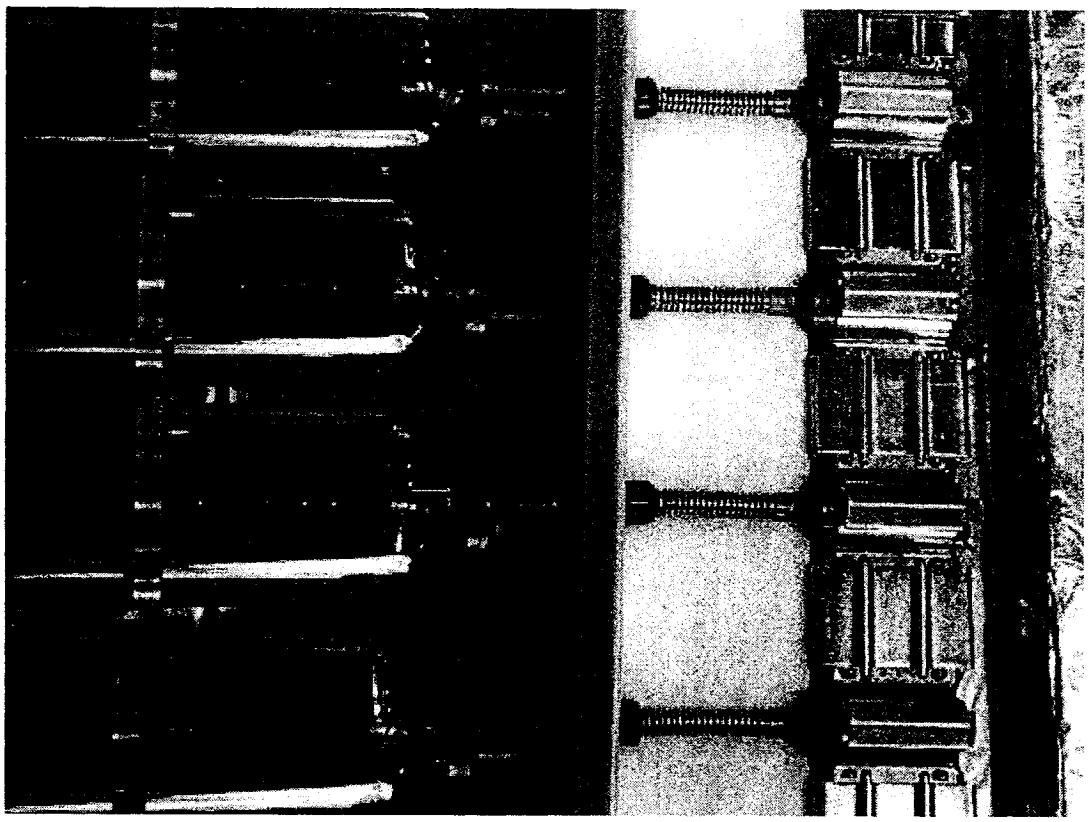

Figure 2.9: Connections of evacuated tubes to the solar cycle (Volker 2004)

2.4.6 Collector Efficiency

In order to compare collectors, testing institutions usually estimate efficiency curves based on measurements of collector performance. These curves are given for different irradiances E and a variety of temperature differences between collector T_C and ambient air T_A. The commonly used empirical equation for the collector efficiency eta_C is:

$$eta_C = eta_0-(a_1\cdot(T_C-T_A)+a_2\cdot(T_C-T_A)^2)/E \qquad (2.5.1)$$

The three parameters eta_0, a_1 and a_2 are estimated by collector test measurements; eta_0 is also referred to as optical efficiency. Figure 2.10 shows typical collector efficiencies for a flat-plate collector. The thermal losses increase as temperature difference between collector and ambient air rises. At low solar irradiances, the efficiency decreases at a faster rate.

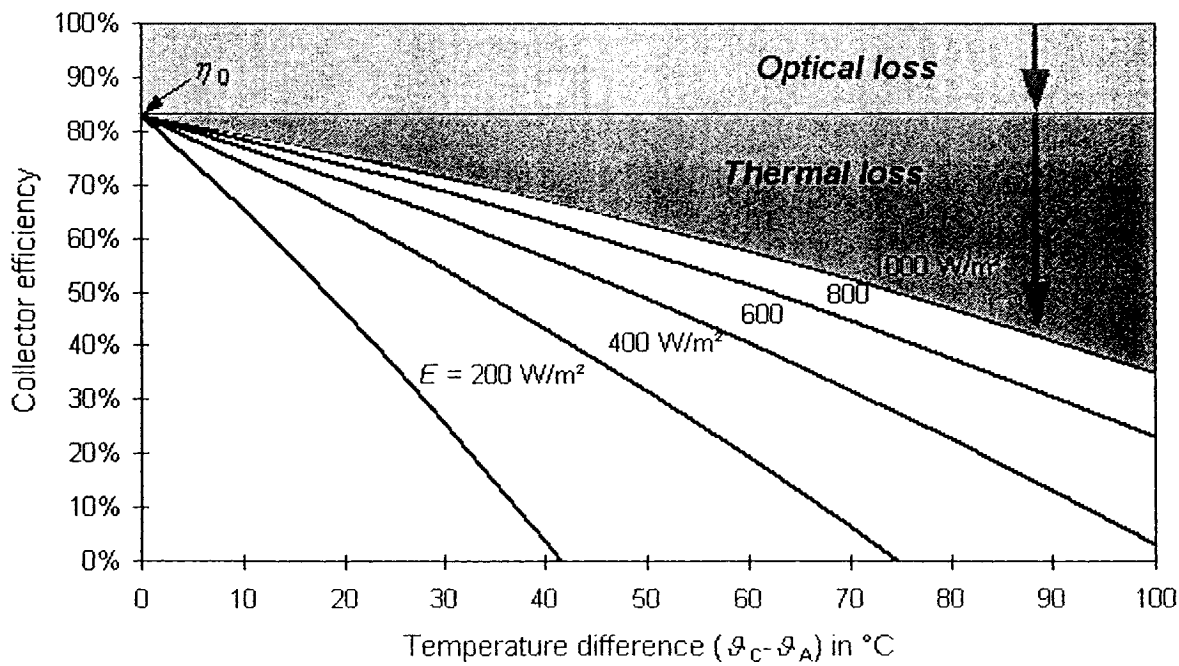

Figure 2.10: Collector efficiencies at different irradiances and temperature differences (Volker 2004)

2.5 Thermal Insulation

In order to accurately simulate the heat transfer characteristics through the walls of a home, a review of insulation technologies was conducted. Current technology usually involves 2" x 6" wood wall construction filled with fiberglass insulation, yielding about R20 ft2h°F/Btu or RSI3.5 m2°K/W. Problems with this method include thermal bridging through the wood studs as well as air infiltration through gaps or imperfections in the insulation. This could be due to settling of the batts, incorrect installation, or simply the fact that it would be impossible to have a perfect seal with such a material. This insulation can also deteriorate over time due to moisture infiltration, causing the thermal insulation value to diminish significantly.

Leading edge technology, leading to higher R values, less air infiltration, and reduced thermal bridging, involves using rigid insulation attached to the wood sheathing on the exterior of the home, followed by an air barrier such as Tyvek. Inside the home is the usual fiberglass insulation and vapor barrier. Polyurethane spray insulation is an alternative method that is available but not yet become commonplace in the market and yields a slightly higher R value yet is comparable in price to rigid insulation. The foam can be sprayed on the exterior of the home, which serves as a vapor barrier, thermal insulation and sound proofing. Inside the home the usual fiberglass insulation can be used without fear of unwanted air infiltration since the foam spray insulation seals the building envelope extremely well.

Vacuum technology can be used to inhibit convection and conduction. The "ultimate" example of vacuum insulation is the Dewar's Flask, commonly known as a "Thermos bottle". In a Dewar's Flask the space between the dual walls of a cylinder is completely (99.999999%) evacuated. With virtually no molecules of gas available heat transfer by conduction and convection are almost eliminated and therefore thermal conductivities are extremely low - 0.000576 W/(m · K) (R 250) or better.

Nevertheless, it is mechanically difficult to support such a pressure differential between the outside and inside of the flask. This certainly limits the structural configurations and the choice of materials for fabrication. Additionally, since even a few molecules of gas will destroy its insulation value, the cylinder walls must be absolutely impermeable to gas and moisture. Also because radiation travels best through a vacuum where there is nothing to hinder its path the wall materials are limited to either specially treated glass or metal, both have a tendency to conduct considerable amounts of heat at areas where the walls are joined together. Commercial products of vacuum insulation panels (VIPs) provide around R30 with a thickness of 16mm. The insulating value in the centre of a VIP is approximately R250, however with edge losses and the allowance of some minor air movement this value drops to about R30.

2.6 Windows

Current technology in the construction industry consists of double glazed, low emissivity (low-e) argon filled window yielding an R value of about R3.3. Leading edge technology includes triple-glazed, double low-e argon filled windows, with fiberglass thermally broken framing. This is rarely seen in residential homes due to increased costs and the opinion from some engineers that the reduction in solar heat gain coefficient (SHGC)

does not justify for the improved thermal insulation. These windows can yield R values of about RSI 1 m2°C/W, have much less problems with condensation, and insulate much better leading to greater thermal comfort in the home (especially those with a large amount of glazing area), greater energy savings, and better soundproofing as well.

A window that is more popular in Germany that has a significantly higher R value uses wood for the frame and the gas used to fill the space between the glazings is low-conductivity xenon rather than argon. Such windows have R values of around R12 at the center of the window, which is more than double the R value when using argon gas.

Another leading edge window technology is windows that include a single glazing, followed by a motorized Venetian shade, followed by two more glazings. This allows heat gains to be rejected much more effectively to the outside compared to the interior placement of shading, yet the shades are still protected from the outdoor elements. This is the product of the future since it represents an energy efficient window and integrates the control of solar radiation, which is key to integrated design of building facades whether residential or commercial.

A third leading-edge window technology is semi-transparent photovoltaic windows. These windows incorporate photovoltaic cells in the window add shading and electricity generation to an existing window. One PV window that takes this one step further is what is known as an artistic PV window. This type of window incorporates art and photovoltaics in an existing window. Since PV windows are regular windows with the addition of PV cells, the thermal properties of the window do not change and are therefore as energy-efficient. The only change would be the daylight transmission

properties due to the placement of PV cells in the window, and this can be a design variable when designing the building.

Future window technology includes electrochromic, thermochromic, and photochromic windows. These technologies involve changing window transmission properties based on an electrical signal, a reaction to thermal conditions, or a reaction to daylight conditions respectively.

To make an electrochromic window, a thin, multi-layer assembly is sandwiched between traditional pieces of glass. The two outside layers of the assembly are transparent electronic conductors. Next is a counter-electrode layer and an electrochromic layer, with an ion conductor layer in-between. When a low voltage is applied across the conductors, moving ions from the counter-electrode to the electrochromic layer cause the assembly to change color. Reversing the voltage moves ions from the electrochromic layer back to the counter-electrode layer, restoring the device to its previous clear state. The glass may be programmed to absorb only part of the light spectrum, such as solar infrared.

Early research indicates that the technology can save substantial amounts of energy in buildings, and electrochromic glazings may eventually replace traditional solar control technology such as tints, reflective films and shading devices.

Several thermochromic technologies are being explored, but gel-based coatings seem to be the most promising. "Cloud Gel", a product now on the market, is a thin plastic film that can be incorporated into almost any window assembly. The response temperatures of "Cloud Gel" can be adjusted depending on need and location.

In addition to automatically changing from clear to diffuse in response to heat, the glazings also turn white and reflective, reducing the transmission of solar heat. That can

reduce air conditioning costs significantly when it's hot outside. Because you can no longer see through the window once it loses its transparency, this glazing is probably best suited for skylights rather than view windows.

While this type of technology may seem like a good idea, it has its drawbacks for saving energy. Photochromic windows work well to reduce glare from the sun, but they don't control heat gains. That's because the amount of light that strikes a window doesn't necessarily correspond to the amount of solar heat it absorbs. Because the sun is lower in the sky during the winter months, for example, its rays may strike a window more intensely in the cold season than in the summer, when the sun is higher in the sky. In this case, a photochromic window would darken more in the winter than in the summer, although winter is the time when solar heat would be beneficial.

Another problem is that, while this technology works fine on small, eyeglass-sized pieces of glass, it has yet do be done successfully on a large-scale, commercial level for window-sized pieces.

Despite some problems, "smart windows" hold the promise of reducing energy demand and cutting air conditioning and heating loads in the future. They offer the next major step in windows that are increasingly sophisticated and energy efficient [Pasini (2006)].

2.7 Electric Lighting and Daylighting Controls

2.7.1 Dimming

For this thesis, only fluorescent dimming luminaries were considered, due to their superior energy performance. Modern ballast designs use solid state electronic components and digital controls to more precisely regulate both the current and voltage

flowing through the electrical circuit. Digital dimming works by sending a control signal to the digital ballast, which then interprets that command and produces the appropriate control voltage which is used to precisely dim the fluorescent light, thus significantly improving its performance over analog signals. For this reason linearity and accurate and repeatable dimming proportionality is excellent. The DALI protocol, which stands for Digital Addressable Lighting Interface, uses a 16 bit packet format which transmits 8 bits of address information and 8 bits of control information. DALI has many useful features including controlling the dimming level between 1% and 100%, querying the status of the lamps and ballast, and since each ballast is assigned a unique address the scene selection and programming can be done for any number of single or multiple luminaries, irrespective of location. DALI has a limit of 64 devices per zone, and if more devices are required more zones are added [Unger (2001)].

2.7.2 Photosensor Control Algorithms

The photosensor control algorithm is the component of the lighting control system that is unique among manufacturers. It is this algorithm which takes as an input the electrical signal from the photosensing device, and then determines whether to maintain the current light level, raise it, or lower it. Also, in more advanced systems it would be the control algorithm that would determine the appropriate position of the blinds and set the parameters necessary to adjust ambient heating or cooling to be delivered by the HVAC. There are three main types of control algorithms: open-loop, closed-loop, and integral reset, which determine the operation of the dimming system.

Sensors for open-loop systems are often mounted on the exterior facade to detect only daylight and then dim indoor lighting in proportion to the daylight level".

Park and Athienitis (2003) also use an open loop control system for lighting and motorized Venetian blinds but with a sensor usually located on the inner surface of the exterior facade and pointed away from the window to avoid strong directional and specular effects.

Closed-loop proportional controllers have the photocell so that it can detect both daylight and electric light. The controller adjusts the electric light output so that the dimming level is a linear function of the difference between the photosensor signal and the desired light level. Closed-loop systems use negative feedback to respond to changing conditions. Negative feedback is a method of error-correcting whereby an increase in an input signal level causes a decrease in the output signal, and vice-versa. Therefore an increase in daylight levels will result in a decrease in electric light [Rubenstein et al (1989)].

A closed-loop algorithm was chosen for use in the Solar Home since it represents the most accurate method of controlling interior lighting conditions based on daylight and electric light. Currently, the industry does not have appropriate control algorithms that will control blinds and lighting to optimize both whole building energy performance and indoor environment.

2.8 Software for solar building design and motivation for the approach followed

Software that can be used for detailed building simulation such as TRNSYS (Welfonder et al. 2003) are not convenient for routine building design that is aimed at optimization of building envelope options. Consideration of building-integrated solar technologies such as photovoltaics that constitute the roof requires their simultaneous consideration as a

thermal zone element and an electricity generating device whose efficiency depends on its temperature. Newer software such as Energy 10 (Balcomb 1997) are a good step in the direction of development of a solar design tool. However, they can not model all the technologies considered in this thesis, such as motorized blinds controlled based on solar radiation and room temperature.

It was therefore decided to utilize a flexible modeling environment – Mathcad, using as a basis the electronic book by Athienitis (1999). Mathcad is an open mathematical programming environment suitable for developing complex mathematical models and solving them numerically. The electronic book facilitated the development of the program developed in this thesis by providing models for components such as solar radiation transmission through windows.

CHAPTER 3

SIMULATION MODEL AND RESULTS

3.1 Introduction

This chapter describes the models that were designed to simulate the custom features than can be found in a net-zero energy house, such as a PV-thermal system and thermal storage. Figure 3.1 illustrates a conceptual diagram of the net-zero energy home that was modeled in this chapter.

In particular, it shows air passing under a solar heated photovoltaic roof, obtaining heat from the panels, which also generate more electricity because they are cooled. The heat is stored in a hollow core floor with or without phase-change thermal storage and with a heat exchanger (air-to water) that may be connected to a hot water tank or a heat pump.

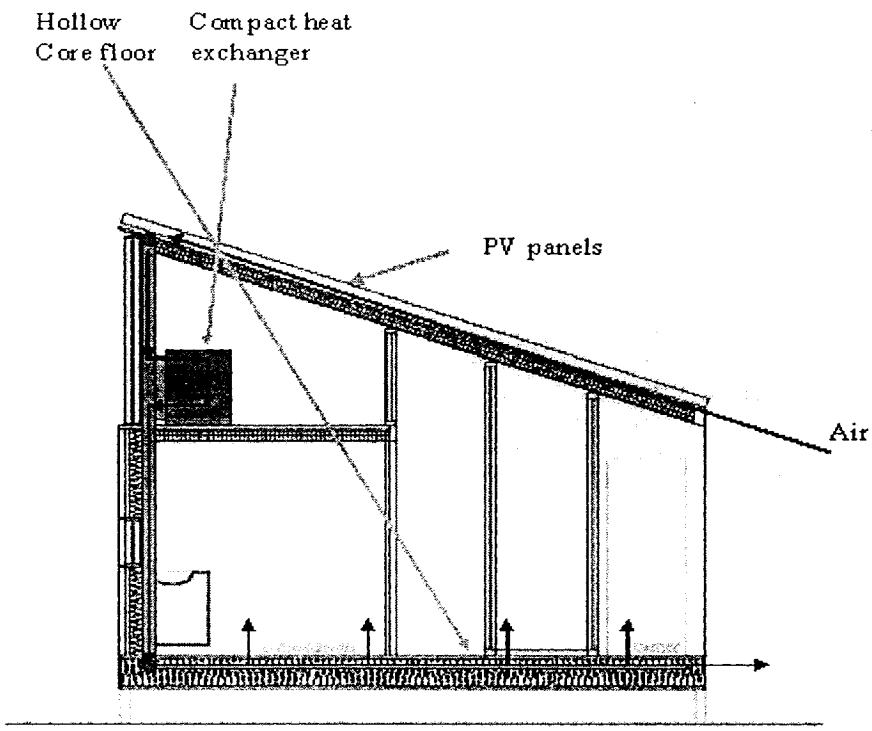

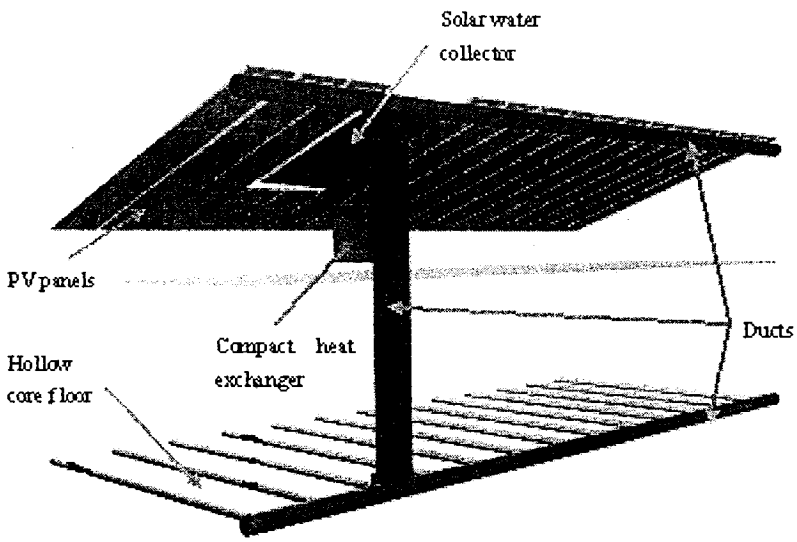

Figure 3.1: Conceptual Diagram of Net-Zero Energy Solar Home

A more detailed look at the individual systems, their mathematical representations, and their interaction to form the thermal network of the home are described in this chapter as well. Such systems include the windows, thermal insulation, thermal storage, and PV-thermal system. Heat transfer between surfaces and from heat sources (such as solar radiation) are modeled, as well as the effects of air infiltration on temperature variation within the space at any desired time step. Most modeling is done through calculation of equivalent resistance or conductance and capacitance (i.e. thermal storage) and solving networks as an electrical network (RC circuit). Heat flow is analogous to current, temperature is analogous to voltage, thermal storage is analogous to capacitance, and thermal resistance is analogous to a resistor or a capacitor. The only difference is that heat flow has units of power, current does not. Each section of the house will be described using this method in detail in the sections that follow. The program described in the following sections integrates electrical, thermal, and lighting to give a more complete picture. Modeling of heat gains, shading (interior, exterior, in cavity), lights aspects of solar radiation, and the net efficiency of the PV-thermal system are all achieved.

The exterior temperature profile for Washington D.C. was chosen since it was the location for the 2005 Solar Decathlon Competition and the Canadian entry in this competition represented a case study for the results of the research in this thesis (Refer to Chapter 4). The temperature profile was based on the maximum daily average temperature for the month September [WeatherNetwork (2006)]. This very hot, clear design day was chosen to vary between 15°C at night and 25°C during the day. The ground temperature is assumed to be constant and approximately equal to outside

temperature. However, the ground temperature has almost no impact on calculations since the house is assumed to be sitting on a foundation of concrete posts 1' above ground level. Manufacturer's specifications are assumed to be correct for windows, insulation, and other building materials. The conductivity, heat capacity, and density of concrete and water are approximated.

3.2 Model Descriptions

3.2.1 House Integration Model

This module integrates all of the models along with the floor model in order to get a complete picture of the behavior of the house as a system. Figure 3.2 shows the thermal network for the room air node.

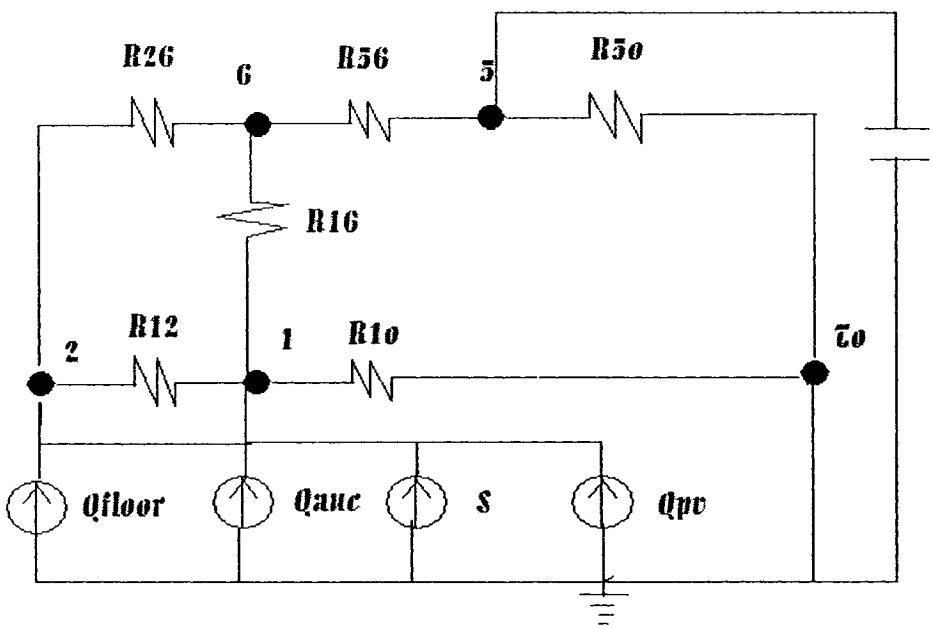

Figure 3.2: Thermal Network

Where:

1: Room air

2: Floor surface

5: Middle layer of unheated surfaces

6: Inner layer of unheated surfaces

Qfloor: Equivalent heat source representing heat flow from floor to room air

Qaux: Heat flow from auxiliary source (i.e. heat pump)

S: Heat flow from solar radiation

Qpv: Heat flow from air from PV cavity

Equation 3.2.1 (Athienitis, 1999) is an example of the resistance between the room air and the outside. It is made up of three thermal resistances in parallel: windows, doors, and infiltration.

$$R_{1o} := \frac{1}{U_{inf} + \sum_{ii}\left(\frac{Aw_{ii}}{R_W} + \frac{Ad_{ii}}{Rd}\right)} \tag{3.2.1}$$

The following are finite difference equations that describe the nodes in the brick, air, and at the floor surface. These equations are for one control volume, the equations can then be slightly modified to describe other control volumes and then all of the equations are solved simultaneously with an appropriate time step. The time step selected was 5 minutes since the goal of the analysis is to control the air temperature in a home, which will not change rapidly and will ultimately be controlled by some sort of a heat pump which cannot be turned on and off frequently.

Equation 3.2.2 describes all of the heat flow into the brick node. It consists of a network of thermal resistances between the brick and:

1. The previous brick control volume ($T1c_p$)
2. The surrounding air ($T2a_p$)
3. The surface of the floor ($Ts2_p$)

$$\frac{T1_{a_p} \cdot U_{1b\_2b} + T2_{c_p} \cdot U_{2a\_2c} + Ts2_p \cdot U_{2a\_r}}{U_{1b\_2b} + U_{2a\_2c} + U_{2a\_r}} \tag{3.2.2}$$

Equation 3.2.3 describes all of the heat flow into the air node. It consists of a network of thermal resistances between the air and:

1. The adjacent brick
2. The air in the previous control volume

$$\frac{T2_{a_p} \cdot U_{1a\_1c} + T1_{c_p} \cdot U_{a(p)}}{U_{1a\_1c} + U_{a(p)}} \tag{3.2.3}$$

Equation 3.2.4 describes all of the heat flow into the floor surface temperature node. It consists of a network of thermal resistances between the air and:

1. The unheated surfaces of the house (walls, ceiling)
2. The average ambient room air
3. The floor thermal storage system
4. The fraction of solar radiation incident (70% of solar radiation through windows hits floor, 75% of which is incident on false floor, and then the area of one control volume as a fraction of total false floor surface area hits the actual control volume)

$$\frac{\frac{T_{6,p}}{R_{26}} + \frac{T_{1,p}}{R_{12}} + \frac{T1a_p}{R_{1a\_r}} + 0.7 \cdot .75 \cdot St_p \cdot F}{\left(\frac{1}{R_{26}} + \frac{1}{R_{12}} + \frac{1}{R_{1a\_r}}\right)} \tag{3.2.4}$$

The heat flow from the floor to the room air is calculated using equation 3.2.5. It is the volumetric air flow of the air surrounding the bricks multiplied by the difference in air temperature between that bricks (T_4) and the room air (T_1).

$$q_{floor} := \left[c_a \cdot \rho_a \cdot air\_width \cdot air\_height \cdot 1200 \cdot V2(p) \cdot V(p) \cdot \left(T4c_p - T_{1,p}\right)\right] \tag{3.2.5}$$

3.2.2 Floor Model

The floor thermal storage system consists of bricks, which have been soaked in PCM (0.48 butyl stearate, 0.50 propyl palmitate, 0.02 fat acid), spaced out in a staggered fashion above the main floor of the house, forming a sort of "false floor", in which air will pass between the bricks. A 2D control volume thermal network model was developed to calculate the outlet air temperature of the air as it flows through the floor. Note that there are three cases of air flow through the floor:

1. Hot air from roof PV-thermal system flows through the floor and then leaves the house (or just a small portion is circulated as fresh air)
2. Room air is re-circulated through the floor by an air-handling unit to extract the store heat from the previous step, or "coolness" stored from the next option.
3. Cool outdoor night air is passed though the floor at night during summer for free cooling.

Thus, this false floor will act as a large duct, carrying the air from one end of the house to another. A typical subnetwork of a floor section is shown in Fig. 3.3. Because there is

insulation below and above the bricks, the floor acts like an isolated thermal storage system. It is represented by the equivalent heat source Qfloor in Fig. 3.2.

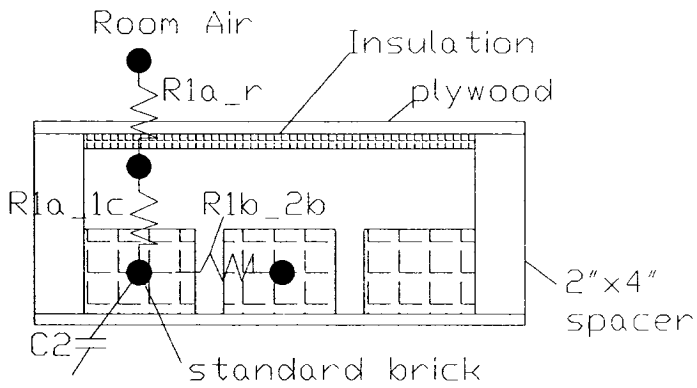

Figure 3.3: Floor thermal storage system (typical subnetwork – repeated in 2D)

The butyl styrate is used to increase the thermal capacity of the bricks, leading to approximately 36 kWh of thermal energy storage assuming a 10°C temperature difference between the brick and the ambient air (see equation 3.2.6).

$$C2 := \rho_b \cdot c_b \cdot brick\_width \cdot brick\_height \cdot brick\_length \qquad C2 = 1.501 \times 10^{-3} \frac{kW \cdot hr}{degC} \qquad (3.2.6)$$

$$C2 := C2 \cdot 1200 \cdot 2 \cdot 10 degC \qquad C2 = 36.026 kW \cdot hr$$

The thermal capacity of the bricks for one control volume is calculated using equation 3.2.6. The total capacitance is shown by taking the capacitance of a single ordinary brick, multiplying by the quantity of bricks (1200), multiplying by the additional heat capacity by soaking the brick in PCM (x2), and finally assuming a temperature difference between the bricks and surrounding air.

The conductance of the heat flow path between adjacent bricks is shown in equation 3.2.7. It takes into account the dimensions of one control volume of brick as well as the thermal conductivity.

$$U_{1b\_2b} := \frac{k_b \cdot brick\_width \cdot brick\_height}{brick\_length} \tag{3.2.7}$$

The resistance between the brick and the air surrounding the brick is calculated in equation 3.2.8. The resistance is calculated by adding in series the thermal resistance of the brick itself with the thermal resistance of the film coefficient at the boundary between the brick and the air.

$$R_{1a\_1c} := \left[\frac{brick\_height}{(2 \cdot k_b \cdot brick\_length \cdot brick\_width)} + \frac{1}{(h_o \cdot brick\_length \cdot brick\_width)} \right] \tag{3.2.8}$$

The resistance between the air surrounding the bricks and the room air, which is basically separated by a layer of plywood and hardwood flooring as well as two film coefficients on either side of the wood floor, is described in equation 3.2.9.

$$R_{1a\_r} := \frac{1}{(h_i \cdot brick\_length \cdot brick\_width)} + \frac{flr\_thick}{k_{wood} \cdot brick\_length \cdot brick\_width} + \frac{1}{(h_o \cdot brick\_length \cdot brick\_width)} \tag{3.2.9}$$

3.2.3 PV-Thermal System

A model was developed to calculate the rise in temperature of the air drawn through the cavity under PV panels. One such system as implemented in the Solar Decathlon Home is described in detail in Chapter 4. A conceptual diagram of the PV-thermal cavity including the locations of the temperature nodes used for calculating the heat transfer processes is shown below.

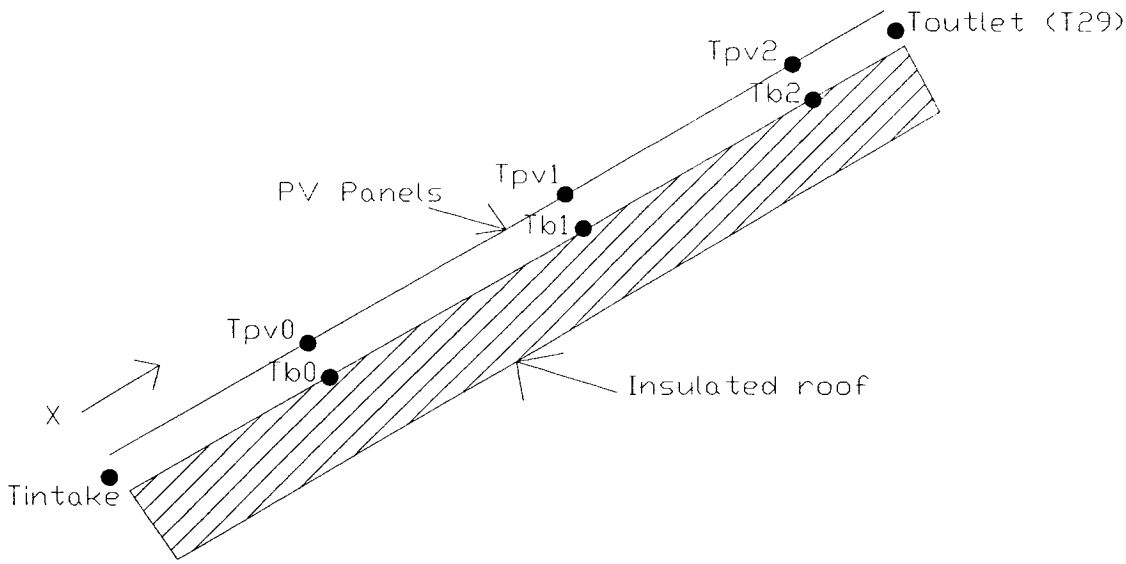

Figure 3.4: Conceptual diagram of PV-thermal air cavity

The method of simulating the rise in air temperature in the PV cavity was simulated using a one-dimensional model to calculate the heat transfer from the PV panel to the air. The rise in air temperature was calculated using nodal analysis by breaking up the air cavity into several nodes and iterating explicitly until convergence is attained. Equation 3.2.10 (Athienitis, 1999) is the general equation used to calculate the air temperature at a node. It is basically the average of the PV panel temperature and the room temperature plus the rise in the intake air temperature described by an exponential equation that is dependent on the distance between the node and the inlet.

$$T0_{d,0} := \frac{T_{pv_0} + T_{b_0}}{2} + \left[T_{intake_d} - \frac{\left(T_{b_0} + T_{pv_0}\right)}{2} \right] \cdot e^{\frac{-X_1 \cdot 2}{a}} \qquad (3.2.10)$$

Figure 3.5 illustrates the temperature profile of the fresh air in the PV cavity. The roof is split, using wood strapping, into 18 cavities, where each cavity has three panels. The assumed values are:

- Velocity of air in the cavity, V = 1.0 m/s
- Outside temperature, $T_0 = 20^oC$
- Instantaneous solar radiation incident on PV, G = 800 W/m^2

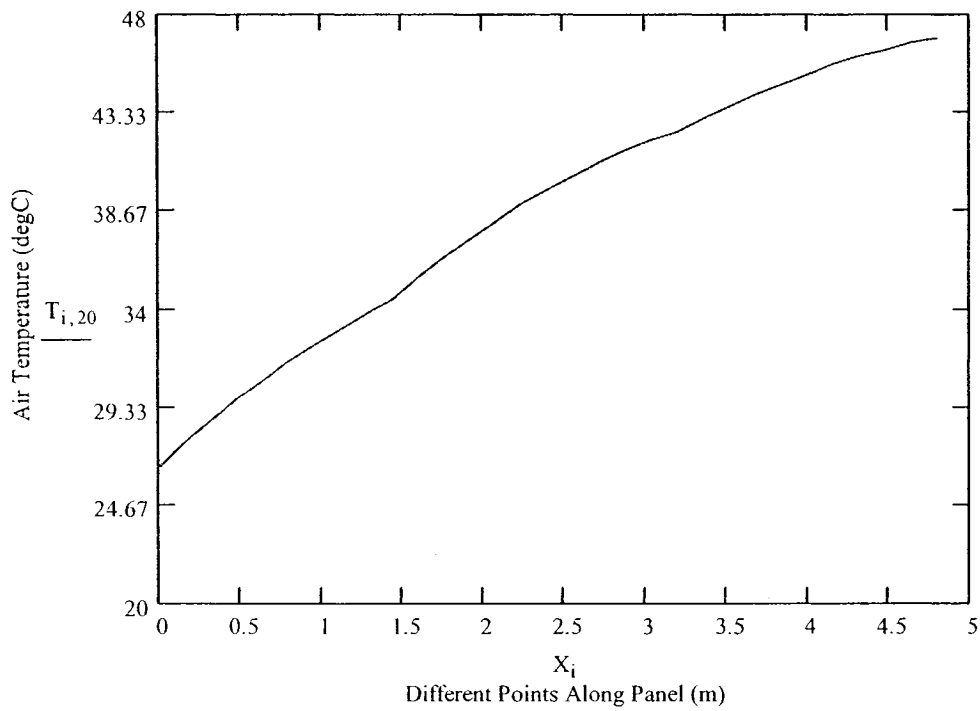

Figure 3.5: Temperature variation of air in PV cavity vs. distance in cavity

The thermal energy gained by the air flowing through the cavity which can then be used as a heat source for heating water or the space is calculated as follows:

$$q_{air} := Ml \cdot \rho_{air} \cdot c_{air} \cdot (Toutlet - Tintake) \qquad (3.2.11)$$

For example, at noon on a summer day with an outside ambient temperature of 25°C, the thermal energy gained in the PV cavity, calculated using equation 3.2.11, is 768 W.

A model was also developed to calculate the optimal tilt angle of the PV array for any geographical location and any time of year in terms of quantity of daily incident solar radiation. The model was used to determine the optimal tilt angle for the roof of the Solar Decathlon Home (see Chapter 4) during the time of the competition, which was the first week of October in Washington D.C. Figure 3.6 shows the result of the simulation.

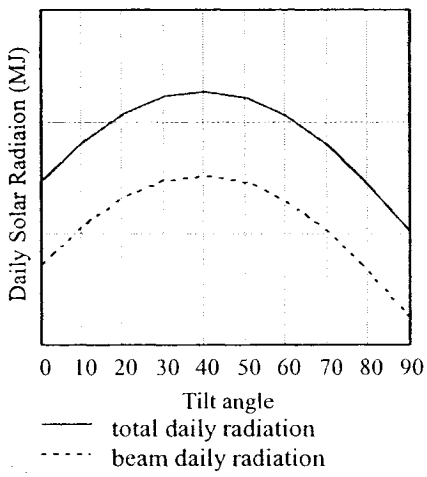

Figure 3.6: Graph of Daily Incident Solar Radiation versus Tilt Angle

The model reveals that a tilt angle of approximately 40° would be optimal, but basically any variation within 10° has minimal impact. The tilt angle of the home was therefore chosen to be 30° in order to strike a balance between architectural decisions and energy needs.

In order to validate the model, the average electrical and thermal energy output of the PV array, as shows in Table 3.1, were compared to results from Tripanagnostopoulos (2004). Tripanagnostopoulos found that an average ratio of 3:1 was found for thermal energy generation versus electricity generation from an unglazed PV-thermal system. Result

observed in Table 1 yield similar results throughout the year, indicating the model to be in agreement with past research.

Table 3.1: Electrical and Thermal Energy Captured from 50m^2 PV Array

Month	Jan	Feb	Mar	Apr	May	Jun	Jul	Aug	Sep	Oct	Nov	Dec
Daily Avg. Solar Radiation (kWh)	131	179	224	232	255	274	283	248	218	153	93	87
Electricity Generated (kWh)	9.2	12.5	15.7	16.2	17.9	19.2	19.8	17.4	15.3	10.7	6.5	6.1
Thermal Energy (kWh)	30.2	42	58.1	73.2	82.6	83.7	80.3	71.1	56.6	41.1	29.5	24.7
Total Energy (kWh)	39.4	54.5	73.9	89.4	100.5	102.9	100.1	88.5	71.9	51.8	36.0	30.8
System Efficiency (%)	30.0	30.4	33.0	38.5	39.4	37.6	35.4	35.7	33.0	33.9	38.7	35.4

3.2.4 Shading Model

A model was created that calculates the amount of solar radiation that is absorbed by the shading device and emitted to the room air through radiation. R_1 represents the thermal resistance from the shading the device to the outside, R_2 represents the thermal resistance from the shading device to the inside room air, T_b is the temperature of the blind throughout the day depending on the amount of solar radiation (I) in W/m^2, and Q is the amount of heat in terms of W.

$$R_1 := \frac{1}{h_o} + R_w + \frac{1}{h_{gap}} \tag{3.2.12}$$

$$R_2 := \frac{1}{h_i} \tag{3.2.13}$$

$$T_{b_{it}} := \frac{R_1 \cdot R_2 \cdot \tau_w \cdot \alpha_b \cdot I_{12,1} + To_{it} \cdot R_2 + T_i \cdot R_1}{R_1 + R_2} \tag{3.2.14}$$

$$Q_{blind\_room} := \frac{T_b - T_i}{\frac{1}{h_i}} \tag{3.2.15}$$

To simulate a shading control algorithm, a model was created which simply allows only a percentage of the solar radiation to enter the window between certain times of day as specified by the schedule. Figure 3.7 illustrates the following control scheme: 90% shading between 9am and 5pm and 20% shading the remainder of the day. It assumes 80% transmittance of the blinds when they are fully open (i.e. Venetian blinds), with a 70% reduction in their closed position.

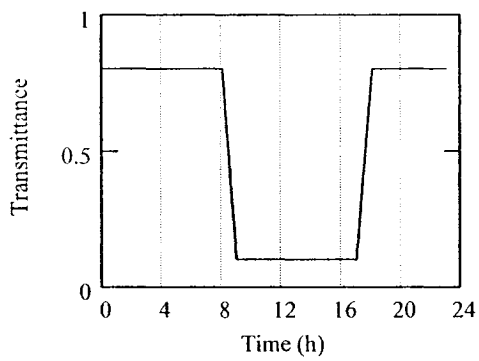

Figure 3.7: Graph of typical daily shading algorithm (summer)

3.2.5 Window Model

The resistance of a window is calculated using the concept of heat transfer coefficients, meaning the actual resistance of the glazings themselves are ignored in terms of

insulating value, only the trapped air (or gas) between the glazings and the low-emissivity coatings are considered (see equation 3.2.16 from Athienitis, 1999). The variables hi, hc, hr, and ho represent the interior surface, convective, radiative, and exterior heat transfer coefficients respectively.

$$R_w := \frac{1}{hi} + \frac{2}{hc + hr_{low\_e}} + \frac{1}{h_o} \tag{3.2.16}$$

In order to calculate the heat gains through the windows the angle of refraction, component reflectivity and transmittance of a single glazing as shown in equations 3.2.17, 3.2.18, and 3.2.19 from Athienitis, 1999 respectively must be determined. The variable *a* in equation 3.2.20 is simply a placeholder.

$$\theta'_{it,iw} := \operatorname{asin}\left(\frac{\sin(\theta_{it,iw})}{n_g}\right) \tag{3.2.17}$$

$$r_{it,iw} := \frac{1}{2}\cdot\left[\left(\frac{\sin(\theta_{it,iw} - \theta'_{it,iw})}{\sin(\theta_{it,iw} + \theta'_{it,iw})}\right)^2 + \left(\frac{\tan(\theta_{it,iw} - \theta'_{it,iw})}{\tan(\theta_{it,iw} + \theta'_{it,iw})}\right)^2\right] \tag{3.2.18}$$

$$a_{it,iw} := \exp\left[-\frac{kL}{\sqrt{1 - \left(\frac{\sin(\theta_{it,iw})}{n_g}\right)^2}}\right] \tag{3.2.19}$$

$$\tau_{it,iw} := \frac{\left(1 - r_{it,iw}\right)^2 \cdot a_{it,iw}}{1 - \left(r_{it,iw}\right)^2 \cdot \left(a_{it,iw}\right)^2} \tag{3.2.20}$$

The properties of a double-glazed window with two low-e coatings including the reflectance of the outer glazing, the transmittance, and the absorptance of the inner and

outer glazings are calculated using equations using equations 3.2.21 through 3.2.24 (Athienitis, 1999) respectively.

$$\rho o_{it,iw} := r_{it,iw} + \frac{r_{it,iw}\cdot\left(1 - r_{it,iw}\right)^2\cdot\left(a_{it,iw}\right)^2}{1 - \left(r_{it,iw}\right)^2\cdot\left(a_{it,iw}\right)^2} \tag{3.2.21}$$

$$\tau e_{it,iw} := \frac{\left(\tau_{it,iw}\right)^2}{1 - \left(\rho o_{it,iw}\right)^2} \tag{3.2.22}$$

$$\alpha i_{it,iw} := \alpha s_{it,iw}\cdot\frac{\tau_{it,iw}}{1 - \left(\rho o_{it,iw}\right)^2} \tag{3.2.23}$$

$$\alpha o_{it,iw} := \alpha s_{it,iw} + \alpha s_{it,iw}\cdot\frac{\tau_{it,iw}\cdot\rho o_{it,iw}}{1 - \left(\rho o_{it,iw}\right)^2} \tag{3.2.24}$$

The incident solar radiation that enters the windows and is absorbed by the inner (G_{ai}) and outer glazings (G_{ao}) is calculated using the direct component (G_b) as well as the diffuse component (G_d) that includes reflected from the ground (I_{dg}) and the sky (I_{ds}). Equations 3.3.25 through 3.2.28 are from Athienitis, 1999.

$$Gd_{it,iw} := \tau ed_{iw}\cdot\left(Ids_{it} + Idg_{it}\right) \tag{3.2.25}$$

$$Gb_{it,iw} := Ib_{it,iw}\cdot\tau e_{it,iw} \tag{3.2.26}$$

$$Gao_{it,iw} := \alpha o_{it,iw}\cdot Ib_{it,iw} + \alpha o_{it,iw}\cdot\left(Ids_{it} + Idg_{it}\right) \tag{3.2.27}$$

$$Gai_{it,iw} := \alpha i_{it,iw}\cdot Ib_{it,iw} + \alpha i_{it,iw}\cdot\left(Ids_{it} + Idg_{it}\right) \tag{3.2.28}$$

The solar radiation absorbed in the glazings and released to the room air for use in the room air heat balance equations is shown in equation 3.2.29 (Athienitis, 1999).

$$Qgg_{it} := \sum_{iw}\left[\frac{1}{R_w \cdot h_o}\cdot\left(\alpha_{o_{it,iw}}\cdot I_{it,iw}\right) + \frac{1}{R_w}\cdot\left(R_w - \frac{1}{h_{iw}}\right)\cdot\left(\alpha_{i_{it,iw}}\cdot I_{it,iw}\right)\right]\cdot Aw_{iw} \qquad (3.2.29)$$

3.2.6 Solar Radiation Incident on Interior Surfaces

The solar radiation incident on the interior walls and floor of the house are calculated in equation 3.2.20 (Athienitis, 1999) in order to take into account the thermal storage properties of ordinary interior construction materials such as gypsum, hardwood flooring, ceramic, etc. The shading factor *shadefac* is included because it will determine the amount of transmitted solar radiation through the window that will reach the walls and floor. The 0.3 factor assumes that 30% of all the transmitted solar radiation reaches the walls, and the remaining 70% will reach the floor. This is a safe assumption as long as there are no devices such as light shelves or large flat object directly beside the window inside the house.

$$S_{it,iw} := 0.3 \cdot Gt_{it} \cdot \frac{A_{iw}}{\sum_{iw} A_{iw}} \cdot shadefac_{it} \qquad (3.2.30)$$

3.2.7 Temperature Profile

The outdoor temperature profile is simulated using a sinusoidal waveform with a period of 24 hours with the peak temperature at 2pm and the minimum at 2am. Refer to Figure 3.8 for the summer design day temperature profile with a mean temperature of 20°C and a deviation of 5°C. Equation 3.2.32 (Athienitis, 1999) describes the temperature profile.

$$w1 := \frac{2 \cdot \pi}{24 \cdot hr} \qquad Tomean := 17 \cdot degC \qquad DT := 10 \cdot degC \tag{3.2.31}$$

$$To_{it} := \left(Tomean + \frac{DT}{2} \cdot \cos\left(w1 \cdot t_{it} - 1.25\pi \right) \right) \tag{3.2.32}$$

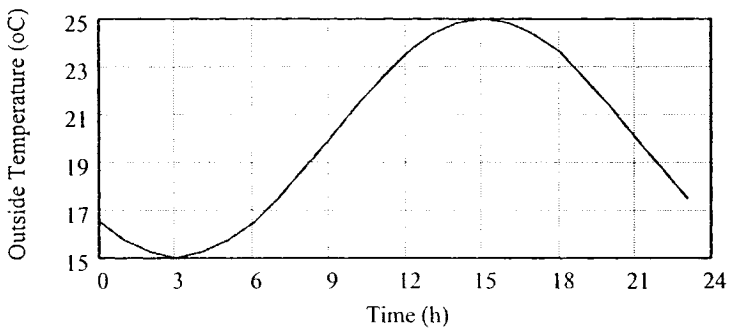

Figure 3.8: Temperature curve over 1-day

3.2.8 Solar Radiation

Solar radiation is calculated using several steps according to Hottel's Clear Sky Model. The following angles are necessary in order to determine the solar radiation incident on any surface at any time of day.

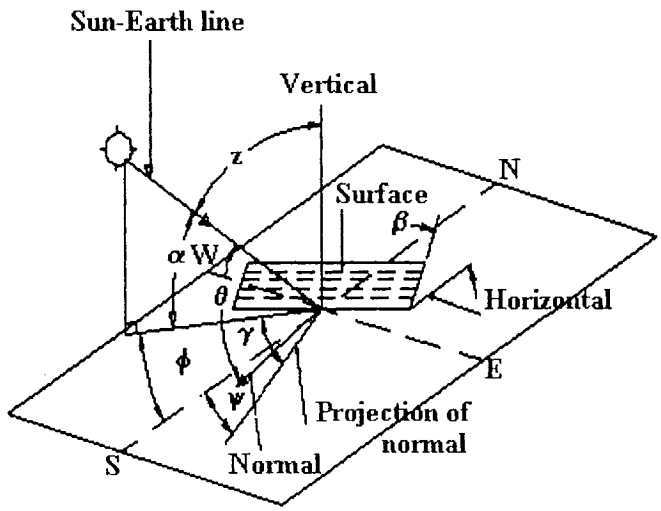

Figure 3.9: Solar Radiation Geometry for an Inclined Plane (Athienitis, 1998)

- δ: Declination angle, equal to the angular position of the sun at solar noon with respect to the equatorial plane
- α: Solar altitude, equal to the angle between the sun's rays and the vertical
- z: Zenith angle, equal to the angle between the sun's rays and the vertical
- φ: Solar azimuth, equal to the angle between the horizontal projection of the sun's rays from due south (positive in the afternoon)
- γ: Surface solar azimuth, equal to the angle between the projections of the sun's rays and of the normal to the surface on the horizontal plane
- ψ: Surface azimuth, equal to the angle between the project of the normal to the surface on a horizontal plane and due south (east is negative)
- β: Tilt angle between the surface and the horizontal ($0 - 180^{o}$)
- θ: Angle of incidence between the solar rays and a line normal to the surface

$$\delta := 23.45\,\text{deg}\cdot\sin\left(360\cdot\frac{284 + n_d}{365}\cdot\text{deg}\right) \tag{3.2.33}$$

$$\alpha = \operatorname{asin}\left(\cos(L)\cdot\cos(\delta)\cdot\cos(h) + \sin(L)\cdot\sin(\delta)\right) \tag{3.2.34}$$

$$z = 90\cdot\text{deg} - \alpha\cdot\text{deg} \tag{3.2.35}$$

$$\phi = \operatorname{acos}\left(\frac{\sin(\alpha)\cdot\sin(L) - \sin(\delta)}{\cos(\alpha)\cdot\cos(L)}\right)\cdot\frac{h}{|h|} \tag{3.2.36}$$

$$\gamma = \phi - \psi \tag{3.2.37}$$

$$\theta = \operatorname{acos}\left(\cos(\alpha)\cdot\cos(|\gamma|)\cdot\sin(\beta) + \sin(\alpha)\cdot\cos(\beta)\right) \tag{3.2.38}$$

Using the angles described above (Athienitis, 1999), it is then possible to find the solar radiation incident on any surface by adding the sum of the direct beam, diffuse sky

(reflected from the atmosphere, clouds, etc.), and diffuse ground solar radiation (reflected off surfaces in the plane of the earth). First the extraterrestrial solar radiation normal to the earth's surface, which is a relative to the day of the year, is calculated using equation 3.2.39 (Athienitis, 1999).

$$I_{on} := 1353 \frac{watt}{m^2} \cdot \left(1 + 0.033 \cos\left(360 \frac{n_d}{365} \cdot deg\right)\right) \tag{3.2.39}$$

Direct beam solar radiation is then calculated using equation 3.2.40 (Athienitis, 1999), which is a factor of the angle of incidence.

$$I_{b_{it,iw}} := \left(I_{on} \cdot \tau_{b_{it}} \cdot \cos\left(\theta_{it,iw}\right)\right) \tag{3.2.40}$$

Diffuse sky radiation is calculated in equation 3.2.41 (Athienitis, 1999) as a factor of solar altitude, beam atmospheric transmittance, and tilt angle. For example, the tilt angle for a window would be 90^{o}.

$$I_{ds_{it}} := I_{on} \cdot \sin\left(\alpha_{it}\right) \cdot \left(0.2710 - 0.2939 \tau_{b_{it}}\right) \cdot \frac{1 + \cos(\beta)}{2} \tag{3.2.41}$$

Diffuse ground radiation is calculated in equation 3.2.42 (Athienitis, 1999) as a factor of the solar altitude, beam atmospheric transmittance, tilt angle, and ground reflectivity. The reflectivity used in most cases was 0.2.

$$I_{dg_{it}} := \left[I_{on} \cdot \sin\left(\alpha_{it}\right) \cdot \left(0.2710 - 0.2939 \tau_{b_{it}} + \tau_{b_{it}}\right)\right] \cdot \rho_g \cdot \frac{1 - \cos(\beta)}{2} \tag{3.2.42}$$

3.2.9 Wall Resistances

This calculation of the thermal capacitances and resistances of the walls and ceiling are described in this section. Equation 3.2.43 describes the thermal resistance of a wall where f_f represents the fraction of insulation area to wood stud area, R is the value of the insulation in m2°C/W, Rext is the value of the exterior layer of insulation in m2 °C/W, h1 is the interior film heat transfer coefficient, and ho is the exterior film heat transfer coefficient.

$$R_l := \frac{1}{\frac{1 - f_f}{\left(R + \frac{1}{h_o} + \frac{1}{h_l} + Rext\right)} + \frac{f_f}{\left(R_f + \frac{1}{h_o} + \frac{1}{h_l} + Rext\right)}} \tag{3.2.43}$$

3.3 Simulations

When simulating the performance of the house to maintain a comfortable indoor environment, all of the loads that act as heat sources must be considered in addition to weather conditions. These include: the PCM bricks, HVAC, windows, appliances, lights, and internal gains from visitors. All of these must be considered when calculating optimal insulation values for the wall, ceiling and floor, and for determining the cooling and heating requirements in order to size mechanical systems appropriately.

The program uses a transient finite difference analysis with a time step of 300 seconds to calculate the behavior of the house as a system for a 1 week period and it is assumed that a heat pump is supplying auxiliary heating/cooling. The air that passes through the floor and into the room is modeled as a heat (or cool) source for simplification. The room air

temperature is calculated using the previous air temperature from the floor, rather than the current air temperature. This is still quite accurate and much easier to simulate. Other simplifications including assuming uniform heat flow and heat storage through thermal storage, uniform temperature gradient in thermal storage and room air, and all walls at same temperature, so no heat exchange between them. The heat transfer between the walls and ceiling and the walls and floor are considered since there could be a noticeable temperature difference. The results from the simulations in this Chapter were used to determine features of the building envelope and mechanical systems for the Solar Decathlon Home described in Chapter 4.

3.3.1 Windows

The following table summarizes the simulation results found for various amounts of double-glazed window area for both summer in Washington and winter in Montreal. Shading for the summer design day assumed the shades are closed between 9am and 5pm.

Table 3.2: Effect of window area on cooling and heating loads for design days

Window area (%)	Cooling Load – Summer Design Day (kWh) (with shading)	Heating Load – Winter Design Day (kWh) (no shading)
15	10.5	19.5
25	10.5	12
35	10.5	9
45	10.5	6

Simulations show that the cooling load is not affected much by window size if the windows are efficient and a good shading control technique is used. A window area for the south facing façade of approximately 45% was chosen to reduce the heating load in

the winter, which is the dominating season in northern climates such as Canada. About 3.5kWh and 2kWh of electricity would be required to cool and heat the house respectively when using a heat pump with a COP of 3.

The solar radiation (W/m^2) over a 24 hours period on September 21st in Washington D.C. entering the house through the windows is shown in Figure 3.10. Note that noon is represented on the time scale as 0.

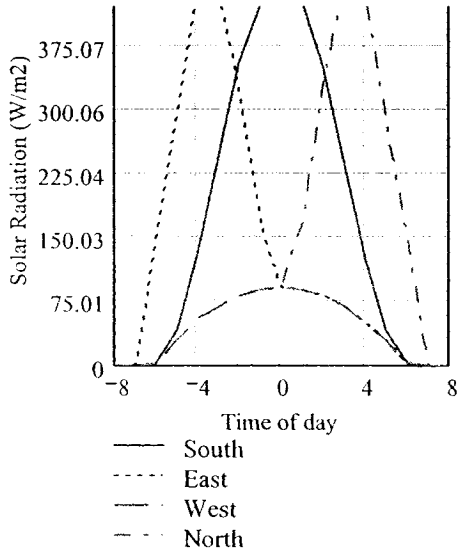

Figure 3.10: Daily solar radiation through windows

3.3.2 Shading

Motorized shading is key to energy efficient house design since it is not practical to assume occupants will be diligent enough to constantly adjust blinds to an optimal position based on the interior and exterior conditions of the home at any given point in time. Typical home will have around 15% south facing window area, however passive solar designs such as the one simulated in this thesis and built for the Solar Decathlon can have around 30% south facing window area. This translates into an average of 50 kWh of

solar radiation transmitted through the windows on a clear sunny winter's day, found by integrating the graph of solar radiation transmitted through the window seen in Figure 3.11.

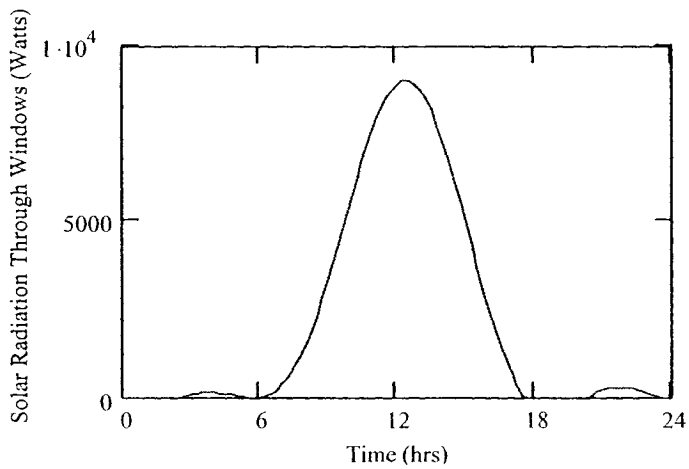

Figure 3.11: Solar Radiation Transmitted Through Windows

Therefore, having a shading system that is controlled with heat gains in mind can greatly affect the energy consumption of a home. Control algorithms that were used to control shading and DALI electric lights in the Solar Decathlon Home are presented in Chapter 4.5. Results from the home are presented in Chapter 5 that show the temperature profile of the home with the shades controlled automatically.

Simulations were run to show the benefits of having blinds either outside the house or in the window cavity. The following example follows the same principle that the program uses to calculate the heat absorbed by the shading device which is then radiated into the room:

Outside Temperature: 20°C

Room Temperature: 20°C

Solar Radiation Incident on Blind: 500 W/m^2

Absorptance of Blind: 25%

*With the above assumptions, the blind reaches a temperature of approximately 35°C. The blind absorbs 125 W/m² of solar radiation, so for a 2m² blind this represents a load of **250W**, which is quite significant during the hottest hours of the day when the cooling load is already at its highest.*

Based on the above calculation, the shading device was therefore assumed to be outside the windows.

Due to time limitations, calculating the shading position to satisfy the interior lighting conditions based on an average illuminance could not be done within the scope of this thesis. The shades were instead controlled solely according to heating and cooling requirements. On a partly cloudy day during the heating season for example, the shading device would allow more light to enter the house since there would be less risk of overheating. On a sunny day in the cooling season however, the shading device would be positioned to allow a minimal amount of solar radiation to avoid overheating, even though as the calculation above shows with the shading device inside the house significant heat gains can still be experienced.

For the summer design day that is a sunny day with a temperature that varies between 15°C and 25°C, the cooling load over a 24 hours period is 13.5 kWh with the blinds open at 80% the entire day. However, with the blinds open at 80% except between 9am and 5pm the cooling load is reduced to 10.5 kWh.

3.3.3 Thermal Insulation

Simulations were performed for different levels of insulation in the walls and ceiling to determine the optimal amount in terms of cost versus performance. The following table

summarizes the heating load for the winter design day, which was chosen over the summer design day since in the winter there is a much greater difference in temperature (ΔT) between the outside temperature and the inside temperature. The floor is assumed to be adiabatic due to the false floor containing the thermal storage.

Table 3.3: Summary of surface areas and thermal resistance values

Condition	Walls (RSI)	Ceiling (RSI)	Infiltration	Heating Load (kWh)
1	4	5	0.5 ach	13.5
2	5	6	0.5 ach	6
3	6	7	0.5 ach	6
4	7	8	0.5 ach	6
5	7	9	0.5 ach	6

Table 3.3 shows that the heating load does not change with increasing wall and ceiling insulation greater than RSI 5 m2°C/W and RSI 6 m2°C/W respectively, meaning these are the optimal insulation values for the home.

3.3.4 Room Air Temperature – Summer Design Day

The design day for summer represents a clear, sunny week in Washington D.C. in October with a sinusoidal outdoor temperature varying between 15°C and 25°C. The simulation also includes the heat gains due to occupants, which is assumed to be 2 kW for 3 hours. The performance of the house during a very hot week can be seen in the following graph. The variation of the mean room air temperature can be seen over a 5-day period. The room air cooling setpoint is set at 24.4°C. It can be seen that the heat pump provides cooling to the house when the temperature begins to exceed the 24.4°C

limit. The average daily cooling load is estimated at 10.5 kWh, without the use of the thermal storage.

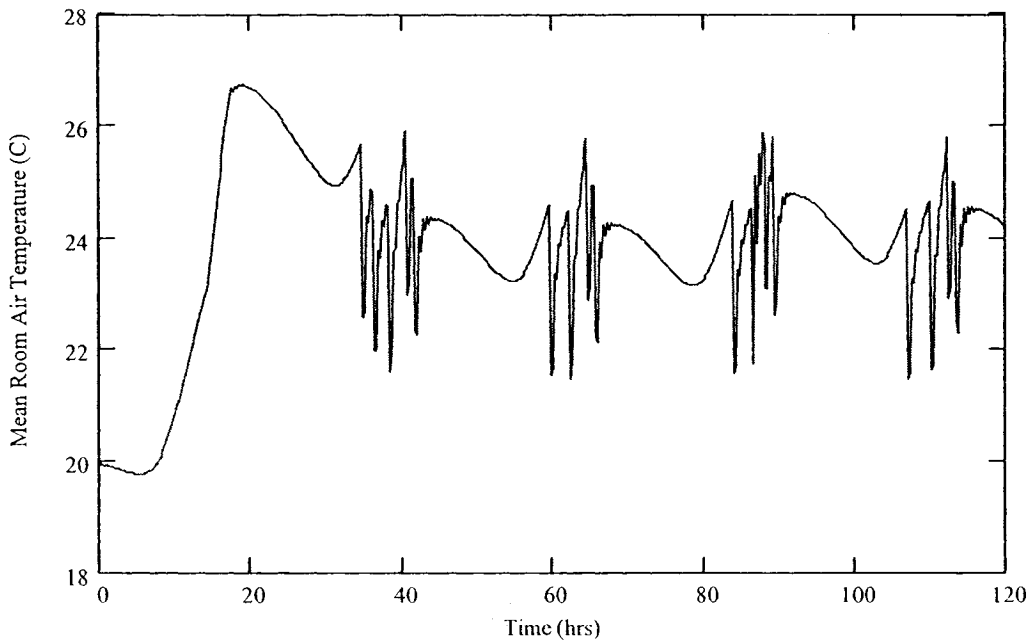

Figure 3.12: Temperature variation within house over 5-day period without thermal storage

When including the thermal storage capabilities of the floor to reduce the cooling load, the cooling load is reduced to 4.5 kWh. The use of the thermal storage however must be strategically planned. In this case, for example, the night air is passed through the floor at 0.5m/sec between the hours of 10pm and 8am. The room air is then circulated through the floor between 2pm and 5pm to cool the outside air which must be supplied for fresh air purposes. The air conditioning is also restricted to being used between the hours of 10am and 6pm, since the system might be tempted to use supplemental cooling after 6pm

if the house is too hot, but it will be in the process of naturally cooling down as long as the exterior temperature is less than the setpoint.

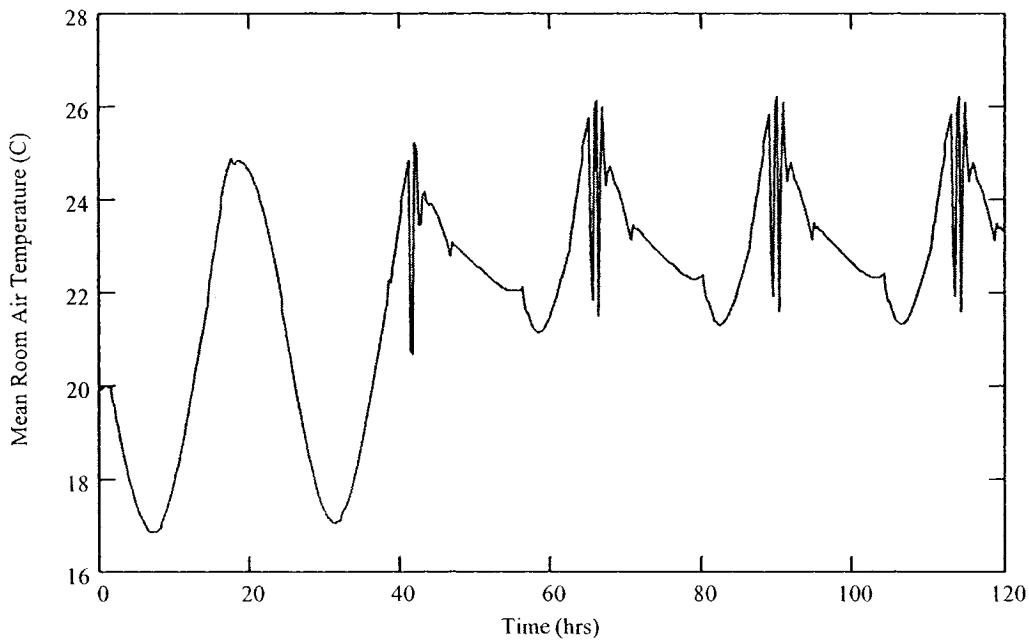

Figure 3.13: Temperature variation within house over 5-day period with use of thermal storage

This proves that with the use of an intelligent control algorithm a significant amount of energy can be saved for cooling needs.

3.3.5 Room Air Temperature - Winter Design Day

The winter design day represents a clear, cold day in Montreal, Canada, with a sinusoidal outside temperature between -20°C at night to -10°C during the day. By allowing the temperature within the house to go as low as 18°C at night, a significant amount of electrical heating is required without the use of thermal storage as can be seen in the following graph. The daily heating load was calculated as 6 kWh.

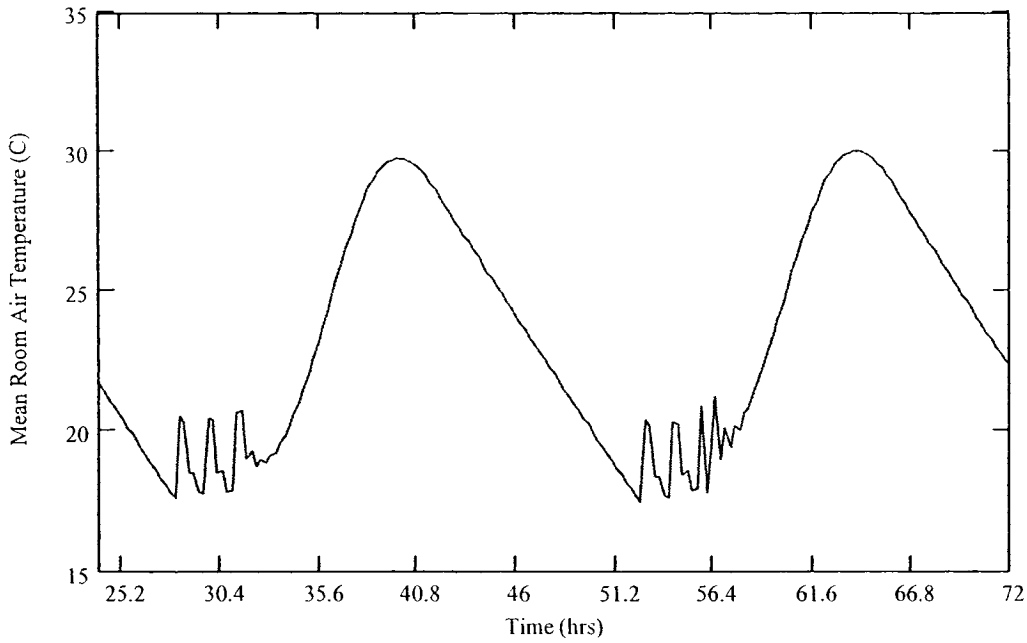

Figure 3.14: Temperature variation within house for winter design day in Montreal, Canada without thermal storage

With the use of the trombe wall and the thermal storage in the floor to aid with reducing the heating load, the following graph shows their effects. As can be seen, the heat pump comes on much less often, leading to a daily heating load of 3 kWh.

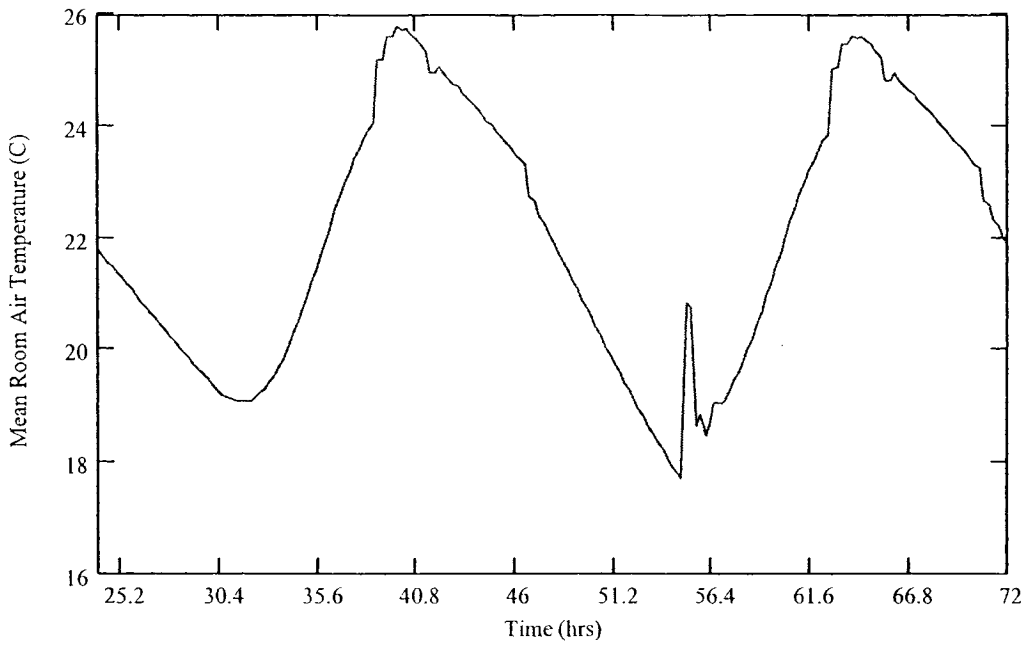

Figure 3.15: Temperature variation within house for winter design day in Montreal, Canada with use of thermal storage

3.3.6 Room Air Temperature – Annual Simulations

Annual simulations were performed for the thermal performance of the house in Washington D.C. for the 21st day of each month. Each day is assumed to be sunny, with a daily temperature according to Table 3.4. The following table summarizes the information found on theweathernetwork.com regarding Solar Radiation, average temperature, and hours of sunlight for Washington D.C. used for the annual simulations.

Table 3.4: Weather and solar radiation data from theweathernetwork.com for Washington D.C.

Temperature(^{o}C)	Jan	Feb	Mar	Apr	May	Jun	Jul	Aug	Sep	Oct	Nov	Dec
Maximum	6	8	14	19	25	29	31	31	27	21	15	8
Minimum	-2	-1	3	8	14	19	22	21	17	10	5	0
Mean	1	3	8	14	19	24	27	26	22	15	10	4
Hours of Sun	145	152	204	228	261	283	281	263	225	204	150	133
Irradiation (kWh/m^2)	3.8	4.7	5.6	6.2	6.3	6.3	6.3	6.1	5.6	4.8	3.9	3.4
Clearness Index	0.42	0.45	0.47	0.48	0.49	0.51	0.51	0.49	0.50	0.49	0.44	0.40

The following table summarizes the results found using data for average days. Figures 3.16 to 3.19 show the temperature variation within the house for an average day in winter (January 15th), spring (April 15th), summer (July 15th), and fall (October 15th).

Table 3.5: Summary of annual temperature variations and thermal loads for average days in Washington D.C.

Temp(°C)	Jan	Feb	Mar	Apr	May	Jun	Jul	Aug	Sep	Oct	Nov	Dec
Max (w/o thermal storage)	25	26	29	29	26	25	25	25	25	25	26	26
Min (w/o thermal storage)	19	18	21	23	24	23	23	23	22	22	20	19
Thermal Load - kWh (w/o thermal storage)	6	0	0	0	7.5	15	18	18	15	6	0	0
Max (with thermal storage)	23	25	26	24.5	26	25	25	25	25	24	24	24
Min (with thermal storage)	19	19	22	20.5	22	23	23	23	20	20	21	20
Thermal Load - kWh (with thermal storage)	3	0	0	0	0	9	12	9	1.5	0	0	0
Shading Strategy	No shading	No shading	70% : 12pm – 2pm	70% : 10am – 3pm	70% : 9am – 5pm	70% : 9am – 5pm	70% : 9am – 5pm	70% : 9am – 5pm	70% : 9am – 5pm	70% : 9am – 5pm	70% : 9am – 5pm	70% : 11am – 3pm

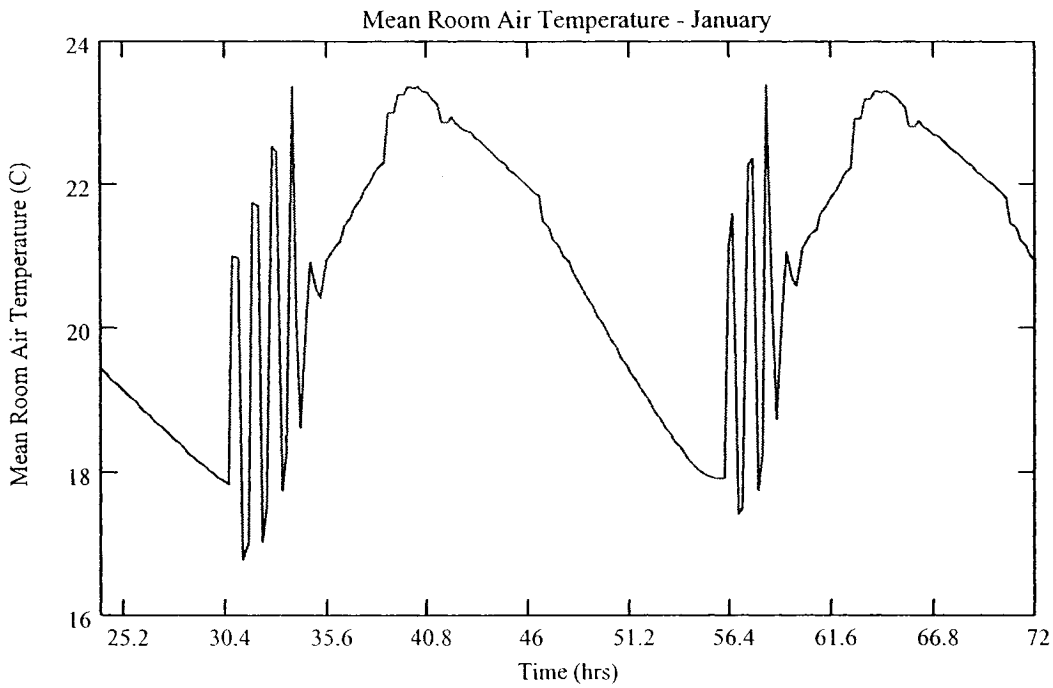

Figure 3.16: Mean room air temperature for average day in Washington D.C. – January

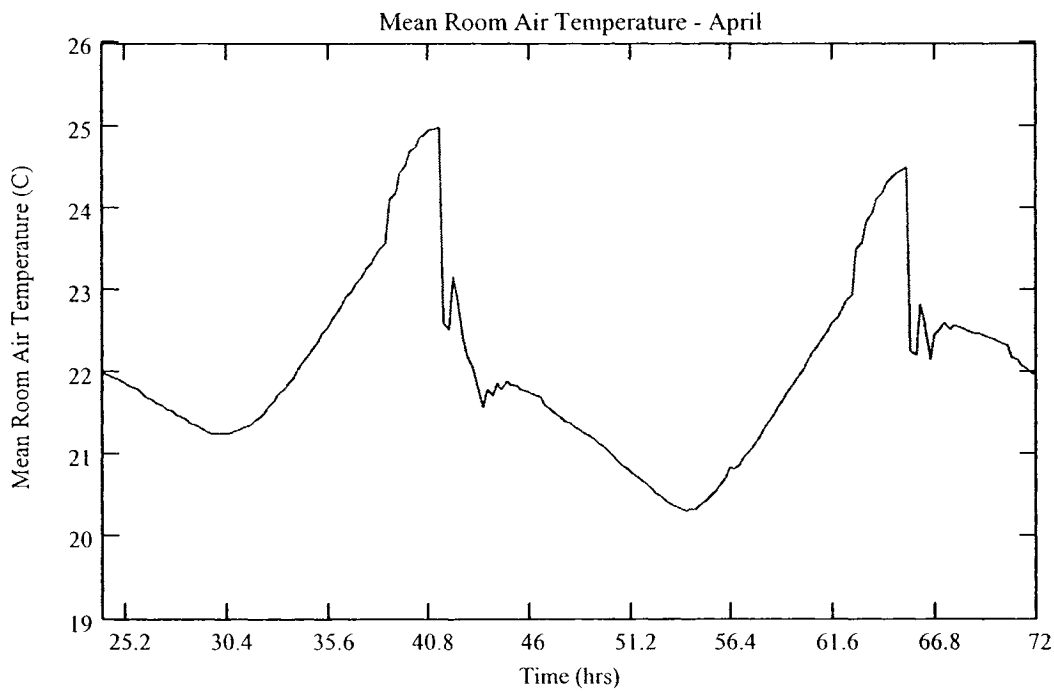

Figure 3.17: Mean room air temperature for average day in Washington D.C. – April

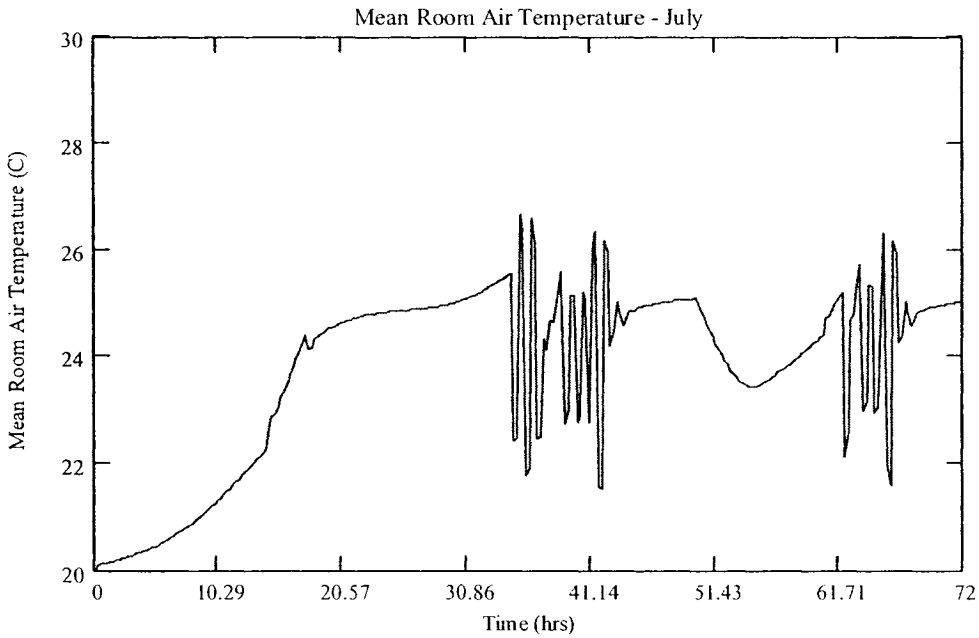

Figure 3.18: Mean room air temperature for average day in Washington D.C. – July

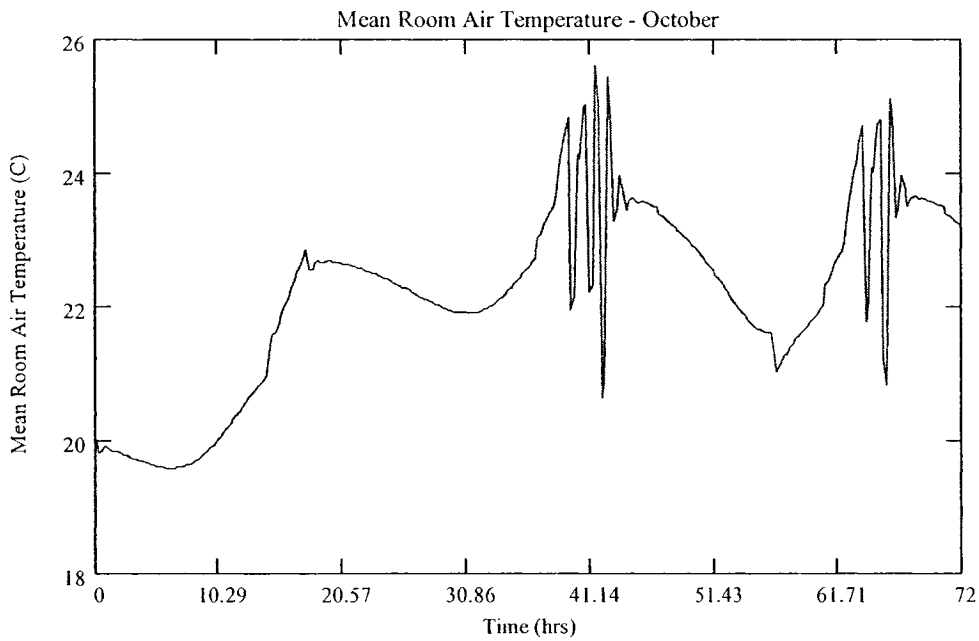

Figure 3.19: Mean room air temperature for average day in Washington D.C. – October

The results show that for a climate such as that found in Washington D.C., the Solar House performs exceptionally well since the only time of year electricity is required for the purposes of thermal comfort is during the months of June – September. It should be noted that the numbers represented thermal energy, and with a heat pump with a COP of 3.0 the electricity consumption for the months of June – September would be 3 kWh, 4 kWh, 3 kWh, and 0.5 kWh. It should also be noted that the months that require the most electricity are also the months that have the most amount of sunlight, which is ideal due to the use of photovoltaics.

3.5 Conclusion

The program developed gives a good idea of the thermal behavior a home with various custom features. The home is shown to have a cooling load of only 10.5 kWh for the summer design day and a 6 kWh heating load for the winter design day using the optimal combination of windows, shading, insulation, and thermal storage as determined by the program. According to simulation, energy performance does not increase significantly beyond insulation levels of RSI 5 $m2^{\circ}C/W$ in the walls and RSI 6 $m2^{\circ}C/W$ in the ceiling. A window area of 45% was found to be optimal for winter performance and had minimal impact on heat gains in the summer using exterior shading that is properly controlled. The PV-thermal system can general over 700 W of thermal energy during a typical summer day which can be used for space or water heating, or stored in the thermal storage which can hold over 36 kWh of thermal energy for later use. The combined PV-Thermal system generates on average three times as much thermal energy compared to

electrical energy, indicating that PV-Thermal systems should be implemented whenever possible if cost effective.

CHAPTER 4

TEST CASE: CANADIAN SOLAR DECATHLON HOME

4.1 Introduction

The Solar Decathlon is an international competition designed to increase public awareness of the viability of photovoltaic systems on homes. The competition was hosted by the US Department of Energy and took place during the first three weeks of October 2005 in Washington D.C. It was the second such competition, the first of which occurred in September 2002. Concordia University and the University of Montreal entered a joint partnership to represent the only Canadian team to ever enter this competition. In order to stand out amongst the 16 American teams out of a total of 18 teams (1 team from Spain), the Canadian team decided to incorporate innovative energy saving techniques. One of the techniques was the ability to capture the heat generated by the PV array and use it to reduce overall load usage. The warm air has several uses including space heating, domestic hot water heating, and drying clothes. In order to validate the design options, the program described in this thesis was used to model the thermal behaviour of the house as well as the thermal and electrical characteristics of the PV array. Control algorithms described in this thesis were used to optimize the usage of the thermal and electrical energy throughout the year.

4.2 Specifications of the Home

Following the simulations described in Chapter 3, elements of the building envelope of the Solar Decathlon Home were chosen. Although the ideal level of insulation for the walls and ceiling were determined to be RSI 5 and RSI 6 respectively (Table 3.3), slightly higher levels of insulation were chosen due to practical purposes of filling in the available space for insulation in the wall and ceiling cavities. Therefore, the walls insulated to RSI 6.2 $m2^{\circ}C/W$ and the ceiling to RSI 8.8 $m2^{\circ}C/W$ as follows:

- Walls: 3.5" polyurethane spray foam @ RSI 1.25/inch + 2" rigid outside @ RSI 0.88/inch + sheathing, gypsum, air barrier
- Ceiling: 7" polyurethane spray foam @ RSI 1.25/inch, gypsum

Since the optimal window area was determined to be 45% of the south facing wall (see Table 3.2), this was chosen as the as for the Decathlon Home. The large, south-facing windows in the living room are double-glazed, low-e, argon-filled with fibreglass framing and insulated spacers. The remainder of the windows are triple-glazed windows since a higher level of insulation takes priority over solar transmission. The approximate total R value of the triple-glazed windows is R 5.3 (RSI 0.95), the double-glazed windows is R 3.2 (RSI 0.56). Motorized shading is used to control automatically heat gains and lighting with the use of temperature and daylight sensors. The shades are described from the manufacturer to have a 3% transmission of light, however upon testing it was revealed that approximately 10% of the light is transmitted, 68% is reflected, and 22% is absorbed. The algorithm that controls the position of the shade is based on temperature, daylight, and time based conditions. The electric lighting is used to supplement daylight when required. The electric lighting consists of digital dimmable

ballasts (DALI) and fluorescent bulbs which are very efficient and easily controlled as discussed in Section 2.7 of the Technology Review. A Siemens automation system integrates the control of lighting and shading. Heating and cooling in the house is provided by a water-source heat pump with an average COP of 4 (can go up to 7). Heat sources for the hot tank include PV air, the solar thermal collector, and outside air. The heat pump is composed of two compressors, one 9000 BTU and one 12000 BTU, which can be used individually or together to more closely address the heating and cooling needs. The peak capacity of 21000 BTU is equivalent to approximately 6kW, which was determined in the simulations to be the ideal capacity to meet the needs of the home for the design days. An energy recovery ventilator conditions fresh air to reduce heating/cooling load while maintaining a healthy indoor environment. Built in to the floor of the house are PCM (phase-change material) soaked bricks providing approximately 36 kWh of energy storage as calculated in Section 3.2.2.

4.3 PV System

The main PV system on the roof consists of a 7 kW Photovoltaic (PV) system that generates electricity and heat at the same time. One of the main purposes of using both electricity and heat generated by the PV modules is to increase the total efficiency of the system. By harnessing both electricity and thermal energy, the overall energy efficiency of the system increases from roughly 7 - 10% to 30 - 40% [Pasini (2005)]. The roof area is approximately 13.5m by 5.5m, which can accommodate many different arrangements of panels depending on their dimensions and means of installation. The PV system

consists of forty BP 175 W solar modules and one solar heating collector. The solar panels are 1.595 m x 0.79 m producing 175 W with a maximum voltage of 35.7V and a maximum current of 4.9A. The module conversion efficiency is rated at 13.9%.

The forty panels are all connected in pairs producing twenty strings, each capable of charging a 48V battery bank. The twenty strings run within a crawl space underneath the roof and connect to a junction box. Each input string has a respective pullout fuse rated at 15A. The outputs from the junction boxes run through respective DC breakers each rated at 60A. The strings then go into individual charge controllers. From the charge controllers five more DC breakers are used before connecting everything together in a combiner box. The output of the combiner box connects to the battery bank. The bank is comprised of twelve 4V deep-cycle batteries. Each battery has a capacity of 1900Ah at the 100 hour discharge rate, meaning when the batteries are discharged slowly over a period of 100 hours they will give 1900Ah. The faster a battery is discharged, the less the energy that can be extracted from them. The batteries are all connected in series, making the voltage 48V. Two outputs are taken from the batteries, each of which goes through DC disconnects rated at 175A. Each of these two circuits is connected to 4kW inverters that output 120VAC. The two inverters are synchronized out of phase to produce both 120VAC and 240VAC. This output of the inverters is connected to a standard AC panel, which feeds all the electrical circuits of the house. Figures 4.1 to 4.3 illustrate the key components of the PV system of the Solar Decathlon House.

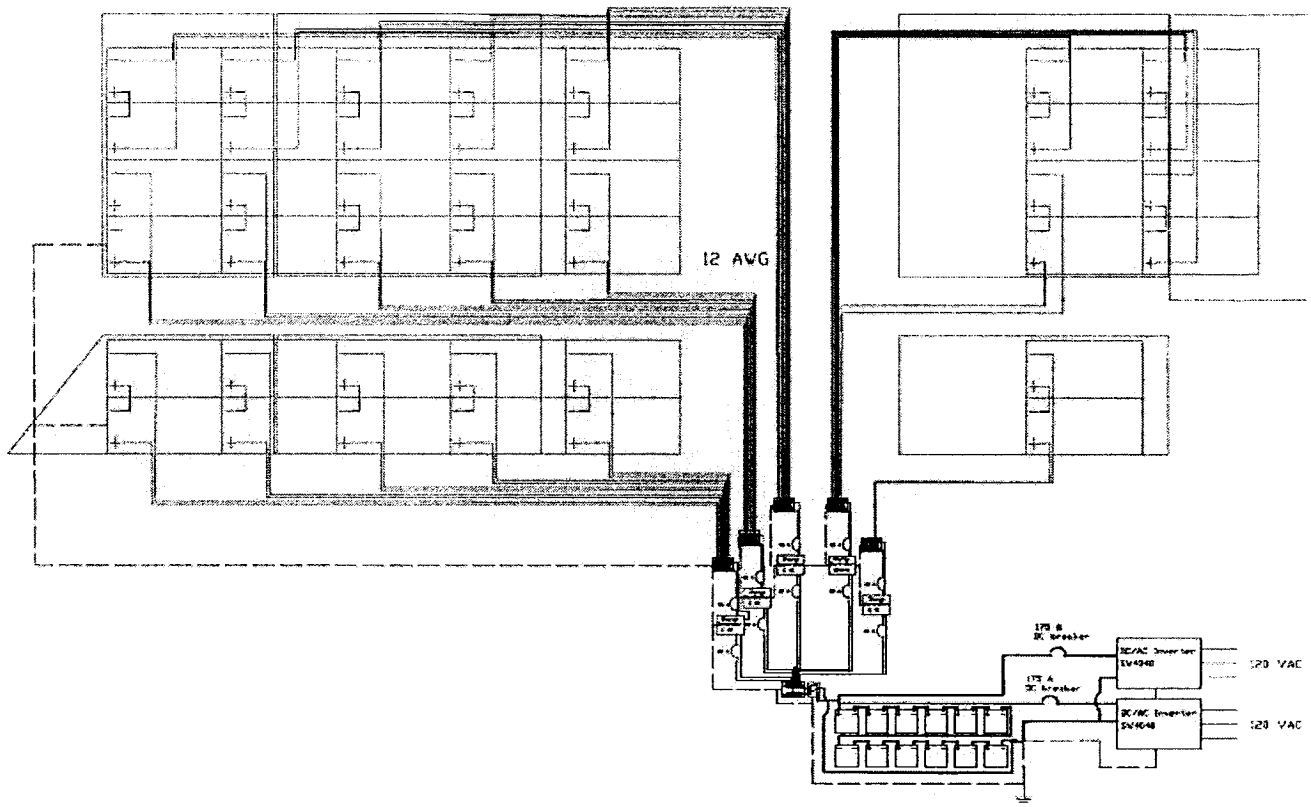

Figure 4.1: Schematic of Solar Decathlon PV System

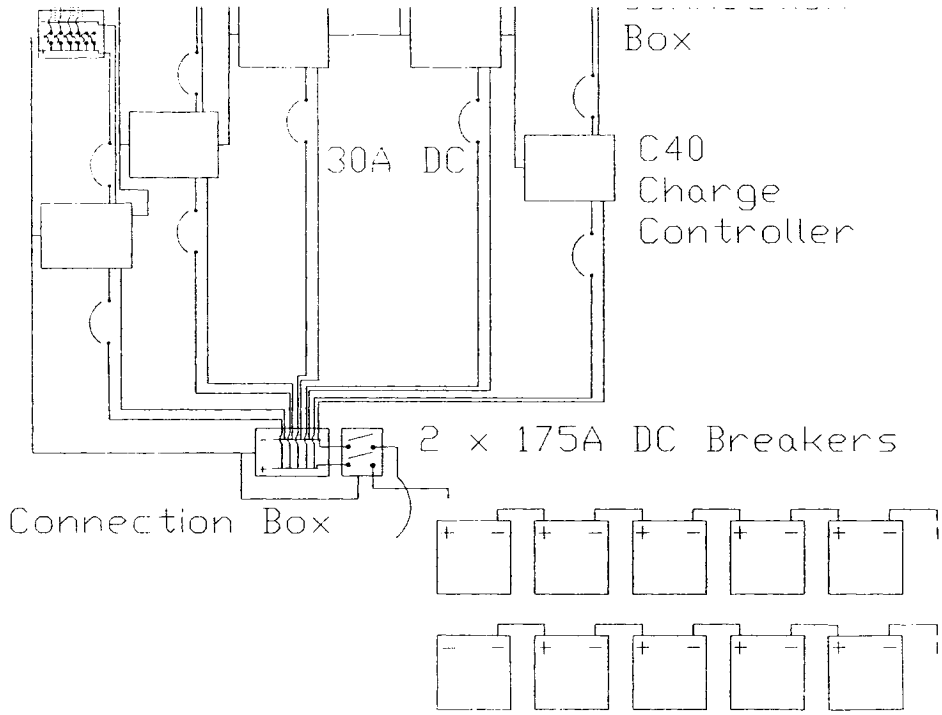

Figure 4.2: Close-up of charge controllers, DC breakers, and connection box

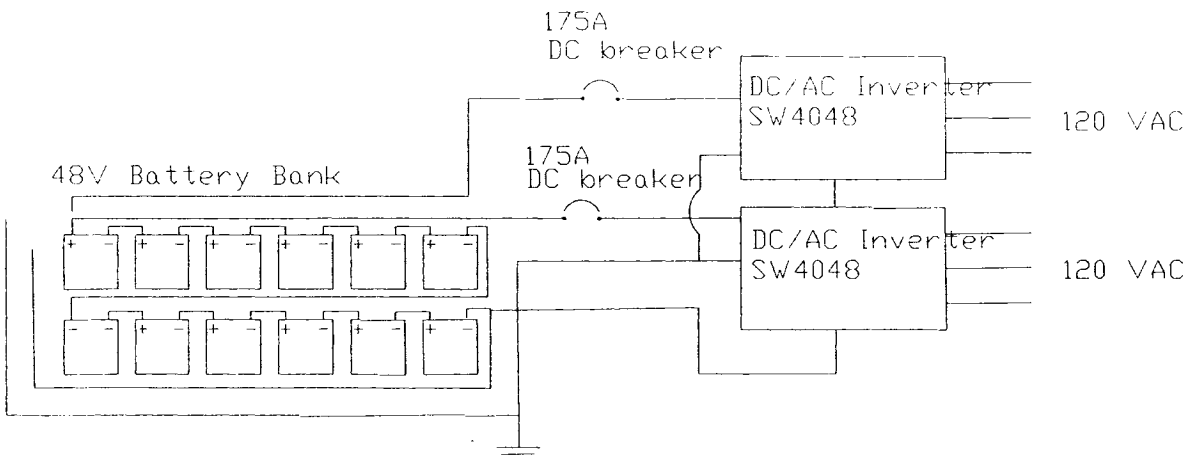

Figure 4.3: Close-up of battery bank, DC breakers, and inverters

A benefit of the BP Solar module is the fact that they were manufactured frameless, allowing the design and installation of a custom framing system that lends well to PV-Thermal and BIPV (Building Integrated Photovoltaics). One interesting framing system that works well with frameless, glass panels is from the company Solrif, based in Switzerland. The Solrif framing system allows the integration of PV modules onto rooftops in a manner similar to roof tiles. The panels overlap slightly in order to form a waterproof rain screen to avoid the common scenario of placing the PV modules on an existing roofing material. This method allows the PV modules themselves to act as the roofing material, effectively increasing their usage and lowering the overall cost of the system when installed on a new application [Pasini (2005)]. The process of attaching the framing to the panels begins by first placing a strip of electrically insulating tape around the border of each panel to prevent a short circuit with the metallic frame in case a tear occurs in the backing of the panel. A thin bead of caulking is then placed around the edge of the panel, followed by the each of the four edges of the frame. The edges are then screwed together, which concludes the framing process, lasting approximately 10 minutes per panel.

Two 1.0m by 2.0m solar thermal collectors, each consisting of 10 evacuated tubes, were placed on the east most portion of roof. Each solar thermal collector is capable of producing 900W peak of thermal energy for the purpose of heating water. The reason evacuated tubes were chosen was for the fact that Canada has a very cold climate and evacuated tubes lose very little heat, as described in Section 2.4.

A strategy for arranging and connecting the PV modules was developed. This strategy takes into consideration factors such as incident solar radiation and panel temperature,

both of which affect their efficiency. Therefore, the string of panels that are located at the front part of the roof at a different slope should be connected to one charge controller. The panels on the main portion that are at similar vertical heights were also connected to the same charge controller since they will experience similar levels of radiation and air temperature in the cavity under them. The panels were mounted on 1" x 2" wood strapping in order to form cavities under each vertical row of panels. This forms the channel through which air passes. The strapping which forms the air cavity as well as the PV panel support structure, the air cavity and overlap can be seen in Figure 4.4.

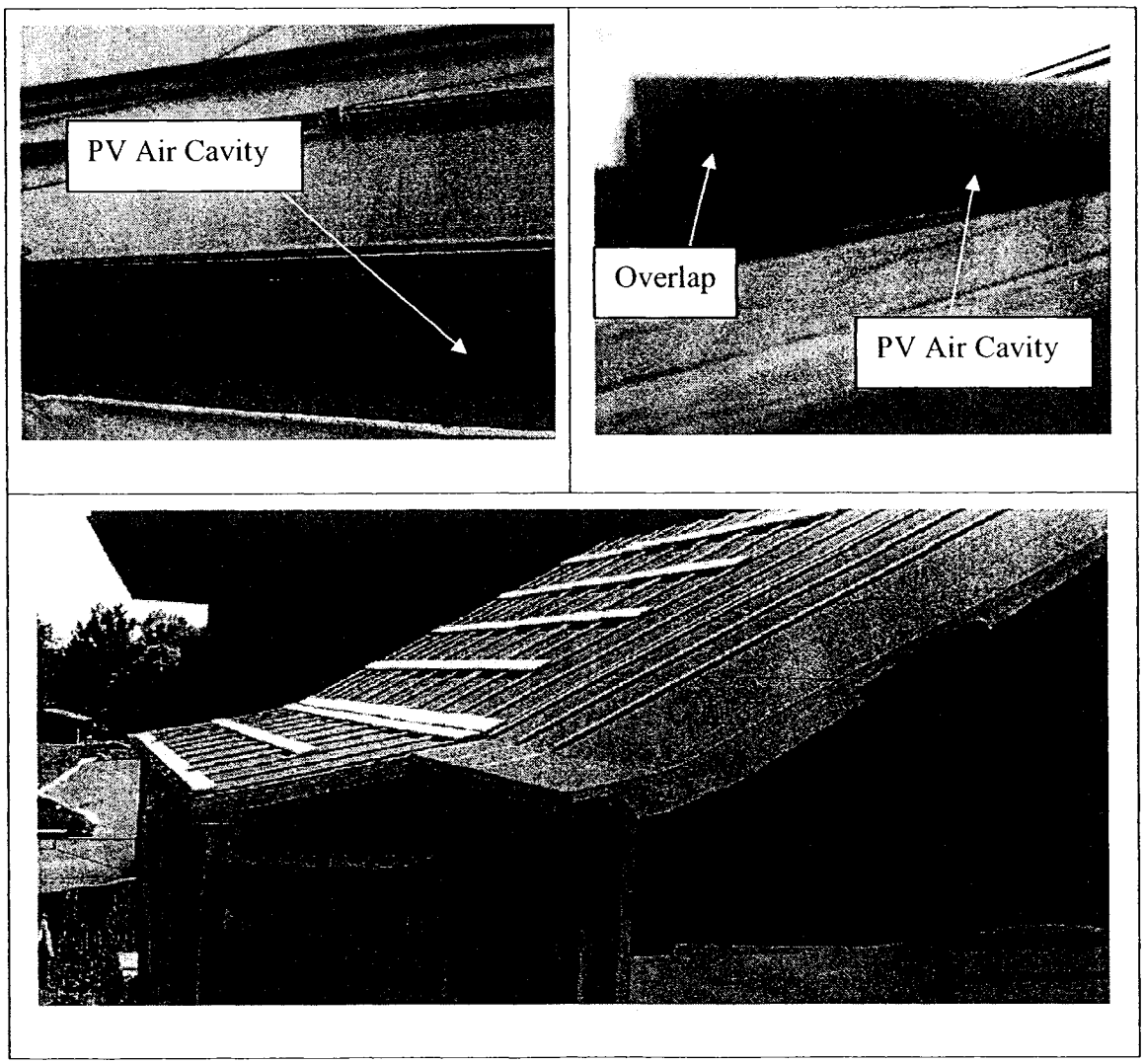

Figure 4.4: Photo of air cavity under PV panels (top left), framing overlap (top right), and strapping

The air is then collected near the peak of the roof where it is drawn into a duct attached to the underside of the peak of the roof. The duct then leads to the mechanical room where the air is used for water pre-heating or as the inlet to the heat pump (see Figure 4.5).

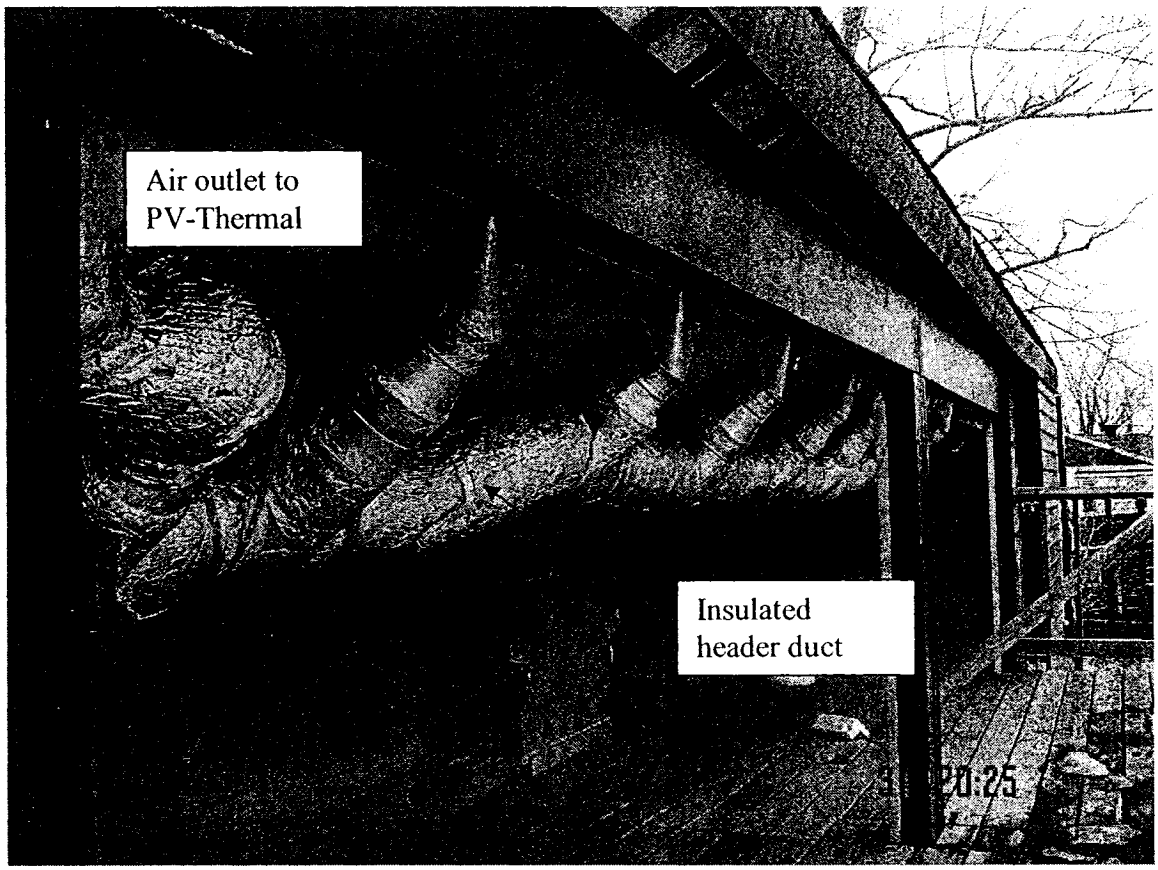

Figure 4.5: Picture of PV-Thermal Duct

The roof's high level of insulation keeps most of the heat generated from the PV panels from radiating to the attic. A photo of the house is shown in Figure 4.6 below.

A junction can be seen between the PV panels and the shingles which cover the remainder of the roof, which was necessary since the dimensions of the solar panels and space for the solar thermal collectors did not allow for complete coverage of the roof. The ideal case would be to completely cover the roof in PV panels by sizing the roof with a

specific PV panel in mind, and then placing the solar thermal collectors on the façade of the house.

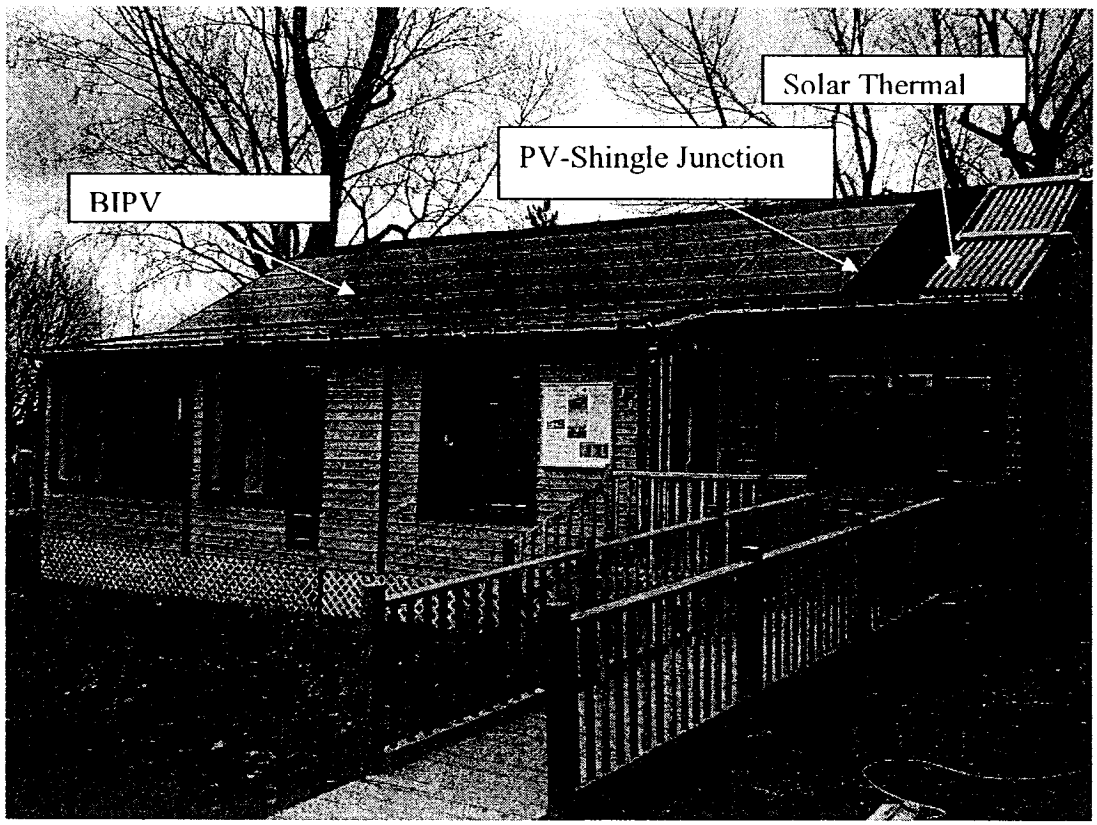

Figure 4.6: Canadian Solar Decathlon Home, Loyola Campus, Concordia University

4.4 Balance of PV-Thermal System

A PV system that generates electricity and captures heat as well in order to be used for other purposes is a complex system that has to be designed very thoroughly in order to obtain the best module efficiency and capture as much heat as possible. Figure 4.7 illustrates the major components of the PV-Thermal system the house uses.

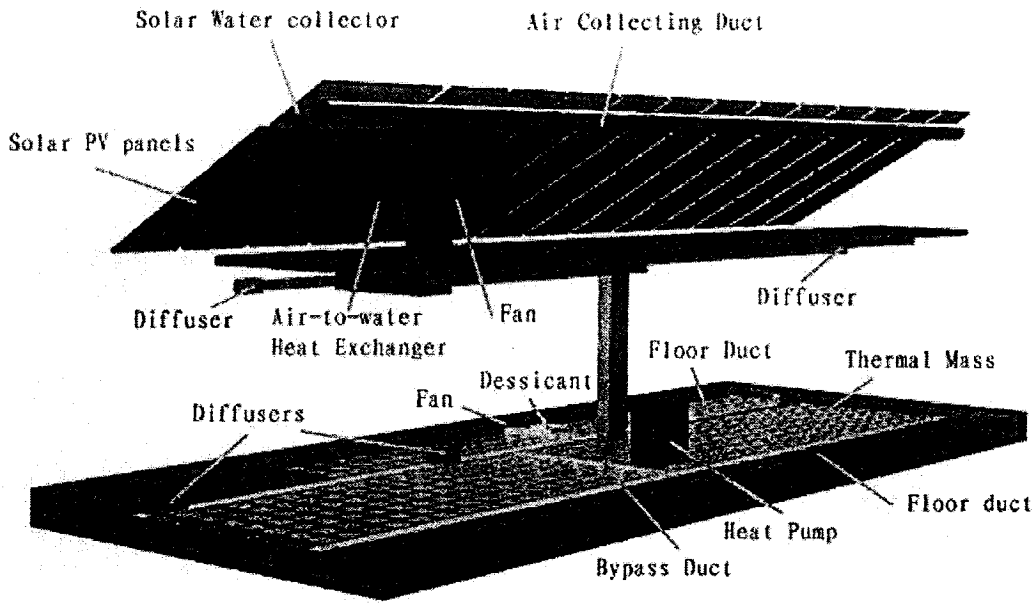

Figure 4.7: Schematic of PV/T System (Courtesy of Yu Xiang Chen, 2005)

The PV-Thermal system consists of an air-collecting duct that runs along the peak of the roof that collects the warm air from the PV cavity. The air is drawn through the duct to a second floor mechanical room using a variable speed fan. The air can be used to either pre-heat domestic hot water, preheat the liquid for the inlet of the heat pump, or heat the thermal mass consisting of PCM-soaked bricks under the floor. The system consists of various dampers, diffusers, and fans in order to route the air through the appropriate path depending on the situation. The two most common scenarios of air routing and usage are as follows:

1. Cooling situation: In the summer, if the night air is cool, air will be drawn through the thermal mass in the floor in order to reduce the cooling load the following day.

2. Heating situation: On a cold, sunny winter day, air from the PV will be used to heat the liquid for the inlet of the heat pump in order to increase the coefficient of performance.

4.5 Daylighting and Electric Lighting Control

Based on the simulations performed on the Canadian Solar Decathlon House using the program described in this thesis, simple control algorithms were developed and implemented into the control system that was used to control the DALI lighting and motorized shading in the house. A flowchart describing the basic logic behind the control of the lighting and shading can be seen in Figures 4.8 and 4.9 below. The variables in the Figure are defined as follows:

Occ.Sensor: Occupancy sensor

int.temp: Interior room temperature

Light_sensor: Output of interior illuminance meter

Light_setpoint: Value of desired illuminance at pre-defined target

blind_pos: Position of blinds described as percentage relative to fully-open state

out.temp: Outside air temperature

solar.rad: Solar Radiation incident on south-facing window

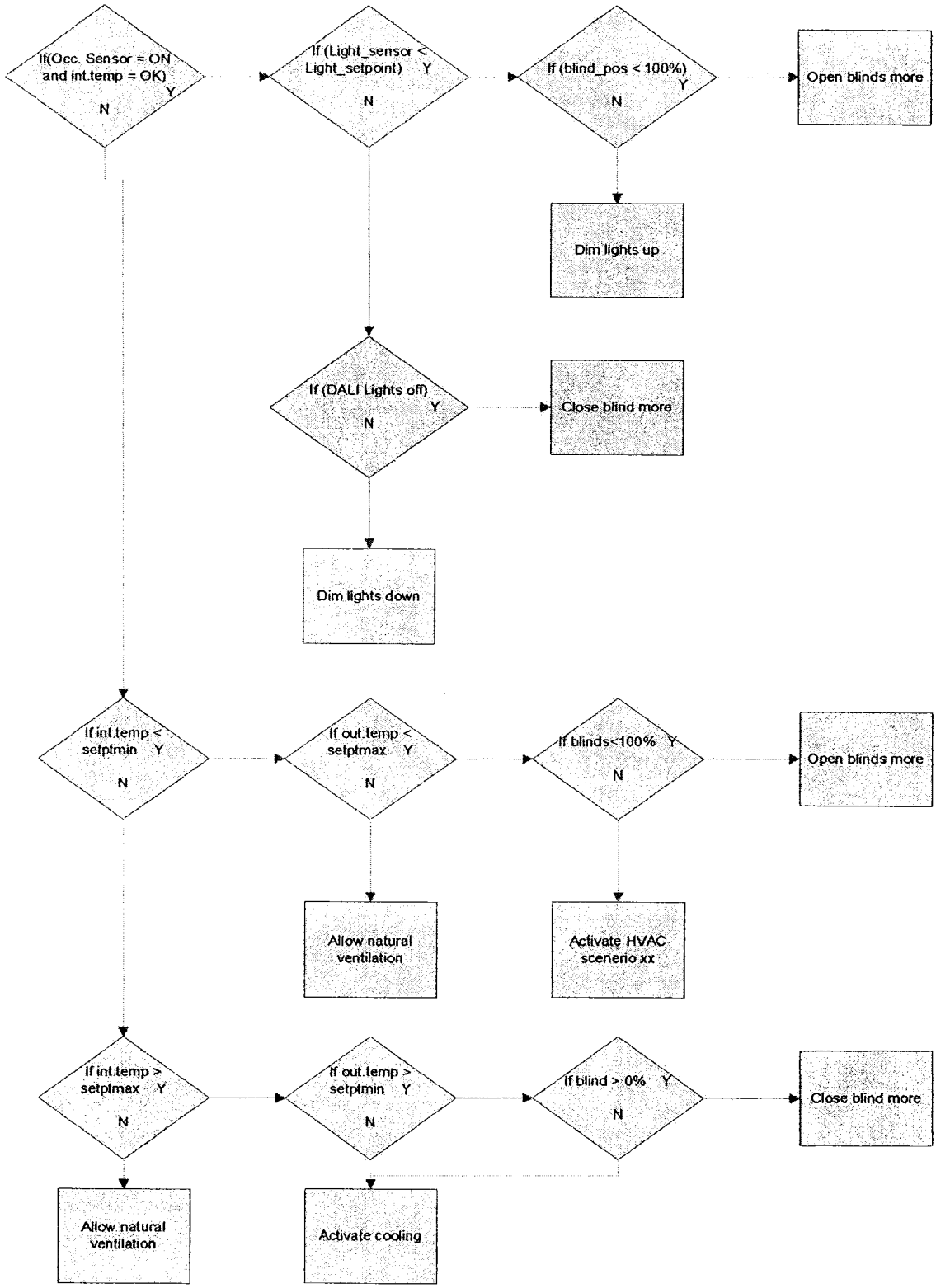

Figure 4.8: Flowchart Illustrating Control Algorithm for Electric Lighting and Shading, and HVAC

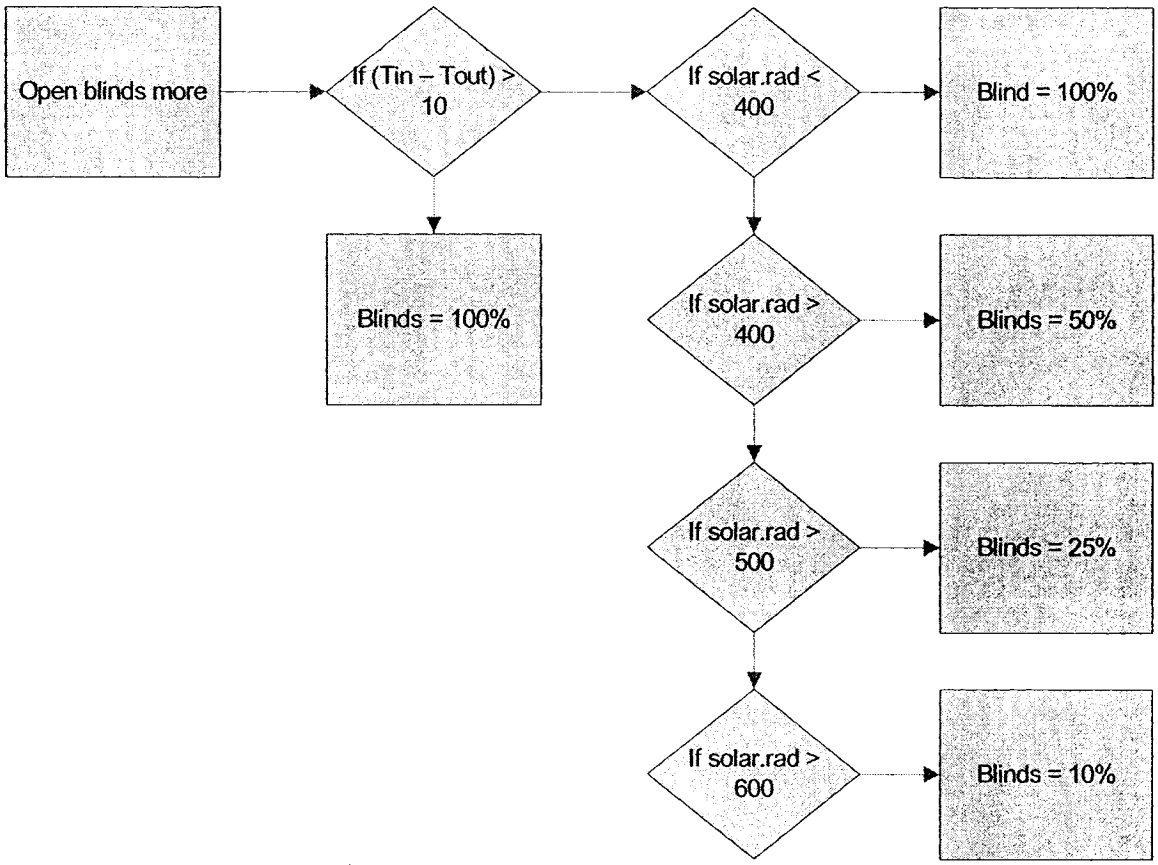

Figure 4.9: Control Algorithm for Motorized Shading

The above control algorithm uses proportional control of the motorized shading based on solar radiation and the difference in temperature between the outside air temperature and the room air temperature. The control algorithm uses daylight to act as the primary heating source, so when it is not sufficient the HVAC system is activated to supply the balance of the heating load (refer to Figure 4.8).

4.6 Conclusion

The Canadian Solar Decathlon Home served as an implementation of the design and control suggestions made in this thesis. The house can serve as a research facility for validation of the program developed in this thesis and for other projects related to energy efficiency in homes and mechanical systems.

CHAPTER 5

VERIFICATION OF PV-THERMAL AND THERMAL STORAGE MODELS

5.1 Test Facility

The test hut is a 12' x 10' mockup of a house that incorporates a PV-thermal and thermal storage system. The roof consists of eight 190W solar panels. The panels are connected in four strings, each string containing two panels in series. Each vertical row of panels contains a duct near the peak of the roof that leads to the main collector duct. The panels are mounted using 1" x 3" wood strapping attached to the existing shingle roof along with wood framing that holds the panels to the strapping.

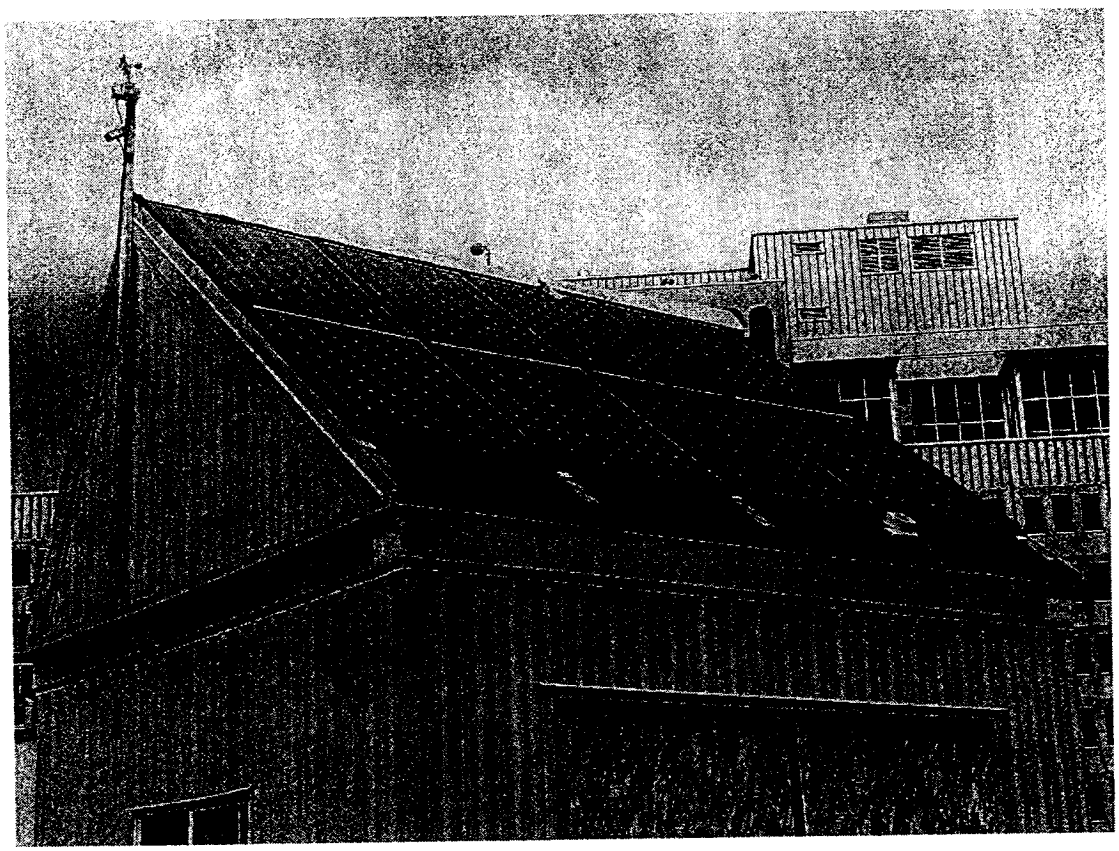

Figure 5.1: Photo of test room located on rooftop of Concordia University BE building

Thermocouples are located near the entrance and end of the air cavity. On a sunny day a 30°C rise in air temperature was noted in the PV air cavity (see Figure 5.2) which is approximately 2.64m in length. Temperature sensors are also located inside the test hut at the inlet to the false floor as well as the outlet of the false floor. The false floor consists of a secondary floor system built overtop the existing floor. It is made of 2" x 4" pieces of wood, spaced at 16"cc with a layer of 5/8" thick plywood on top that forms the walking service. In between the 2" x 4" wood are PCM-soaked bricks. The bricks are used for storing thermal energy, meaning they can be used in the spring, fall and winter for heating and in the summer for cooling.

5.2 Results

Figure 5.2 shows the temperature of the air at different points in the system measured during a warm, sunny day during July 2005. Tintake is the temperature of the ambient outdoor air, Toutlet is the temperature of the air after passing under the solar array, Tfloor_in is the temperature of the air at the inlet of the false floor, Tfloor_out is the temperature of the air after passing through the bricks in the false floor, and Sol_rad is the solar radiation incident on the solar array. The air that passes between the bricks is observed to fall 12.5°C, meaning this energy is being absorbed by the bricks and stored for later use.

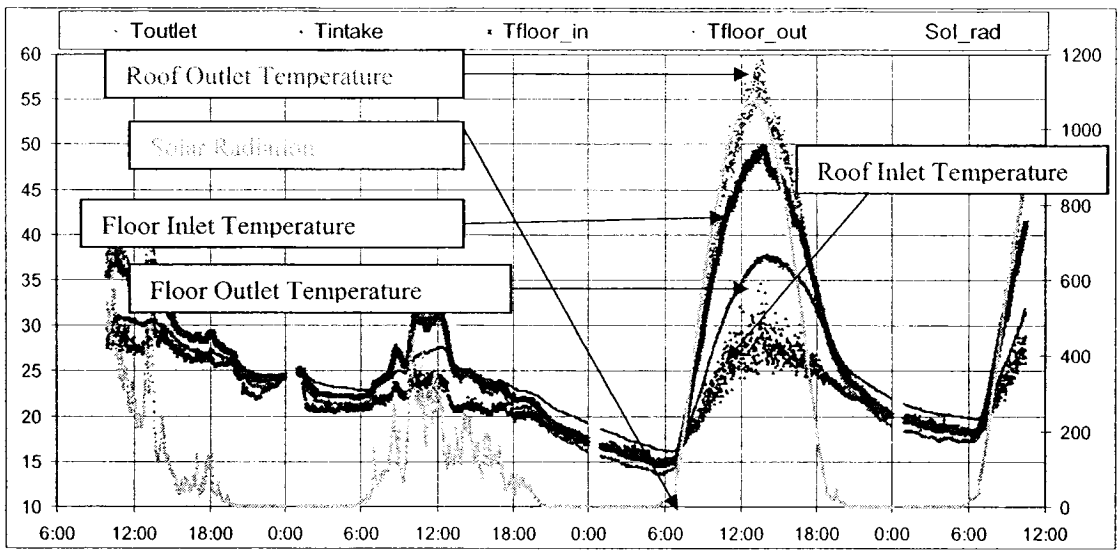

Figure 5.2: Air temperature at different points in HVAC system

The model developed in Chapter 3 was used to simulate the rise in air temperature under similar conditions as measured in Figure 5.2. Figure 5.3 below presents the results.

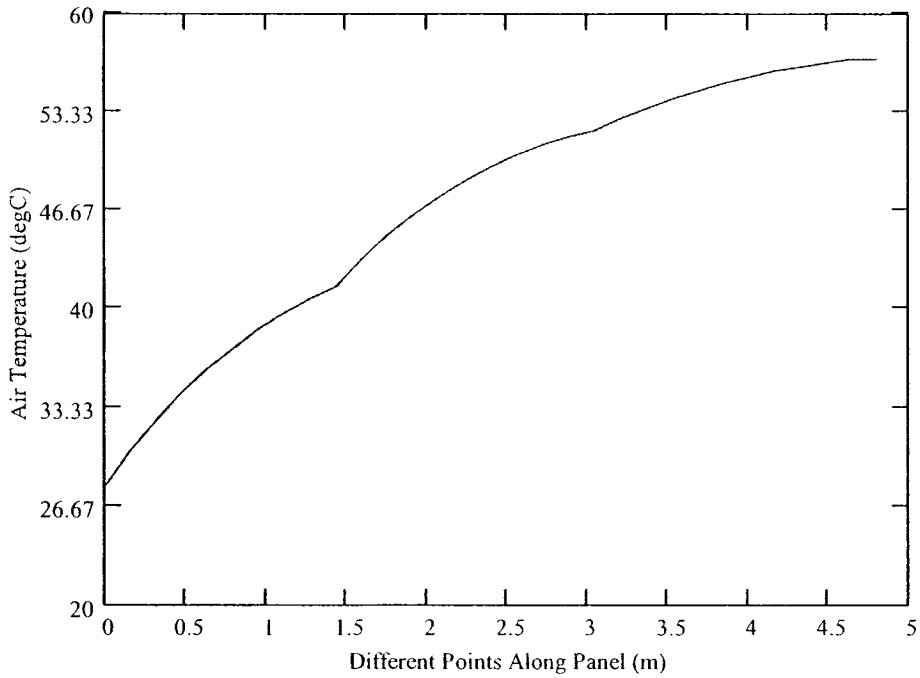

Figure 5.3: Simulation of PV Air Temperature Rise

Measurements of the Solar Decathlon Home were performed in order to validate the software model developed in Chapter 3. Figure 5.4 shows the outdoor temperature profile and room temperature profile measured every 5 minutes along with the solar radiation averaged over every hour for a relatively clear winter day. Measurements show that the room temperature varies between approximately 18°C and 23°C, the outside temperature varies between approximately 8°C and 12°C, and the solar radiation varies between approximately 0 and 600W/m^2.

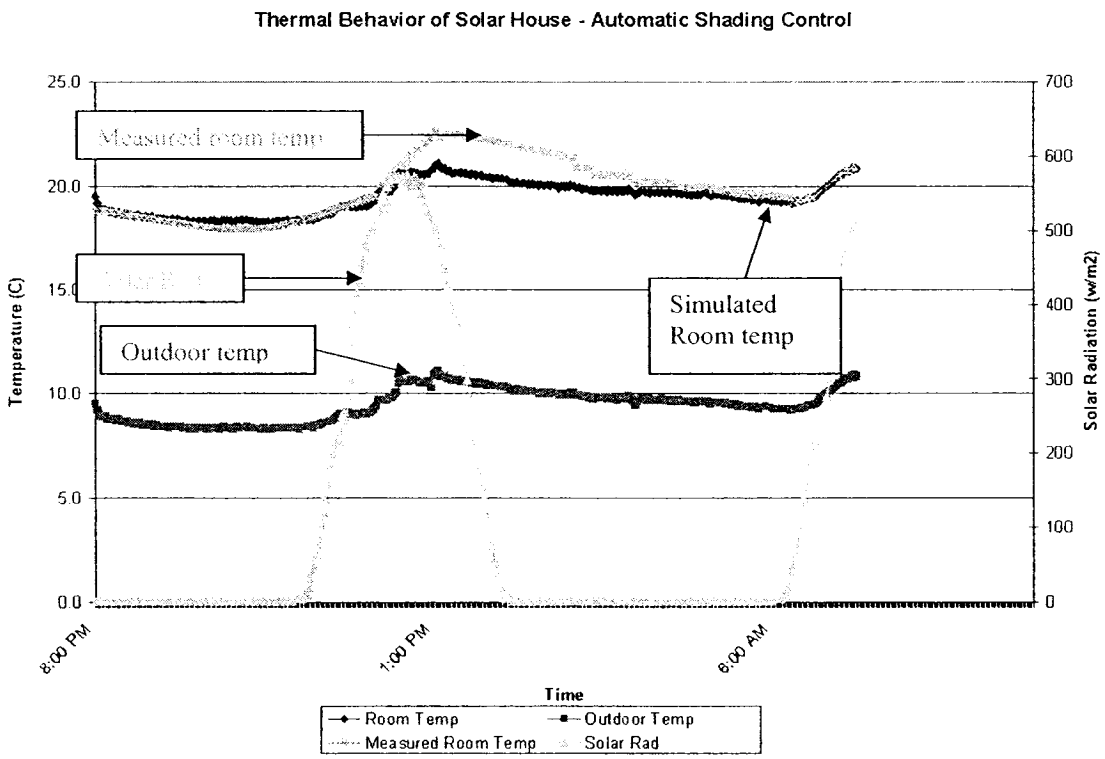

Figure 5.4: Comparison of measured versus simulated room air temperature - automatic shading control

In order to verify the software model described in Chapter 3, an outdoor temperature and solar radiation profile similar to that shown in Figure 5.4 was entered into the model in

order to simulate the room temperature profile. The solar radiation was modeled as a half sinusoid with a peak at 600 W/m^2. It can be seen from Figure 5.4 that the model closely matches the actual measurements taken from the Solar House except during the peak time in the afternoon. This can be explained by the fact that the properties of the thermal mass in the Solar House were not calculated and therefore had to be estimated, which could cause the house to react more quickly to the solar radiation than the model predicts.

5.3 Conclusion

Results from the test facility indicate a 30°C rise in air temperature in the PV cavity, which agree very closely to the results found by performing a simulation using the software developed in Chapter 3. The model can therefore be considered to be quite accurate as long as the model as described holds true. In the case of the room air temperature, the main discrepancy between the simulation and the measured results occurs during the peak hours of the afternoon. Additional testing of the solar house using the thermal mass to store energy during peak times is required in order to truly determine the accuracy of the simulation model.

CHAPTER 6

CONCLUSION

6.1 Conclusion

A program for simulating the performance of a solar home using first principles is presented. The program allows the simulation of multiple energy related systems in a home and linking all of the elements together to get a picture of the thermal behavior of the home as a system. This program is suitable for simulating various design options for a building in unison, however since the possibility of combinations of alternatives is almost endless additional work is required to design a program that also helps to choose or narrow the search of ideal alternatives using energy consumption and cost as the driving factors. However, it needs to be made more user friendly for routine building design. Such programs can be used as engines that run behind more user-friendly interfaces. A case study, the 2005 Solar Decathlon Home, is also presented. The Decathlon Home was designed following the recommendations made by the software that this thesis work produced as well as the review of active solar technology which best suits a net-zero solar powered home in Canada. The house performs very well in both design day simulations – a very cold and clear winter day requires almost no electricity powered heating (~3 kWh), and a very hot and clear summer day requires almost no electricity powered cooling (~4.5 kWh). The house generates approximately 25 kWh of electricity during a typical clear

sunny day in September in Washington D.C., which should be sufficient for two days of operation. The house uses the latest in passive and active solar design principles such as thermal storage in the floor and walls in order to keep the temperature in the space within a reasonable range without the use of much electricity. The house makes use of the thermal energy generated by the PV panels to aid in the heating of the house during the winter as well as the pre-heating of the hot water throughout the year. The house also incorporates the latest in high tech devices such as highly reflective motorized shading, digitally controlled low-power consumption electric lighting, and in-house developed software that integrates all of the systems of the house together to achieve the optimum response. By incorporating all of the above techniques the house uses much less energy than a conventional house without thermal storage and without automated shading techniques. Further work is planned on the integration of the solar and HVAC systems, as well as on their optimal control.

Preliminary testing of the home indicates that it performs similarly to what the software predicts. Concepts outlined in this thesis can be used to design energy efficient and net-zero energy homes in any area of the globe, so long as the design options are simulated with accurate software in order to make informed decisions regarding the home's energy systems.

6.2 Future Work

Additional work is required to integrate daylighting into the program using view factors so that shading can be controlled more precisely to satisfy lighting conditions in addition to thermal gains. Work is also required to determine the effective heat capacity and thermal conductivity of the PCM bricks so that more precise calculations regarding their

thermal storage can be performed. The advancement of programs that take all energy aspects of a home into account must be improved by adding the functionality of custom energy retrofits.

Simple algorithms are required that save energy while keeping controls simple to use, commission and install in order to truly penetrate the market and become truly adopted by users. Continued work is required to improve the user-friendliness of the program as well as integrating it with an accurate lighting simulation program (i.e. one that uses the radiosity method and ray-tracing) is required.

Control hardware is also required which is flexible enough to accept custom control algorithms to allow optimal control of all the energy systems in a home in unison. Existing hardware today limits algorithms to simple logic statements and conflicts can occur when trying to control a single element with multiple variables from sensors, this must be improved to truly observe significant savings in homes.

REFERENCES

AIP (American Institute of Physics), (2006) www.aip.org

ASHRAE, 2001, "Fundamentals of Control", 2001 ASHRAE Fundamentals Handbook (SI)

Athienitis A.K, 1998, "Building Thermal Analysis", 3rd edition, Concordia University, Montreal.

Athienitis, A.K., 1999, "Building Thermal Analysis", Electronic Mathcad Book - 2nd Edition - in Civil Eng. Library, Mathsoft Inc., Boston, U.S.A.

Athienitis, A.K. and Tzempelikos, A., 2002, "A Methodology for Simulation of Daylight Room Illuminance Distribution and Light Dimming for a Room with a Controller Shading Device", Solar Energy, Vol. 72, No. 4, pp. 271-281

Araujo, G., 1998, "Solar Electricity: Engineering of Photovoltaic Systems", James and James Science Publishers Ltd.

Balcomb, J. D., 1997, "ENERGY-10, A Design Tool for Low-Energy Buildings", Proc. Building Simulation '97, International Building Performance Simulation Association, Prague, Czech Republic, Sept. 8-10.

Barnett, Allan, 2003, "The U.S. Photovoltaic Industry Roadmap", Solar Electric Power

Bellia, L. et al, 2002, "Setting up a CCD photometer for lighting research and design", Building and Environment, 37, 1099-1106

Bierman, Andrew and Conway, Kathryn M., 2000, "Characterizing Daylight Photosensor System Performance to Help Overcome Market Barriers", Journal of the Illuminating Engineering Society

Charron, R., 2005, "Integrated Design and Optimization Issues for Zero Energy Solar Homes", Second Canadian Design Engineering Network Conference on Design Education, Kananaskis

Choi, An-Seop et al., 2005, "The Characteristics of Photosensors and Electronic Dimming Ballasts in Daylight Responsive Dimming Systems", Building and Environment, 40, 39-50

Ehrlich, Charles et al, 2001, "Simulating the Operation of Photosensor-Based Lighting Controls", Proceedings of the 2001 Building Simulation 7th International Building Performance Simulation Association Conference, Rio de Janeiro

Galasiu, A.D. et al., 2004, "Impact of Window Blinds on Daylight-Linked Dimming and Automatic On/Off Lighting Controls, Solar Energy", v. 76, pp. 523-544

Galasiu, A.D. and Veitch, Jennifer A., 2003, "A Literature Review on Occupant Preferences and Satisfaction in Daylit Offices", NRC

Heschong Mahone Group, Inc., 2003, "Photocontrol Systems – Design Guildelines", Southern California Edison

HowStuffWorks, http://home.howstuffworks.com

Matrix Energy, www.matrixenergy.ca

Mistrick, Richard et al., 2000, "A Comparison of Photosensor-Controlled Electronic Dimming Systems in a Small Office", Journal of the Illuminating Engineering Society

NEEC (National Energy Efficiency Committee, 2005, (www.neec.gov.sg)

Newsham, G.R et al., 2004, "Effect of Dimming Control on Office Worker Satisfaction and Performance", IESNA Annual Conference Proceedings, Tampa, Florida, pp. 19-41

Newsham, G.R. et al., 2002, "The Effect of Power Constraints on Occupant Lighting Choices and Satisfaction: A Pilot Study", IESNA Annual Conference, Salt Lake City, pp. 115-131

Newsham, G.R. and Veitch, Jennifer A., 1997, "Energy-Efficient Lighting Options: Predicted Savings and Occupant Impressions of Lighting Quality", CLIMA 2000 Conference, Brussels, Belgium

Park, K.W., 2004, "An Illuminance Ratio Prediction Method for Daylighting Control of Buildings", PhD Thesis, Department of Building, Civl & Environmental Engineering, Concordia University.

Pasini, Mark, 2005, "PVT Simulation of the Canadian Solar Decathlon House", Natural Resources Canada

Pasini, Mark, 2006, "Trends in Current, Leading-Edge and Future Residential Home Energy Use", Natural Resources Canada

Pasini, Mark and Athienitis, A.K., 2006, "Systems Design of the Canadian Solar Decathlon House", 2006 ASHRAE Annual Meeting, Quebec City

Paule, Bernard, 2002, "DIAL-Europe: A European integrated daylighting design tool"

Quaschning, Volker, 2004, "Solar Thermal Water Heating", Renewable Energy World, pp.95-99

Reinhart, Christoph F., 2004, "Lightswitch-2002: A Model for Manual and Automated Control of Electric Lighting and Blinds", Solar Energy, 77, 15-28

Roth, Kurt, 2004, "Modulating Compressors for Residential Cooling", ASHRAE Journal

Rubinstein, Francis et al, 1989, "Improving the Performance of Photo-Electrically Controlled Lighting Systems", Journal of the Illuminating Engineering Society

Scholar Programme, 2006, "Photovoltaics – How Does it Work?", http://www.scolar.org.uk/html/school-info/ks4/ks4-2c.html

Silberstein, Eugene, 2002, "Heat Pumps", Thomas Nelson

Smith, C., 1995, "History of Solar Energy", Solar Power.

Solarbuzz, http://www.solarbuzz.com/Technologies.htm

Strong, Steven, 2006, "Building Integrated Photovoltaics", http://www.wbdg.org/design/bipv.php

The Weather Network, www.theweathernetwork.com

Trace Engineering, 2006, "Demystifying Inverters", http://www.westcoastenergyco-op.org/inverters.htm

Tripanagnostopoulos, Y., 2004, "Energy, Cost and LCA Results of PV and Hybrid PV/T Solar Systems", Progress in Photovoltaics: Research and Applications, 13:235-250

Unger, Helmuth K., 2001, "DALI Manual", DALI Activity Group, ZVEI-Division Luminaires

van Cleef, M., 2001, "Superior Energy Yields of UNI-SOLAR Triple Junction Thin Film Silicon Solar Cells compared to Crystalline Silicon Solar Cells under Real Outdoor Conditions in Western Europe", 17th European Photovoltaic Solar Energy Conference and Exhibition, Munich, Germany

Welfonder, T., Hiller, M., Holst, S., and Knirsch, A., 2003, "Improvements on the Capabilities of TRNSYS 15", Proceedings of Building Simulation '03, 1377-1384, International Building Performance Simulation Association, Eindhoven Netherlands.

Wikipedia, 2006, "Photodiode", http://en.wikipedia.org/wiki/Photodiode

Windsun, www.windsun.com

Zigbee Tutorial, Tutorial-Reports.com, http://www.tutorial-reports.com/wireless/zigbee/zigbee-introduction.php

APPENDIX A

House Model

Reference:C:\Program Files\MathSoft\Mathcad 2001i Professional\Solar Decathlon\February Report\H

Reference:C:\Program Files\MathSoft\Mathcad 2001i Professional\Solar Decathlon\February Report\trom

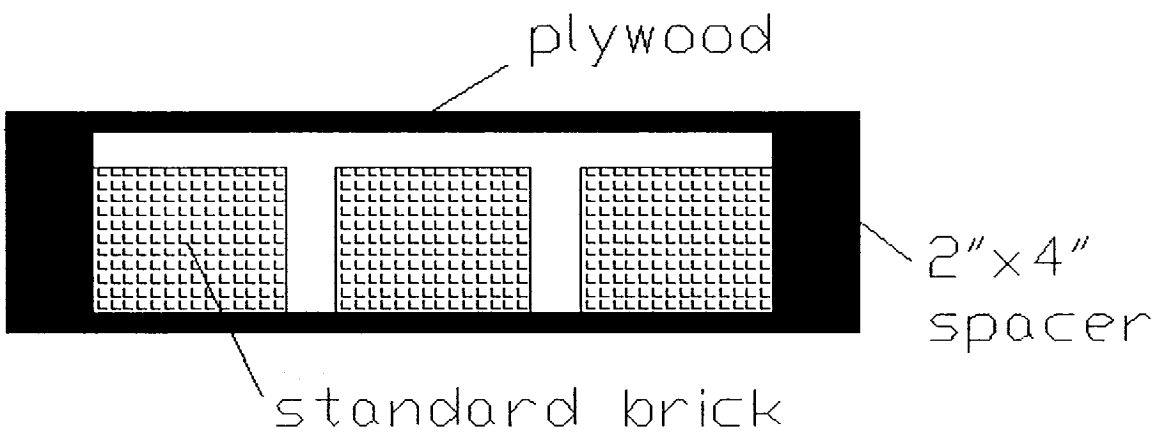

Velocity profile of air through false floor

$V(p) := 1.0$

$V2(p) := 0.5 \cdot \frac{m}{sec}$

$V(p) := if\left[\left(12hr < \frac{t_p}{hr} < 17hr\right) \vee \left(36hr < t_p < 41hr\right) \vee \left(60hr < t_p < 65hr\right) \vee \left(84hr < t_p < 89hr\right) \vee \left(110hr < t_p < 113hr\right), 0.1, V(p)\right]$

$V2(p) := if\left[\left(22hr < \frac{t_p}{hr} < 32hr\right) \vee \left(46hr < t_p < 56hr\right) \vee \left(70hr < t_p < 80hr\right) \vee \left(94hr < t_p < 104hr\right) \vee \left(118hr < t_p < 128hr\right), 0.1\frac{m}{sec}, V2(p)\right]$

Assumptions: - insulation is placed between concrete blocks and soil, therefore assumed to be adiabatic.

- sides of floor are insulated, therefore adiabatic.
- due to symmetry, only half of concrete block is considered.

$degC \equiv 1$

$A_r := 1 \cdot m^2$

$L := 1.0 \cdot m$

size of brick:

$brick\_width := 0.0921 \cdot m$

$brick\_height := 0.0635 m$

brick_length := 0.1937·m

brick_length := L

size of air space:

air_width := 0.11·m

air_height := 0.01905m

air_length := 0.23·m

air properties:

$k_{air} := 0.024 \frac{watt}{m \cdot degC}$

$\nu := 14.5 \cdot 10^{-6} \cdot \frac{m^2}{sec}$

Pr := 0.7

$\rho_a := 1.2 \cdot \frac{kg}{m^3}$

$c_a := 1000 \frac{joule}{kg \cdot degC}$

ordinary brick properties:

$c_b := 840 \cdot \frac{joule}{kg \cdot degC}$

$k_b := 0.7 \cdot \frac{watt}{m \cdot degC}$

$\rho_b := 1100 \frac{kg}{m^3}$

..specific heat

..conductivity

..density

Film coefficients:

$h_i := 8 \cdot \frac{watt}{m^2 \cdot degC}$

$h_o := 20 \cdot \frac{watt}{m^2 \cdot degC}$

floor properties:

$k_{wood} := 0.16 \frac{watt}{m \cdot degC}$

flr_thick := 0.0254·m

Conductance of Air in Cavity:

q(p) := air_width·air_height·V2(p)

$U_a(p) := q(p) \cdot \rho_a \cdot c_a$

Conductances of brick - brick (axial)

$U_{1b\_2b} := \frac{k_b \cdot brick\_width \cdot brick\_height}{brick\_length}$

$U_{2b\_3b} := U_{1b\_2b}$

$U_{3b\_4b} := U_{1b\_2b}$

$U_{4b\_5b} := U_{1b\_2b}$

$U_{5b\_6b} := U_{1b\_2b}$

Conductances of brick - air (radial)

$$R_{1a\_1c} := \left[\frac{brick\_height}{(2 \cdot k_b \cdot brick\_length \cdot brick\_width)} + \frac{1}{(h_o \cdot brick\_length \cdot brick\_width)} \right]$$

$$U_{1a\_1c} := \frac{1}{R_{1a\_1c}}$$

$U_{2a\_2c} := U_{1a\_1c}$

$U_{3a\_3c} := U_{1a\_1c}$

$U_{4a\_4c} := U_{1a\_1c}$

$U_{5a\_5c} := U_{1a\_1c}$

Conductances of air - room (radial)

$$R_{1a\_r} := \frac{1}{(h_i \cdot brick\_length \cdot brick\_width)} + \frac{flr\_thick}{k_{wood} \cdot brick\_length \cdot brick\_width} + \frac{1}{(h_o \cdot brick\_length \cdot brick\_width)}$$

$$U_{1a\_r} := \frac{1}{R_{1a\_r}}$$

$U_{2a\_r} := U_{1a\_r}$

$U_{3a\_r} := U_{1a\_r}$

$U_{4a\_r} := U_{1a\_r}$

$U_{5a\_r} := U_{1a\_r}$

Thermal capacitances of brick and air:

$C1a := \rho_a \cdot c_a \cdot air\_width \cdot air\_height \cdot air\_length$

$$C1a = 1.607 \times 10^{-7} \frac{kW \cdot hr}{degC}$$

. . capacitance of air

$C2 := \rho_b \cdot c_b \cdot brick\_width \cdot brick\_height \cdot brick\_length$

$$C2 = 1.501 \times 10^{-3} \frac{kW \cdot hr}{degC}$$

. . capacitance of brick

$C2 := C2 \cdot 1200 \cdot 2 \cdot 10 degC$

$C2 = 36.026 kW \cdot hr$

$C1b := C1a$

$C1a \cdot 5 \cdot 10 \cdot 10 = 8.033 \times 10^{-5} kW \cdot hr$

$C1c := C1a$

$i := 1, 2 .. 7$

$$St_p := \left[Qggn_0 + 2 \cdot \sum_{n1} Re\left[\left(Qggn_{n1} \right) \cdot \exp\left(j \cdot w_{n1} \cdot t_p \right) \right] \right] + \sum_i \left[Sn_{0,i} + 2 \cdot \sum_{n1} Re\left[\left(Sn_{n1,i} \right) \cdot \exp\left(j \cdot w_{n1} \cdot t_p \right) \right] \right]$$

$$St_p := \frac{St_p + |St_p|}{2}$$

$$TS(p) := \frac{C1a}{U_{1a\_1c} + U_{1b\_2b}}$$

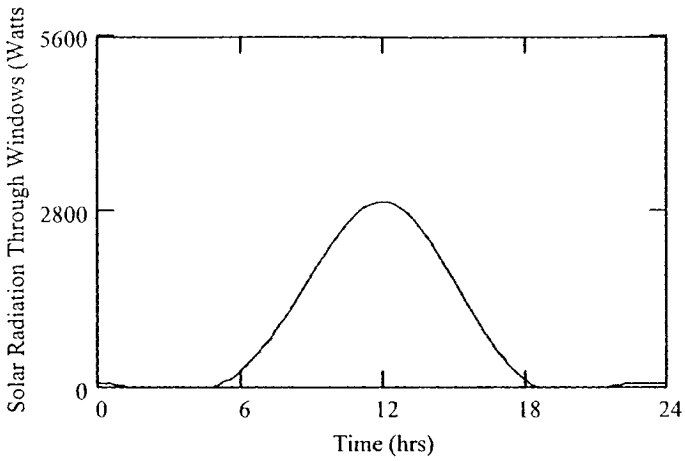

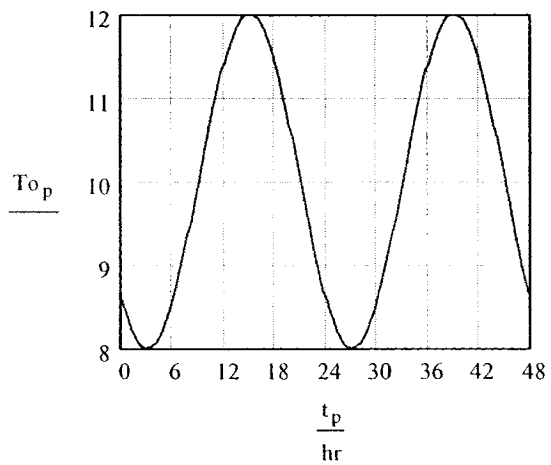

.

start := 0

$F := \frac{1}{200}$

fraction of total solar radiation hitting a surface control volume

$Tb_p := 16 \cdot degC$

$Tsp := 23.3 \cdot degC$

$qcool := 6000 \cdot watt$

$visit\_schedl_p := \left[1 - 1 \cdot \left(mod\left(\frac{t_p}{hr}, 24\right) < 14\right) - 1 \cdot \left(mod\left(\frac{t_p}{hr}, 24\right) > 17\right)\right]$

$qint_p := \left(2000 \cdot watt \cdot visit\_schedl_p\right) + 250 \cdot watt$

modify setpoint to allow it

to be slightly higher during visiting hours

$Tsp_p := if\left[\left(50400 < t_p < 61200 sec\right) \vee \left(136800 sec < t_p < 147600 sec\right), 24.4, 23.3\right]$

$Tsp_p := if\left[\left(14hr < \frac{t_p}{hr} < 17hr\right) \vee \left(38hr < t_p < 41hr\right) \vee \left(62hr < t_p < 65hr\right) \vee \left(86hr < t_p < 89hr\right) \vee \left(110hr < t_p < 113hr\right), 23.3, 23.3\right]$

$Tl_{c_{start}} := 20 \cdot degC$

$Tl_{a_{start}} := 20 \cdot degC$

$T_{1,start} := 20 \cdot degC$

$Ts1_{start} := 20 \cdot degC$

$T2c_{start} := 20 \cdot degC$

$T2a_{start} := 20 \cdot degC$

$T_{2,start} := 20 \cdot degC$

$Ts2_{start} := 20 \cdot degC$

$T3c_{start} := 20 \cdot degC$

$T3a_{start} := 20 \cdot degC$

$T_{5,start} := 20 \cdot degC$

$Ts3_{start} := 20 \cdot degC$

$T4c_{start} := 20 \cdot degC$

$T4a_{start} := 20 \cdot degC$

$T_{6,start} := 20 \cdot degC$

$Ts4_{start} := 20 \cdot degC$

$T5c_{start} := 20 \cdot degC$

$T5a_{start} := 20 \cdot degC$

$qaux_{start} := 0 \cdot watt$

$Ts5_{start} := 20 \cdot degC$

$Tinlet_{start} := 20 \cdot degC$

$qfloor_{start} := 0 \cdot watt$

$M2 := 0.05 \cdot \frac{m^3}{sec}$

$$
\begin{pmatrix}
T1a_{p+1} \\
T1c_{p+1} \\
Ts1_{p+1} \\
T2a_{p+1} \\
T2c_{p+1} \\
Ts2_{p+1} \\
T3a_{p+1} \\
T3c_{p+1} \\
Ts3_{p+1} \\
T4a_{p+1} \\
T4c_{p+1} \\
Ts4_{p+1} \\
Tinlet_{p+1} \\
qaux_{p+1} \\
T_{1,p+1} \\
T_{2,p+1} \\
T_{5,p+1} \\
T_{6,p+1} \\
qfloor_{p+1} \\
Tdiffairpv_{p+1}
\end{pmatrix}
:=
\begin{bmatrix}
\dfrac{Tinlet_p \cdot U_a(p) + T1c_p \cdot U_{1a\_1c} + Ts1_p \cdot U_{1a\_r}}{U_a(p) + U_{1a\_1c} + U_{1a\_r}} \\
\dfrac{T1a_p \cdot U_{1a\_1c} + Tinlet_p \cdot U_a(p)}{U_{1a\_1c} + U_a(p)} \\
\dfrac{\frac{T_{6,p}}{R_{26}} + \frac{T_{1,p}}{R_{12}} + \frac{T1a_p}{R_{1a\_r}} + 0.7 \cdot 75 \cdot St_p \cdot F}{\left(\frac{1}{R_{26}} + \frac{1}{R_{12}} + \frac{1}{R_{1a\_r}}\right)} \\
\dfrac{T1a_p \cdot U_{1b\_2b} + T2c_p \cdot U_{2a\_2c} + Ts2_p \cdot U_{2a\_r}}{U_{1b\_2b} + U_{2a\_2c} + U_{2a\_r}} \\
\dfrac{T2a_p \cdot U_{1a\_1c} + T1c_p \cdot U_a(p)}{U_{1a\_1c} + U_a(p)} \\
\dfrac{\frac{T_{6,p}}{R_{26}} + \frac{T_{1,p}}{R_{12}} + \frac{T2a_p}{R_{1a\_r}} + 0.7 \cdot St_p \cdot F}{\left(\frac{1}{R_{26}} + \frac{1}{R_{12}} + \frac{1}{R_{1a\_r}}\right)} \\
\dfrac{T2a_p \cdot U_{2b\_3b} + T3c_p \cdot U_{3a\_3c} + Ts3_p \cdot U_{3a\_r}}{U_{2b\_3b} + U_{3a\_3c} + U_{3a\_r}} \\
\dfrac{T3a_p \cdot U_{1a\_1c} + T2c_p \cdot U_a(p)}{U_{1a\_1c} + U_a(p)} \\
\dfrac{\frac{T_{6,p}}{R_{26}} + \frac{T_{1,p}}{R_{12}} + \frac{T2a_p}{R_{1a\_r}} + 0.7 \cdot St_p \cdot F}{\left(\frac{1}{R_{26}} + \frac{1}{R_{12}} + \frac{1}{R_{1a\_r}}\right)} \\
\dfrac{T3a_p \cdot U_{3b\_4b} + T4c_p \cdot U_{4a\_4c} + Ts4_p \cdot U_{4a\_r}}{U_{3b\_4b} + U_{4a\_4c} + U_{4a\_r}} \\
\dfrac{T4a_p \cdot U_{1a\_1c} + T3c_p \cdot U_a(p)}{U_{1a\_1c} + U_a(p)} \\
\dfrac{\frac{T_{6,p}}{R_{26}} + \frac{T_{1,p}}{R_{12}} + \frac{T2a_p}{R_{1a\_r}} + 0.7 \cdot St_p \cdot F}{\left(\frac{1}{R_{26}} + \frac{1}{R_{12}} + \frac{1}{R_{1a\_r}}\right)} \\
if\left[\left(24 \cdot hr < \frac{t_p}{hr} < 30 \cdot hr\right) \vee \left(48 \cdot hr < t_p < 54 \cdot hr\right) \vee \left(72 \cdot hr < t_p < 78 \cdot hr\right) \vee \left(96 \cdot hr < t_p < 102 \cdot hr\right) \vee \left(112 \cdot hr < t_p < 118 \cdot hr\right), To_p, T_{1,p}\right] \\
if\left[\left[\left(T_{1,p} - Tsp_p\right) > 1.1\right] \wedge \left[\left(10 \cdot hr < \frac{t_p}{hr} < 18 \cdot hr\right) \vee \left(34 \cdot hr < t_p < 42 \cdot hr\right) \vee \left(58 \cdot hr < t_p < 66 \cdot hr\right) \vee \left(82 \cdot hr < t_p < 90 \cdot hr\right) \vee \left(106 \cdot hr < t_p < 114 \cdot hr\right)\right], qcool, 0\right] \\
\dfrac{\left[\left(\frac{To_p}{R_{1o}} + \frac{T_{6,p}}{R_{16}} + \frac{T_{2,p}}{R_{12}}\right) - qaux_p + \left(1q_{floor}\right)_p\right]}{\left(\frac{1}{R_{1o}} + \frac{1}{R_{16}} + \frac{1}{R_{12}}\right)} \\
\dfrac{\frac{T_{6,p}}{R_{26}} + \frac{T_{1,p}}{R_{12}} + qint_p \cdot 0.2}{\left(\frac{1}{R_{26}} + \frac{1}{R_{12}}\right)} \\
\dfrac{\Delta t}{C_5}\left(\frac{T_{6,p} - T_{5,p}}{R_{56}} + \frac{To_p - T_{5,p}}{R_{5o}} + qint_p \cdot 0.2\right) + T_{5,p} \\
\dfrac{\frac{T_{2,p}}{R_{26}} + \frac{T_{5,p}}{R_{56}} + \frac{T_{1,p}}{R_{16}} + 0.3 \cdot St_p + qint_p \cdot 0.6}{\left(\frac{1}{R_{56}} + \frac{1}{R_{26}} + \frac{1}{R_{16}}\right)} \\
\left[c_a \cdot \rho_a \cdot air\_width \cdot air\_height \cdot 1200 \cdot V2(p) \cdot V(p) \cdot \left(T4c_p - T_{1,p}\right)\right] \\
Tdiff\left(time_p\right)
\end{bmatrix}
$$

inlet temperature for hollc core floor to represent taking outside air during t night and recirculating during the day

inlet temperature for hollow core floor to represent taking outside air during the night and recirculating during the day

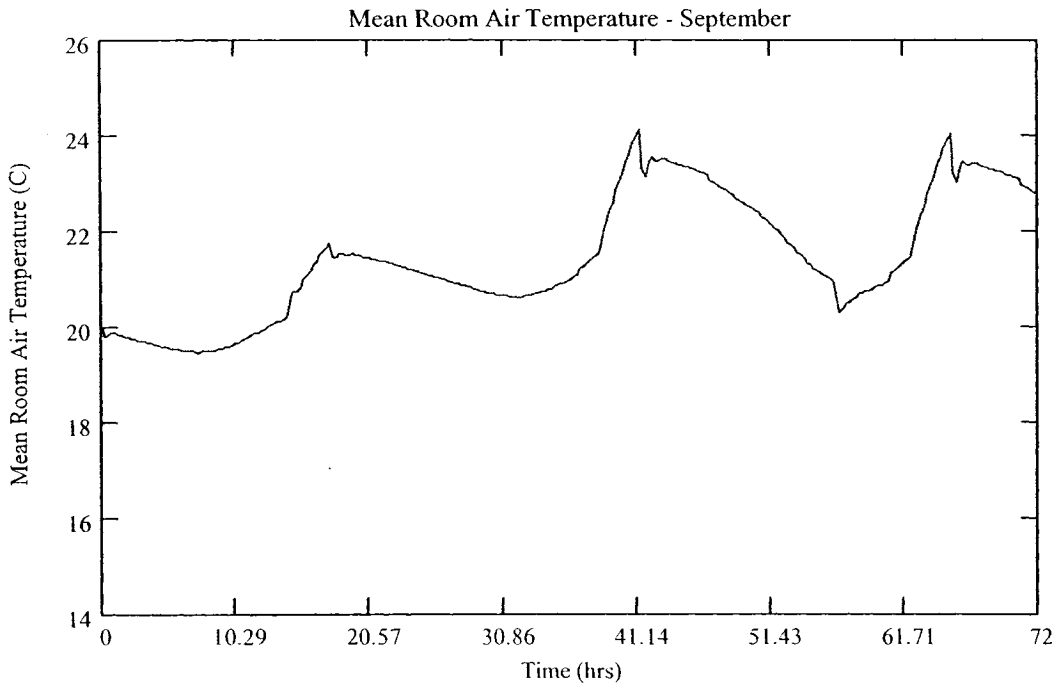
Mean Room Air Temperature - September
Mean Room Air Temperature (C)
26
24
22
20
18
16
14
0
10.29
20.57
30.86
41.14
51.43
61.71
72
Time (hrs)

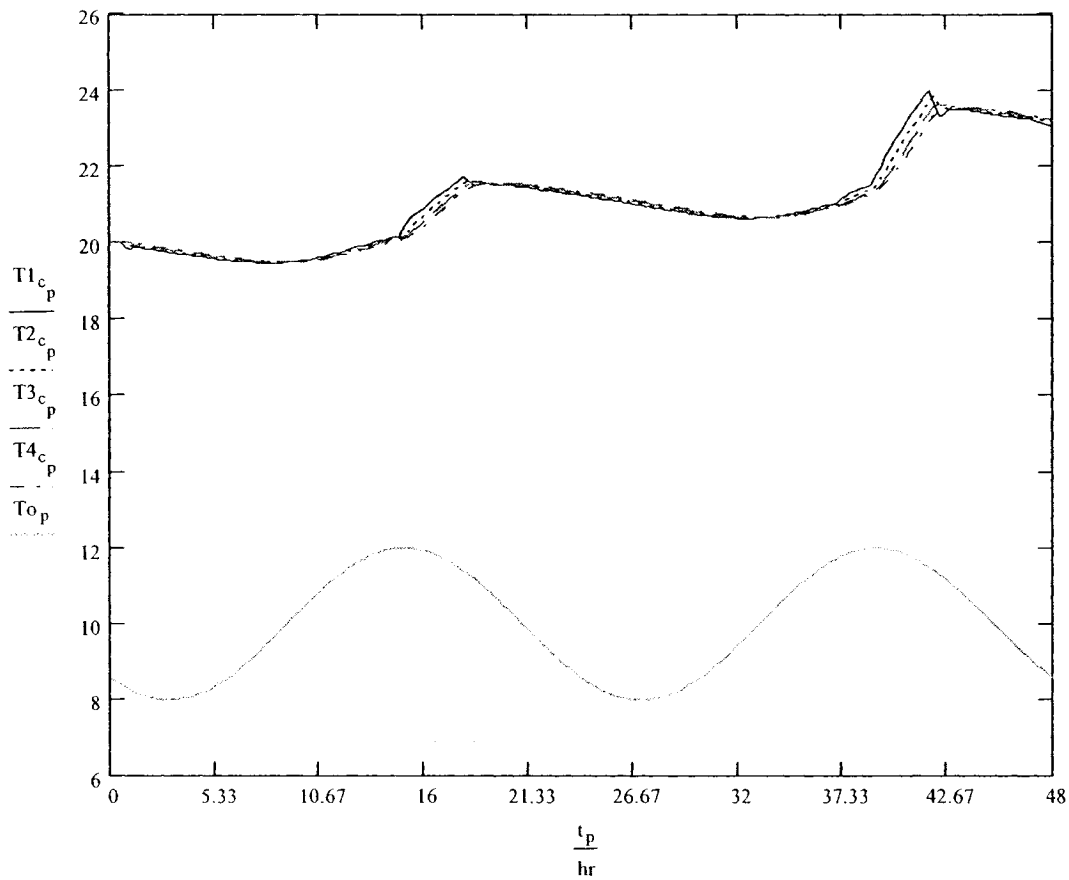
26
24
22
20
18
16
14
12
10
8
6
0
5.33
10.67
16
21.33
26.67
32
37.33
42.67
48
T1cp
T2cp
T3cp
T4cp
Top
tp
hr

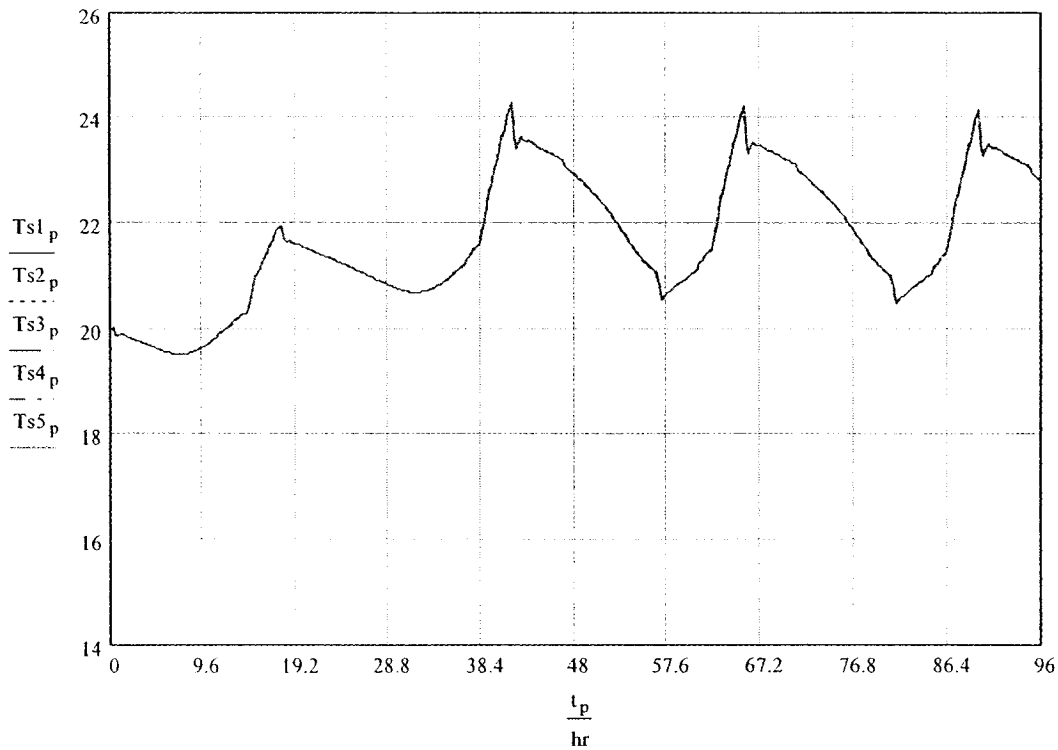

energy consumption by
numerical integration for third day:

$$v := \frac{NT \cdot 4}{5}, \frac{NT \cdot 4}{5} + 1 .. NT - 1$$

$$Qc := \sum_{v} \frac{qaux_v + |qaux_v| + (qaux_{v+1}) + |qaux_{v+1}|}{4} \cdot (t_{v+1} - t_v)$$

$$Qc = 0\,kW \cdot hr$$

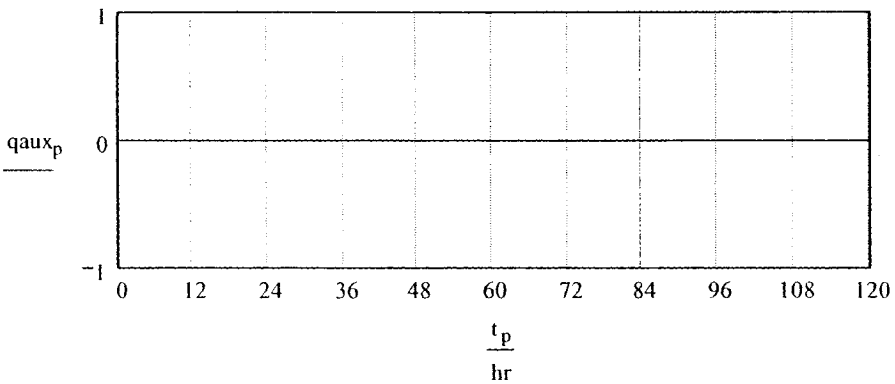

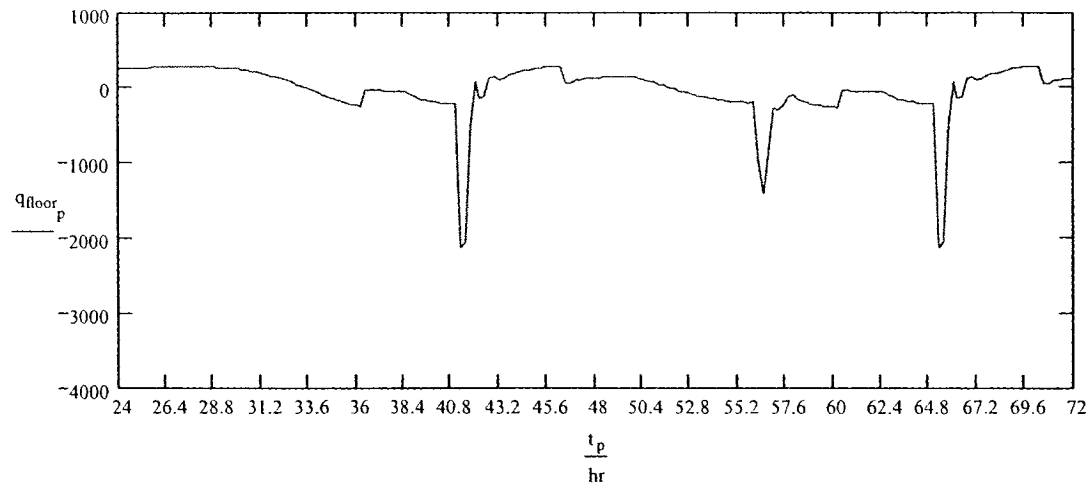

$$\sum_{p=288}^{384} q_{floor_p} \cdot 0.25\,hr = -2.737\,kW \cdot hr$$

$$\sum_{p=288}^{384} q_{floor_p} = -1.095 \times 10^{4}\,kg\,m^{2}\,sec^{-3}$$

Outside Temperature

The outside temperature for a day is modeled by a Fourier series based on NTo+1 values that
are an input to the array below. If more detail is required, NTo may be increased. Then, the
the Fourier series may be used to generate intermediate values as required by the time step of a finite difference model.

$degC := 1$

$Nh := 5$

$n := 0, 1 .. Nh$

...harmonics

$NTo := 23$

$it := 0, 1 .. NTo$

...time index

$t_{it} := it \cdot 1 \cdot hr$

..time

$$w_n := 2 \cdot \pi \cdot \frac{n}{24 \cdot hr}$$

$j := \sqrt{-1}$

The outside temperature is modeled as a single sinusoid, with maximum at 3 pm

$Tomean := 10 \cdot degC$

. mean temperature

$DT := 4 \cdot degC$

. deviation of temperature

$$w1 := \frac{2 \cdot \pi}{24 \cdot hr}$$

$$To_{it} := \left(Tomean + \frac{DT}{2} \cdot \cos\left(w1 \cdot t_{it} - 1.25\pi \right) \right)$$

. . outside temperature

$$Ton_n := \left(\sum_{it} To_{it} \cdot \frac{\exp\left(-j \cdot w_n \cdot t_{it} \right)}{NTo + 1} \right) \cdot degC$$

...Fourier harmonic coefficients

May replace this curve with real data

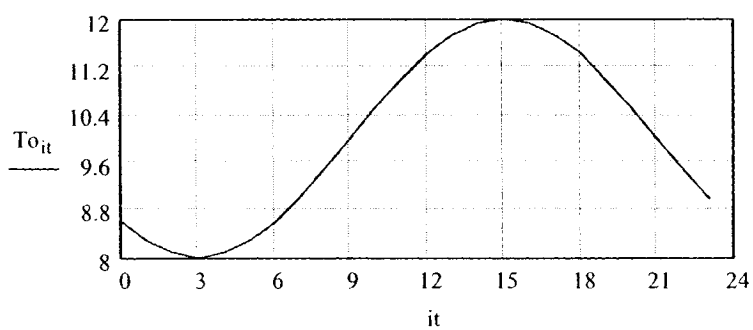

Resistance Model

Reference:C:\Program Files\MathSoft\Mathcad 2001i Professional\Solar Decathlon\February Report\Walls_r1.mcd

The thermal network is shown below FOR FLOOR HEATING.The floor is discretized into two layers (one thermal capacitance and two resistances for each layer). The unheated surfaces are represented by node 6. FOR CONVECTIVE COOLING-HEATING PLACE SOURCE AT NODE 1.

S represents solar radiation transmitted into the room and absorbed by the surfaces (a low value is assummed).

Resistance R1o represents heat loss by infiltration and through the windows and doors.

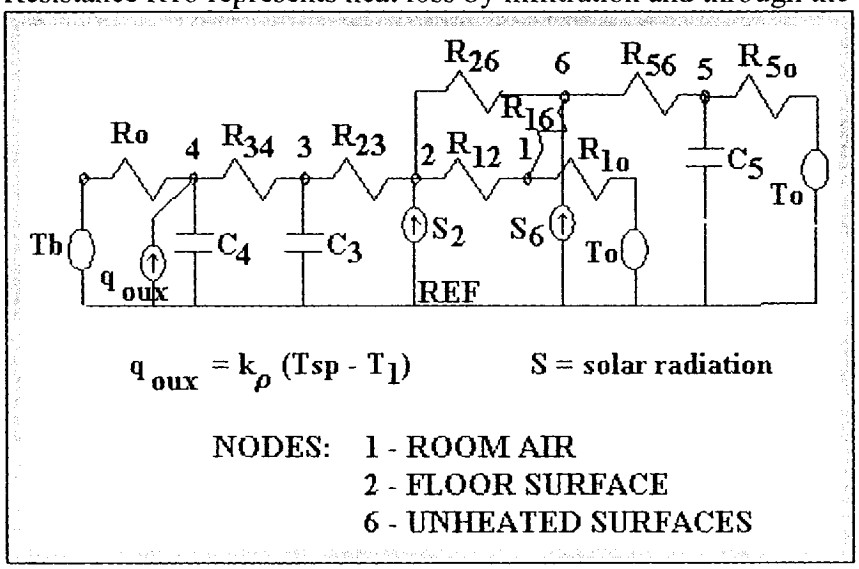

Calaulating the thermal capacitances and resistances :

ach := 0.5

ach= air changes /hour

Calculation of infiltration conductance:

$c_{pair} := 1000 \frac{joule}{kg \cdot degC}$

$\rho_{air} := 1.2 \cdot \frac{kg}{m^3}$

..specific heat and density of air

$U_{inf} := \frac{ach \cdot Vol}{3600 sec} \cdot \rho_{air} \cdot c_{pair}$

$U_{inf} = 27.424 \frac{watt}{degC}$

$C_5 := \sum_{se} A_{se} \cdot L_{se} \cdot c_{se} \cdot \rho_{se}$

..thermal capacitance of interior layer of unheated surfaces

$$R_5 := R_c$$

$$R_{12} := \frac{1}{A_6 \cdot h_6}$$

$$h_{6r} := 4 \cdot \frac{watt}{m^2 \cdot degC}$$

..radiation heat transfer coefficient
between floor and unheated surfaces

$$R_{26} := \frac{1}{h_{6r} \cdot A_6}$$

$$R_{6o} := \sum_{se} \frac{R_{se}}{A_{se}}$$

$$R_{6o} = 1.528 \frac{degC}{watt}$$

$$R_{1o} := \frac{1}{U_{inf} + \sum_{ii} \left(\frac{Aw_{ii}}{R_w} + \frac{Ad_{ii}}{Rd} \right)}$$

$$R_{16} := \frac{1}{\sum_{se} A_{se} \cdot h_{se}}$$

..this represents the thermal resistance
of half of the innermost layer
of the unheated surfaces

$$R_{56} := \frac{1}{\sum_{se} \frac{k_{se} \cdot A_{se} \cdot 2}{L_{se}}}$$

$$R_{26} := \frac{1}{h_{6r} \cdot A_6}$$

$$R_{1o} := \frac{1}{U_{inf} + \sum_{ii} \left(\frac{Aw_{ii}}{R_w} + \frac{Ad_{ii}}{Rd} \right)}$$

$$R_{16} := \frac{1}{\sum_{se} A_{se} \cdot h_{se}}$$

$se := 1, 2 .. 4$

$$R_{5o} := R_{56} + \frac{1}{\sum_{se} \frac{A_{se}}{R_{se}}}$$

$$R_{56} = 6.611 \times 10^{-4} \frac{s^3}{kg\,m^2}$$

$$R_{5o} = 0.069 \frac{s^3}{kg\,m^2}$$

Shading Model

Reference:C:\Program Files\MathSoft\Mathcad 2001i Professional\Solar Decathlon\February Report\S

$t_{it} := t_{it} + 11.99\,hr$

convert time to 24hrs

Shading with blinds or other means according to a predefined schedule:

$$schedule_{it} := \left[1 - 1\cdot\left(mod\left(\frac{t_{it}}{hr}, 24\right) < 9\right) - 1\cdot\left(mod\left(\frac{t_{it}}{hr}, 24\right) > 17\right)\right]$$

$\tau_{b\_open} := .8$

blind-shading effective transmittance when open

$\tau_{b\_redu} := .7$

reduction in transmittance when closed

$shadefac_{it} := \tau_{b\_open} - \tau_{b\_redu}\cdot schedule_{it}$

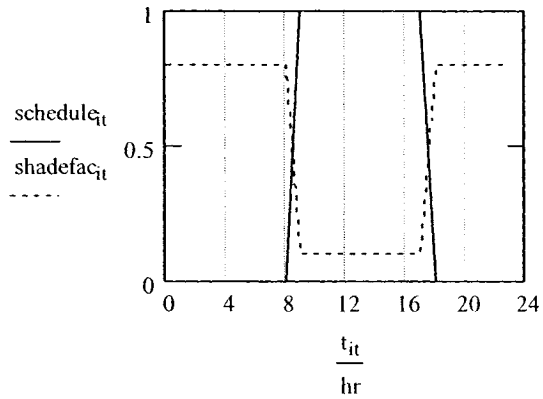

Solar Radiation Model

Solar radiation transmitted through the windows will be modeled as absorbed 70% at the floor surface, and the remainder by the other surfaces in proportion to their areas.

Wall/window azimuth angles:

$iw := 1,2..4$

... window areas

south

east

north

west

$\psi_1 := 0 \cdot deg$

$\psi_2 := -90 \cdot deg$

$\psi_3 := 180 \cdot deg$

$\psi_4 := 90 \cdot deg$

Location data for Washington D.C.:

$Lat := 45 \cdot deg$

..latitude

$\beta := 90 \cdot deg$

..tilt angle

$n_d := 71$

..day number Oct 10

$\rho_g := 0.2$

..ground reflectance

First perform solar geometry calculations

Declination

angle

$$\delta := 23.45 deg \cdot \sin\left(360 \cdot \frac{284 + n_d}{365} \cdot deg\right)$$

$\delta = -4.017 deg$

Sunset time

$$t_s := \left(\operatorname{acos}\left(-\tan(Lat) \cdot \tan(\delta)\right)\right) \cdot \frac{hr}{15 \cdot deg}$$

$t_s = 5.732 hr$

..solar time for solar radiation calculations

Time array:

$it := 0,1..23$

$t_{it} := (it - 11.99) \cdot hr$

$$ha_{it} := 15 \cdot \frac{deg}{hr} \cdot t_{it}$$

..hour angle

(0 at solar noon)

$$ha_s := t_s \cdot 15 \cdot \frac{deg}{hr}$$

..sunset

hour angle

Solar altitude:

$$\alpha_{it} := asin\left(cos(Lat)\cdot cos(\delta)\cdot cos\left(ha_{it}\right) + sin(Lat)\cdot sin(\delta)\right)\cdot\left(\left|t_{it}\right| < \left|t_s\right|\right)$$

Solar azimuth:

$$\phi_{it} := acos\left(\frac{sin(\alpha_{it})\cdot sin(Lat) - sin(\delta)}{cos(\alpha_{it})\cdot cos(Lat)}\right)\cdot\frac{ha_{it}}{\left|ha_{it}\right|}$$

Angle of incidence:

$$\cos\theta_{it,iw} := \cos(\alpha_{it})\cdot\cos\left(\left|\phi_{it} - \psi_{iw}\right|\right)\cdot\sin(\beta) + \sin(\alpha_{it})\cdot\cos(\beta)$$

$$\theta_{it,iw} := acos\left(\frac{\cos\theta_{it,iw} + \left|\cos\theta_{it,iw}\right|}{2}\right)$$

Timestep Model

Reference:C:\Program Files\MathSoft\Mathcad 2001i Professional\Solar Decathlon\February Report\Ou

$$Ton_n := \left(\sum_{it} To_{it} \cdot \frac{\exp(-j \cdot w_n \cdot t_{it})}{NTo + 1} \right) \cdot degC$$

...Fourier harmonic coefficients

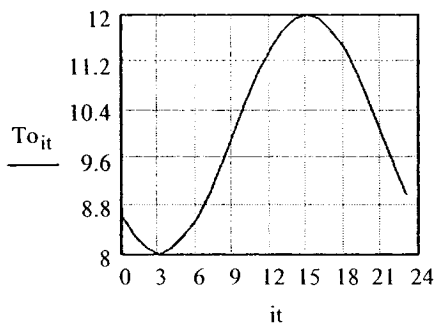

$\Delta t := 900 \cdot sec$

$$NT := 86400 \frac{sec}{\Delta t} \cdot 5$$

$NT = 480$

...number of time steps for two days

$p := 0, 1 .. NT$

$t_p := p \cdot \Delta t$

..times at which simulation is to be performed.

$nl := 1, 2 .. 3$

$$To_p := Ton_0 + 2 \cdot \sum_{nl} Re\left[\left(Ton_{nl}\right) \cdot \exp\left(j \cdot w_{nl} \cdot t_p\right)\right]$$

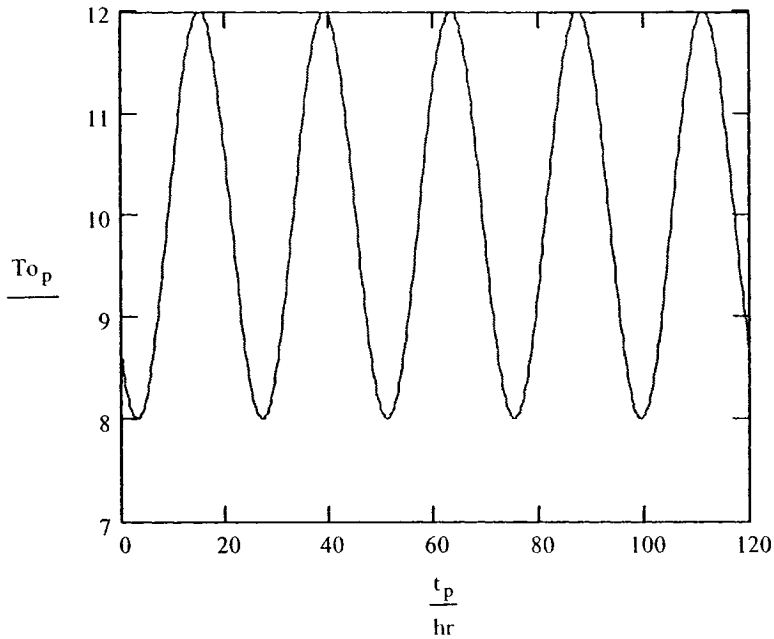
12
11
10
9
8
7
To_p
0
20
40
60
80
100
120
t_p
hr

Wall Model

Reference:C:\Program Files\MathSoft\Mathcad 2001i Professional\Solar Decathlon\February Report\Wi

Reference:C:\Program Files\MathSoft\Mathcad 2001i Professional\Solar Decathlon\February Report\S

$i := 1, 2 .. 7$

$se := 1 .. 5$

$Ad_1 := 1.8 \cdot m^2$

$Ad_2 := 0 \cdot m^2$

$Ad_3 := 1.8 \cdot m^2$

$Ad_4 := 0 \cdot m^2$

Door areas

$Hh := 2.3 \cdot m$

. . wall height

$Lh := 14.6 m$

. . length of house

$Wh := 4.9 \cdot m$

. . width of house

Wall net areas:

$A_7 := 2 \cdot m \cdot 2.5 \cdot m$

$A_7 = 5 m^2$

. . area of trombe wall

$A_1 := Lh \cdot Hh - Aw_1 - Ad_1 - A_7$

$A_1 = 21.78 m^2$

. . area of south wall

$A_2 := Wh \cdot Hh - Aw_2$

$A_2 = 10.9 m^2$

. . area of east wall

$A_3 := Lh \cdot Hh - Aw_3 - Ad_3$

$A_3 = 29.71 m^2$

. . area of north wall

$A_4 := Wh \cdot Hh - Aw_4$

$A_4 = 7.87 m^2$

. . area of west wall

$A_5 := Lh \cdot Wh$

$A_5 = 71.54 m^2$

. . area of ceiling

$A_6 := Wh \cdot Lh$

$A_6 = 71.54m^2$

. . area of floor

$Vol := A_6 \cdot Hh$

. . volume of house

$Rd := 2 \cdot \frac{m^2 \cdot degC}{watt}$

..door thermal resistance

Wall/window azimuth angles:

$\psi_1 := 0 \cdot deg$

$\psi_2 := -90 \cdot deg$

$\psi_3 := 180 \cdot deg$

$\psi_4 := 90 \cdot deg$

Wall absorptances:

$\alpha s_i := 0.7$

$h_5 := 9.0 \cdot \frac{watt}{m^2 \cdot degC}$

$h_6 := 9.3 \cdot \frac{watt}{m^2 \cdot degC}$

$h_7 := 12 \cdot \frac{watt}{m^2 \cdot degC}$

THERMAL RESISTANCE OF WALLS (including air films):

VERTICAL WALLS

Note that thermal storage is considered only for the inner (room-side) layers

1.Inner layer (gypsum
or similar)

$L_1 := 0.03 \cdot m$

$c_1 := 750 \cdot \frac{joule}{kg \cdot degC}$

$\rho_1 := 800 \cdot \frac{kg}{m^3}$

$k_1 := 0.16 \cdot \frac{watt}{m \cdot degC}$

2. Insulation

$R := 3.7 \cdot \frac{m^2}{watt \cdot degC}$

$Rext := 2 \cdot \frac{m^2}{watt \cdot degC}$

$f_f := \frac{3.5}{16}$

$f_f = 0.219$

..fraction of area which is framing - 2"x4" @ 16"cc

2 by 4 wood stud with R-value:

$$R_f := 0.77 \cdot m^2 \cdot \frac{degC}{watt}$$

$$R_l := \frac{1}{\frac{1 - f_f}{\left(R + Rext + \frac{1}{h_o} + \frac{1}{h_l}\right)} + \frac{f_f}{\left(R_f + Rext + \frac{1}{h_o} + \frac{1}{h_l}\right)}}$$

$$R_l = 4.815 \frac{degC \cdot m^2}{watt}$$

Calculation of wall conductance excluding interior layer and film (to be used for admittance calculations):

$$u_l := \frac{1}{R_l - \frac{1}{h_l}}$$

Assume that all exterior walls are of the same construction:

$ii := 1, 2 .. 4$

This needs to be changed for a certain wall if we have e.g. interior bricks rather than gypsum board.

$L_{ii} := L_l$

$R_{ii} := R_l$

$u_{ii} := u_l$

$k_{ii} := k_l$

$\rho_{ii} := \rho_l$

$c_{ii} := c_l$

$$Ts_{it,5} := I_{it,5} \cdot \frac{\alpha s_5}{h_5}$$

For the Roof

$$Ts_{it,iw} := I_{it,iw} \cdot \frac{\alpha s_{iw}}{h_{iw}}$$

For the Vertical Walls

Represent with

Fourier series:

$n := 0, 1 .. Nh$

$$Tsn_{n,se} := \left(\sum_{it} Ts_{it,se} \cdot \frac{\exp\left(-j \cdot w_n \cdot t_{it}\right)}{24} \right)$$

Equivalent or sol-air temperatures:

$Teq_{n,se} := Ton_n + Tsn_{n,se}$

$Teq_{n,6} := Ton_n$

Solar radiation
absorbed by
surfaces :

$$S_{it,iw} := 0.3 \cdot Gt_{it} \cdot \frac{A_{iw}}{\sum_{iw} A_{iw}} \cdot shadefac_{it}$$

$$S_{it,6} := 0.7 \cdot Gt_{it} \cdot shadefac_{it}$$

$\alpha_g := 0.05$

$nl := 1,2..3$

$S_{it,7} := (1 - \alpha_g) \cdot A_7 \cdot G_{it,1}$

Represent with
Fourier series:

$$Sn_{n,i} := \left(\sum_{it} S_{it,i} \cdot \frac{\exp(-j \cdot w_n \cdot t_{it})}{24} \right)$$

Calculation of roof-ceiling thermal resistance :

CEILING:

$$\rho_5 := 800 \frac{kg}{m^3}$$

1. gypsum board

$L_5 := 0.03 \cdot m$

$$c_5 := 750 \frac{joule}{kg \cdot degC}$$

$$k_5 := 0.16 \frac{watt}{m \cdot degC}$$

2. insulation

$$R_{insc} := 6 \cdot m^2 \cdot \frac{degC}{watt}$$

3. air-film (attic)

$$h_a := 12 \cdot \frac{watt}{m^2 \cdot degC}$$

$$R_c := \frac{1}{\frac{1 - f_f}{\left(\frac{L_5}{k_5} + R_{insc} + \frac{1}{h_a} + \frac{1}{h_5} \right)} + \frac{f_f}{\left(\frac{L_5}{k_5} + R_f + R_{insc} + \frac{1}{h_a} + \frac{1}{h_5} \right)}}$$

$$R_c = 6.536 \frac{degC \cdot m^2}{watt}$$

Window Model

Reference:C:\Program Files\MathSoft\Mathcad 2001i Professional\Solar Decathlon\February Report\Sol
Reference:C:\Program Files\MathSoft\Mathcad 2001i Professional\Solar Decathlon\February Report\Outsi

..solar time for solar radiation calculations

$t_{it} := (it - 11.99) \cdot hr$

Calculate transmittance of atmosphere and glazing:

. south windows

$Aw_1 := 1.18 \cdot m^2 + 0.2 \cdot 3.4 \cdot m^2 + .2 \cdot 3.4 \cdot m^2 + 0 \cdot 2.3 \cdot m^2 + 1.4 \cdot m^2$

$Aw_1 = 3.94 m^2$

. east windows

$Aw_2 := 0.37 \cdot m^2$

$Aw_1 := 5 \cdot m^2$

$Aw_2 = 0.37 m^2$

. north windows

$Aw_3 := 0.47 \cdot m^2 + 0.42 \cdot m^2 + 1.18 \cdot m^2$

$Aw_3 = 2.07 m^2$

. west windows

$Aw_4 := 3.4 \cdot m^2$

$Aw_4 = 3.4 m^2$

$hi := 8.3 \cdot \frac{watt}{m^2 \cdot degC}$

$h_1 := 8.3 \cdot \frac{watt}{m^2 \cdot degC}$

$h_2 := h_1$

$h_3 := h_1$

$h_4 := h_1$

..interior film coefficients

. . exterior film coefficient

$h_o := 22 \cdot \frac{watt}{m^2 \cdot degC}$

$hr_{low\_e} := 0.5 \cdot \frac{watt}{m^2 \cdot degC}$

.. radiative heat transfer coefficient (assuming low-e at both sides of the window)

. . conductive heat transfer coefficient

$$hc := 2 \cdot \frac{watt}{m^2 \cdot degC}$$

$$R_w := \frac{1}{hi} + \frac{2}{hc + hr_{low\_e}} + \frac{1}{h_o}$$

$$R_w = 0.966 \frac{m^2}{watt}$$

window resistance (double-glazed)

Beam atmospheric transmittance calculations:

$Al := 0.08$

altitude (km)

modified altitude for

Washington

$r0 := 0.97$

$r1 := 0.99$

$rK := 1.02$

summer

$$a_o := r0 \cdot \left[0.4237 - 0.00821(6 - Al)^2\right]$$

$$a_1 := r1 \cdot \left[0.5055 + 0.00595((6.5 - Al))^2\right]$$

$$k_s := rK \cdot \left[0.2711 + 0.01858(2.5 - Al)^2\right]$$

$$\tau b_{it} := if\left[\left(|t_{it}| < |t_s|\right), a_o + a_1 \cdot \exp\left(\frac{-k_s}{\sin(\alpha_{it})}\right), 0\right]$$

Determine now the glazing properties as a function of time interval j:

Glass

properties:

$kL := 0.02$

..extinction coeff.*glazing thickness

$n_g := 1.53$

..refractive index

Angle of refraction and component reflectivity:

$$\theta'_{it,iw} := \operatorname{asin}\left(\frac{\sin(\theta_{it,iw})}{n_g}\right)$$

$$r_{it,iw} := \frac{1}{2}\left[\left(\frac{\sin(\theta_{it,iw} - \theta'_{it,iw})}{\sin(\theta_{it,iw} + \theta'_{it,iw})}\right)^2 + \left(\frac{\tan(\theta_{it,iw} - \theta'_{it,iw})}{\tan(\theta_{it,iw} + \theta'_{it,iw})}\right)^2\right]$$

Beam transmittance, τ, reflectance, ρo, and absorptance, α, of glazing:

$$a_{it,iw} := \exp\left[-\frac{kL}{\sqrt{1 - \left(\frac{\sin(\theta_{it,iw})}{n_g}\right)^2}}\right]$$

$$\tau_{it,iw} := \frac{\left(1 - r_{it,iw}\right)^2 \cdot a_{it,iw}}{1 - \left(r_{it,iw}\right)^2 \cdot \left(a_{it,iw}\right)^2}$$

$$\rho o_{it,iw} := r_{it,iw} + \frac{r_{it,iw} \cdot \left(1 - r_{it,iw}\right)^2 \cdot \left(a_{it,iw}\right)^2}{1 - \left(r_{it,iw}\right)^2 \cdot \left(a_{it,iw}\right)^2}$$

$$\alpha_{s_{it,iw}} := 1 - \rho o_{it,iw} - \tau_{it,iw}$$

For double glazed windows:

$$\tau_{e_{it,iw}} := \frac{\left(\tau_{it,iw}\right)^2}{1 - \left(\rho o_{it,iw}\right)^2}$$

$$\alpha_{i_{it,iw}} := \alpha_{s_{it,iw}} \cdot \frac{\tau_{it,iw}}{1 - \left(\rho o_{it,iw}\right)^2}$$

$$\alpha_{o_{it,iw}} := \alpha_{s_{it,iw}} + \alpha_{s_{it,iw}} \cdot \frac{\tau_{it,iw} \cdot \rho o_{it,iw}}{1 - \left(\rho o_{it,iw}\right)^2}$$

Determine the solar radiation incident on exterior walls and transmitted by windows

Extraterrestrial normal solar radiation:

$$I_{on} := 1353 \frac{watt}{m^2} \cdot \left(1 + 0.033 \cdot \cos\left(360 \cdot \frac{n_d}{365} \cdot deg\right)\right)$$

Determine beam solar radiation:

$$I_{b_{it,iw}} := \left(I_{on} \cdot \tau_{b_{it}} \cdot \cos\left(\theta_{it,iw}\right)\right)$$

..incident beam radiation

$$G_{b_{it,iw}} := I_{b_{it,iw}} \cdot \tau_{e_{10,iw}}$$

..transmitted beam radiation

$$\tau_{ed_{iw}} := \tau_{e_{11,1}}$$

..approximate value for diffuse transmittance (equal for all windows)

$$\theta_{11,1} = 43.001 deg$$

..incident instantaneous sky diffuse radiation

$$I_{ds_{it}} := I_{on} \cdot \sin\left(\alpha_{it}\right) \cdot \left(0.2710 - 0.2939 \tau_{b_{it}}\right) \cdot \frac{1 + \cos(\beta)}{2}$$

..ground reflected

$$I_{dg_{it}} := \left[I_{on} \cdot \sin\left(\alpha_{it}\right) \cdot \left(0.2710 - 0.2939 \tau_{b_{it}} + \tau_{b_{it}}\right)\right] \cdot \rho_g \cdot \frac{1 - \cos(\beta)}{2}$$

$G_{d_{it,iw}} := \tau_{ed_{iw}} \cdot \left(I_{ds_{it}} + I_{dg_{it}} \right)$

.. transmitted diffuse irradiation (instantaneous)

$G_{b_{it,iw}} := I_{b_{it,iw}} \cdot \tau_{e_{it,iw}}$

..beam transmitted solar radiation; this equation may be modified to include the effect of an overhang based on the equations of section 7.4

Total instantaneous solar irradiation incident on exterior surfaces:

$I_{it,iw} := I_{b_{it,iw}} + I_{ds_{it}} + I_{dg_{it}}$

..on vertical walls

$I_{it,5} := \left[I_{on} \cdot \sin(\alpha_{it}) \cdot \left(0.2710 - 0.2939 \tau_{b_{it}} + \tau_{b_{it}} \right) \right]$

..on roof

Total instantaneous solar radiation transmitted by windows:

$G_{it,iw} := G_{b_{it,iw}} + G_{d_{it,iw}}$

$G_{ao_{it,iw}} := \alpha_{o_{it,iw}} \cdot I_{b_{it,iw}} + \alpha_{o_{it,iw}} \cdot \left(I_{ds_{it}} + I_{dg_{it}} \right)$

..radiation absorbed in outer glazings

$G_{ai_{it,iw}} := \alpha_{i_{it,iw}} \cdot I_{b_{it,iw}} + \alpha_{i_{it,iw}} \cdot \left(I_{ds_{it}} + I_{dg_{it}} \right)$

..radiation absorbed in inner glazings

Incident solar irradiation flux (watts/m^2)

Transmitted solar radiation flux

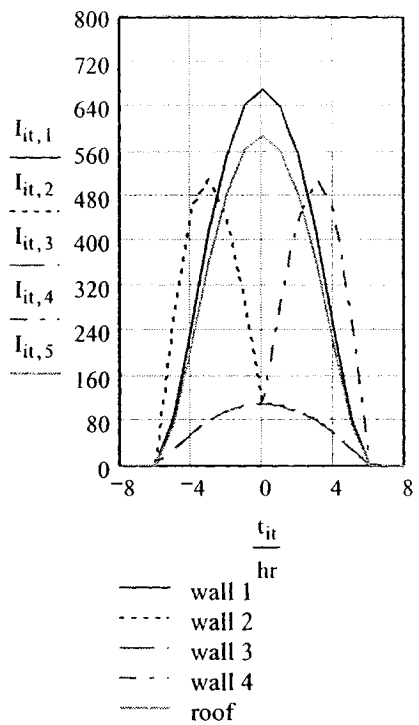

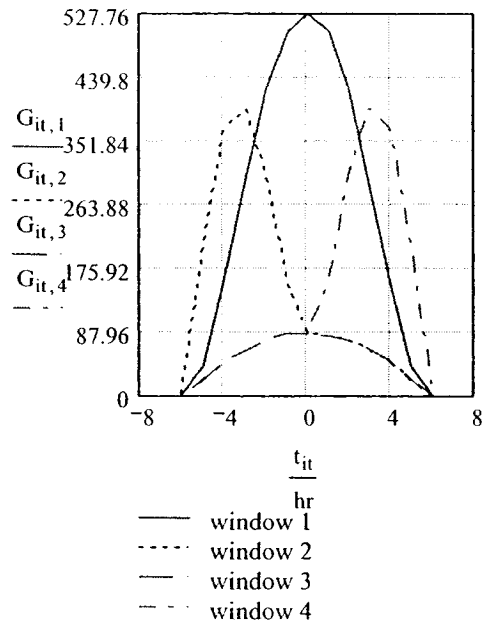

Before performing Fourier series calculations change the time origin from solar noon back to midnight:

$t_{it} := t_{it} + 11.99\,hr$

Solar component of sol-air temperature for exterior surfaces:

Total instantaneous solar radiation transmitted through all windows:

$$Gt_{it} := \sum_{iw} G_{it,iw} \cdot Aw_{iw}$$

$\max(Gt) = 3.329\,kW$

Solar radiation absorbed in glazings and released to room air for the G.F:

$$Qgg_{it} := \sum_{iw} \left[\frac{1}{R_w \cdot h_o} \cdot \left(\alpha_{o_{it,iw}} \cdot I_{it,iw} \right) + \frac{1}{R_w} \cdot \left(R_w - \frac{1}{h_{iw}} \right) \cdot \left(\alpha_{i_{it,iw}} \cdot I_{it,iw} \right) \right] \cdot Aw_{iw}$$

$$Qggn_n := \left(\sum_{it} Qgg_{it} \cdot \frac{\exp\left(-j \cdot w_n \cdot t_{it}\right)}{24} \right)$$

$Qggn_0 = 22.807\,watt$

Solar radiation absorbed in blinds released to room air:

$T_i := 23 \cdot degC$

. . average interior room air temp

$\tau_w := 0.7$

. . transmittance of window

$\alpha_b := 0.15$

. . absorptance of blinds

$$h_{gap} := 8 \cdot \frac{watt}{m^2 \cdot degC}$$

. . heat transfer coefficient of gap between blinds and window

$$h_i := 8 \cdot \frac{watt}{m^2 \cdot degC}$$

. . internal heat transfer coefficient

$$R_1 := \frac{1}{h_o} + R_w + \frac{1}{h_{gap}}$$

. . resistance from blind to outside

. . resistance from blind to interior

$$R_2 := \frac{1}{h_i}$$

$$T_{b_{it}} := \frac{R_1 \cdot R_2 \cdot \tau_w \cdot \alpha_b \cdot I_{12,1} + To_{it} \cdot R_2 + T_i \cdot R_1}{R_1 + R_2}$$

. . temperature of blind

. . heat transfer from blind to room

$$Q_{blind\_room} := \frac{T_b - T_i}{\frac{1}{h_i}}$$